Universidade Federal de Santa Catarina
Centro de Blumenau
Departamento de Engenharia de
Controle, Automação e Computação

Rodrigo Lucas Weber

Implementation of a 24 GHz Radar Combined with Accelerometers for Detection of Passengers in a Moving Vehicle

Developed at IEE S.A.
International Electronics & Engineering

Bissen, Luxembourg
2019

Rodrigo Lucas Weber

Implementation of a 24 GHz Radar Combined with Accelerometers for Detection of Passengers in a Moving Vehicle

Final paper submitted in partial fulfillment of the requirements for the degree of BEng. in Automation and Control Engineering of the Universidade Federal de Santa Catarina.
Advisor: Prof. Dr. Adão Boava

Universidade Federal de Santa Catarina
Centro de Blumenau
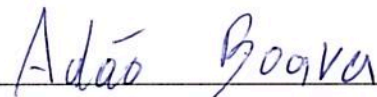Departamento de Engenharia de
Controle, Automação e Computação

Blumenau, Brazil
2019

Rodrigo Lucas Weber

Implementation of a 24 GHz Radar Combined with Accelerometers for Detection of Passengers in a Moving Vehicle

Final paper submitted in partial fulfillment of the requirements for the degree of BEng. in Automation and Control Engineering of the Universidade Federal de Santa Catarina.
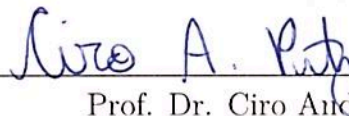
Examination Committee

Prof. Dr. Adão Boava
Universidade Federal de Santa Catarina
Advisor

Prof. Dr. Marcos Vinicius Matsuo
Universidade Federal de Santa Catarina

Prof. Dr. Ciro André Pitz
Universidade Federal de Santa Catarina

Blumenau, July 2019

Acknowledgements

Throughout this very recent period of my life, I have been immensely grateful for all the many great events and opportunities that occurred to me. I am very fortunate for having always such amazing people by my side.

First of all, I could not be more thankful to my academic advisor, Adão Boava, who supported me on my ideas and plans since the first circuits class that I ever had with him. Since the beginning of my graduation in Control and Automation Engineering, Adão has always been both a mentor and a friend, believing on me and helping me to settle an academic record based on inspiration and study. Thank you very much, professor!

I am exceptionally grateful to Dimitri Tatarinov, Udo Schröder, Thomas Stifter, and all those who, at the very first step of this project, believed on my potential and gave me the responsibility of developing this work. Dimitri and Udo, whose great knowledge and advice guided me since my first day at IEE, deserve my very special gratitude. To Steve Dias da Cruz and Jan Sokolowski, who worked directly with me, and to all my colleagues and friends, thank you very much for the companionship in such an important period of my life.

Lastly, but above all else, I would like to express my utmost gratitude and appreciation to my family. *Vó* Rosa, *Vó* Aci, *mãe*, *pai*, *irmão*... they who have been the bedrock of my entire life and, which without them, every single portion of my work and personal growth would not be possible. Thank you very much for your unwavering support, care and love at all times.

Infinita potestas mentis est.

Abstract

In applying a continuous-wave Doppler radar for detection of passengers inside a vehicle, it has been questioned whether the vehicle's movement would interfere on the radar's detection capability. Once the vehicle and radar are moving, not only the passenger's vital signs are detected, but also noise signals caused by engine vibrations, road bumps and relative movements between the vehicle and the passenger. This thesis approaches this question joining a radar and an accelerometer into one single device for supplementary measurement of the vehicle's acceleration and, therefore, its movement. With the accelerometer information about the vehicle's motion, the radar signal can later be filtered to find a cleaner signal of the passenger's vital signs. Additionally, accelerometer belts were crafted and attached to the body of car passengers to measure their acceleration and movement as well. A complete software with user interface for acquiring and processing radar and accelerometer signals was developed for this project and tests have been performed in real road environments. Initial analyses of the collected data have shown that it is indeed possible to detect the vital signs of passengers despite the noise caused by the car's motion. Accordingly, this thesis develops the software and integrates the hardware into a real vehicle system, paving the way for further investigations on the relation between the movements of a vehicle and radar detection.

Keywords: continuous-wave Doppler radar, accelerometer, car passenger detection, breathing detection, vital signs detection.

Resumo

Ao aplicar um radar Doppler de onda contínua para a detecção de passageiros dentro de um veículo, questionou-se se o movimento do automóvel interferiria na capacidade de detecção do radar. Uma vez que o veículo e o radar estão em movimento, não apenas os sinais vitais do passageiro são detectados, mas também os sinais de ruído causados por vibrações do motor, desníveis na estrada e movimentos relativos entre o veículo e o passageiro. Esta tese aborda esta questão unindo um radar e um acelerômetro em um único dispositivo para medição suplementar da aceleração do automóvel e, consequentemente, do seu movimento. Com as informações do acelerômetro sobre o movimento do veículo, o sinal do radar pode ser filtrado posteriormente para encontrar um sinal mais limpo dos sinais vitais do passageiro. Além disso, cintos com acelerômetros foram criados e anexados ao corpo dos passageiros para medir sua aceleração e movimento também. Um software completo, com interface de usuário para aquisição e processamento dos sinais do radar e dos acelerômetros, foi desenvolvido para este projeto e testes foram realizados em ambientes rodoviários reais. Análises iniciais dos dados coletados mostraram que é possível detectar os sinais vitais dos passageiros apesar do ruído causado pelos movimentos do veículo. Assim, esta tese desenvolve o software e integra o hardware em um sistema veicular real, abrindo caminho para novas investigações sobre a relação entre os movimentos de um veículo e a detecção do radar.

Palavras-chave: radar Doppler de onda contínua, acelerômetro, detecção de passageiros, detecção de respiração, detecção de sinais vitais.

List of Figures

List of Tables

Acronyms and Abbreviations

AC	*Alternating Current*
ADC	*Analog-Digital Converter*
AI	*Analog Input*
CW	*Continuous-Wave*
DAQ	*Data Acquisition Device*
DAS	*Data Acquisition Software*
DC	*Direct Current*
DSP	*Digital Signal Processing*
GUI	*Graphical User Interface*
IC	*Integrated Circuit*
IEE	*International Electronics & Engineering*
LIN	*Local Interconnect Network*
MEMS	*Microelectromechanical Systems*
NI	*National Instruments*
PCB	*Printed Circuit Board*
RCS	*Radar Cross-Section*
RR	*Respiratory Rate*
UFSC	*Universidade Federal de Santa Catarina*

Contents

1 Introduction

This thesis reflects the results of the internship for completion of a degree[1] in Control and Automation Engineering. This project was developed at the headquarters of the company IEE S.A. in Luxembourg, with the degree to be obtained from the Federal University of Santa Catarina (UFSC), Brazil.

The subsequent sections of this chapter will introduce the company IEE, some relevant works previously developed, the motivations behind the project, as well as the scope and structure of this thesis.

1.1 Company

Founded in 1989, IEE International Electronics & Engineering S.A. is a Luxembourgish company with global presence and one of the world's leading suppliers of automotive sensing solutions. Since its foundation, IEE has equipped more than 300 million vehicles with its products [2]. In Figure 1, IEE's locations are well presented in a map.
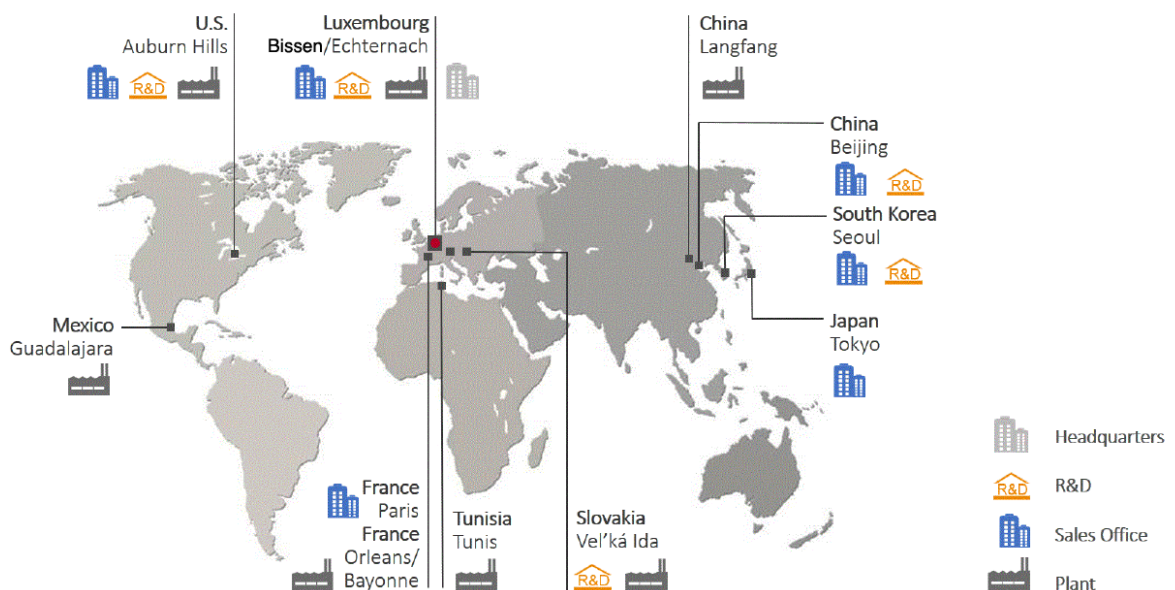
Figure 1 – Map of IEE's locations [2].

The project described in this thesis has been developed at IEE's headquarters, location responsible for the main research topics and product developments. At the beginning of this project, the headquarters office was located in the commune of Contern. However, since May 2019, it has been moved to a new building complex at the Automotive Campus,

---

[1]   300 ECTS degree in accordance with the Bologna Process [1].

in Bissen, Luxembourg. Pictures of the former and new global headquarters are shown in Figure 2 and Figure 3, respectively.

Figure 2 – Former headquarters office in Contern, Luxembourg [2].

Figure 3 – New global headquarters at the Luxembourg Automotive Campus [2].

With 1900 people across eight countries and more than 10% of the workforce dedicated to Research & Development (R&D) activities, IEE is one of the most innovative companies in its sector. IEE holds more than 200 patent families and sells solutions to a range of different markets: Automotive, Building Management & Security, and Medical, Health & Sports [2].

In the early nineties, IEE made its name as a pioneer in passenger presence detection. Over the last 25 years, the company has gone even further and now it is a global leader in automotive safety sensing systems for occupant detection and classification. Among its main products is the *Seat Belt Reminder*®, a foil-based system integrated in the seating area of vehicles, which detects the presence of passengers either through pressure on tactile sensors or through the measurement of the capacitive coupling to the car body [3]. The safety of vehicle occupants is an important issue and robust sensing solutions are essential.

This is not only the view of the automotive industry, it is also backed up by legislative requirements and Euro NCAP[2] incentives.

In the next section, it will be presented some of the previous works performed by IEE in the radar field. The next section will also create a link between the previous projects and the project developed in this thesis.

1.2   Previous developments and motivations

The first development of radar technology in history traces back to the beginning of the 20th century, in Germany. Christian Hülsmeyer, in 1904, was the first who demonstrated and patented the core of the radar principle, namely to detect distant objects by the reflection of electromagnetic waves [4, 5].

The word *radar* is originally an acronym of <u>ra</u>dio <u>d</u>etection <u>an</u>d <u>r</u>anging and, in 1943, the term was adopted internationally through an agreement [6]. Today, radar has been incorporated as a noun in the vocabulary of many languages and does not represent its initial meaning anymore. Some radar types, for example, do not include the ranging feature, but are still called a radar. In Chapter 2, a background of the radar theory will be presented, along with more details about the radar functionality and principles.

At IEE, the development of radar was firstly brought to question as a solution for child presence detection in a vehicle's interior. IEE's stakeholders looked for a system capable of detecting newborns possibly forgotten inside a car, even if they were asleep. Fatalities of children caused by hyperthermia in locked parked cars steadily increased between 1992 and 2005 and, in 2018, it has reached its historic maximum, with 52 deaths in United States alone [7, 8].

This phenomena is partially caused by the fact that parents leave their children on the rear seat of a car and often forget about them while shopping or running errands. Leaving small children in a locked car can become life-threatening after only 15 minutes, even if the weather is cloudy and the outside temperature does not go above 20°C.

With this concern in mind, IEE allocated in-house research and development to address the issue. In 2013, IEE made the first experiences with a radar tester kit of 6 GHz. Soon after, it was able to detect passengers and children using off-the-shelf components, MATLAB and National Instruments' devices. In that same year, the first prototype based on off-the-shelf components was presented to a customer and, in 2014, a 24 GHz radar device already entered its first serial development phase. The product was then named as *VitaSense*® [9].

The radar solution for detection of passengers has been chosen over optical, infrared, and ultrasonic technologies due to its advantages over these systems. The radar system

---

[2]   The European New Car Assessment Programme (Euro NCAP) is a European car safety performance assessment programme and notable vehicle safety rating system.

is not impacted by interior or ambient temperature, illumination, air flow and pressure. The radar waves are able to penetrate sunshades of child restraint systems (CRS), cloth, fabrics and even winter clothing. It has a robust occupant detection performance, detects a wide range of human characteristics, discriminates inanimate objects and is able to distinguish breathing motions from background noise.

This project makes use of the same *VitaSense*® 24 GHz radar device, which is placed inside a vehicle and used to detect the passengers' movements. The transmitter, which can be invisibly mounted behind the vehicle's headliner, emits radio signals that are reflected by occupants or objects. Because an occupant moves, the signal he or she reflects is different from that of an inanimate object. This allows the interior motion detector to discriminate between a person and an object. IEE's interior motion detector is able to detect even minor movements of vehicle occupants. In fact, it is so sensitive that it can even detect the breathing of sleeping babies [2].

However, during further radar application developments at IEE, questions regarding the interference of the car movements on the radar's detection capabilities were raised [3, 10, 11]. If the car is not parked anymore and it is now moving, could the radar still detect passengers with same effectiveness? Would the breathing signals be overlapped by the car movements in such a way that passengers could not be detected? If a car is moving, and if both its passengers and other inanimate objects can move in its interior, would this be a problem to discriminate between passengers and objects?

All the questions above are to be investigated with the development of this thesis. The main goal of this project was to prepare such a system that could measure and evaluate the radar signals in relation to the car movements, while simultaneously measuring the passengers movements as well.

In the next section, the scope and structure of this thesis are provided.

1.3   Scope of the internship

Partial focus of this project laid on the development of a complete software with user interface for acquisition and analysis of radar and accelerometer signals. The radar and accelerometer details and functionalities are described in Chapter 2. Another core part of the project consisted of joining the radar and accelerometer hardware into one single device for further testing. Other main goals and requirements included, but were not limited to: development of a test setup with data acquisition devices; design of test belts for acquisition of passenger's body acceleration; integration of the system into a real vehicle's interior; execution of driving tests and gathering of data for post-processing and analysis.

In Chapter 2, it is presented a technical background on the radar functionality and working principles of the accelerometer devices used in this project.

In Chapter 3 and Chapter 4, the development of the project is detailed and subdivided into two groups: hardware and software. In hardware, the components of the project are shown in details. In software, the program and its graphical user interface are explained, along with its main functions.

In Chapter 5, the vehicle setup and the system integration are depicted.

In Chapter 6, the performed tests are described. The collected data is presented and results of the tests are investigated.

In Chapter 7, it is presented an outlook of the project and IEE's perspectives on the topic of this thesis.

2 Technical Background

This chapter will provide a background on the knowledge and tools used in this project. The first section will introduce the theory and applications behind the continuous-wave radar based on the Doppler-shift. In Section 2.2, it will be presented an introduction about accelerometers and, more specifically, about the type of accelerometer used in this project.

2.1 Radar overview

A radar is a device or system used for the detection and location of objects. The operation of a radar consists of transmitting an electromagnetic wave and detecting the characteristics of the echo received. The transmitted wave is modulated by a particular type of waveform, a pulse-modulated sine wave for example, and is used for comparison with the echo signal. A fundamental structure of a radar consists of a transmitting antenna, emitting electromagnetic radiation generated by an oscillator of some sort, a receiving antenna, and an energy-detecting device, or receiver [12].

As seen in [13], the radar operation can be summarized as follows:

- The radar radiates electromagnetic energy from an antenna to propagate in space.

- Some of the radiated energy is intercepted by a reflecting object, usually called a *target*, located at a distance from the radar.

- The energy intercepted by the target is reflected, or scattered, in many directions.

- Some of the reradiated energy is returned to and received by the radar antenna, also known as the *echo* energy.

- After amplification of the echo signal by a receiver and with the aid of proper signal processing, a decision is made at the output of the receiver as to whether a target echo signal is present or not. At this stage, depending on the type of radar, other information of the target – like its speed and/or position in space – can be estimated as well.

Radar devices are seen in a wide range of applications. Radars can be used in short distances, as for precise detection of high-speed movements in sports; while also being applied in ultra-long ranges, reaching the nearest planets of our solar system [14]. Radar targets can be aircrafts, ships, missiles, people, birds, insects, precipitation, air turbulence, lands, sea, icebergs, undergrounds, meteors, planets, etc. A radar can be small enough to

hold in the palm of one hand or large enough to occupy the space of many football fields [13]. It all depends on the application and on the type of device used.

Nowadays, there is a high number of radar types that have been already developed. Each radar type can yield more or less information and parameters about the target observed. Some of the main types of radar are [13]: pulse radar, which radiates a repetitive series of almost-rectangular pulses; continuous-wave (CW) radar, which applies a continuous sine wave for detection of relative velocity of moving targets; frequency-modulated continuous-wave (FMCW) radar, which uses frequency modulation of the sine wave to allow additional measurement of the range to the target, among many other types that are not interesting to cite here. Since the radar used in this project is a continuous-wave (CW) radar, detailed descriptions of the other types of radars will be suppressed here in this thesis.

2.1.1   Continuous-wave radar

The transmitter of a continuous-wave radar generates a continuous, unmodulated, sinusoidal oscillation of frequency f_o, which is radiated by the transmitting antenna. A portion of the radiated energy is intercepted by the target and is scattered, some in the direction of the radar, where it is collected by the receiving antenna, and receiver. If the target is in motion with a velocity v_r relative to the radar, the received signal will be shifted in frequency from the transmitted frequency f_o by an amount of $\pm f_d$. The shift in frequency is known as the Doppler effect, or Doppler shift, and will be explained in details in Section 2.1.2.

Comparing to the other radar systems, advantages of continuous-wave (CW) radars are its apparent simplicity and the potential minimal spread in the transmitted spectrum. The latter reduces the radio interference problem and simplifies all microwave preselection and filtering [13]. Another advantage is that CW radars are not affected by stationary targets in the environment.

A CW radar continuously radiates with power P_T, whereas a reflective object leads to a receiving power P_R at the radar receiver. The received-echo-signal power is considerably smaller than the transmitter power; it might be as little as 10^{-18} that of the transmitted power [12] – sometimes even less, with the relationship P_R/P_T amounting up to 10^{-20} [15].

The equation which relates the received power with the transmitted power can be seen below, generally known as the radar equation [15]:

$$P_R = P_T \cdot \frac{G_T \cdot G_R \cdot \lambda^2}{(4\pi)^3 \cdot R^4} \cdot \sigma \; , \tag{2.1}$$

where P_R is the power received by the radar, P_T the radiated power by the radar transmitter, G_T the gain of the transmitting antenna, G_R the gain of the receiving antenna, λ

the radar wavelength, R the distance between the radar and its target, and σ the radar cross section – with further explanation about the antenna gain and radar cross section below.

Interesting to note is that radar devices employ directive antennas to channel, or direct, the radiated power P_T into some particular direction [12]. Therefore, the gain G of an antenna represents the increase in the radiated power in the direction of the target, when comparing with the power that would have been radiated from an isotropic antenna[1].

The radar cross section (RCS) is also an important topic in radar analysis and, different than the term may suggest, the RCS is not related to the radar device itself, but a characteristic of its target. The RCS has the unit of area (for example, square meters) and is a measure of the signal energy that the target reflects back into the direction of the radar. Military planes, for example, can be engineered in a way that its surface would have a really low reflection signal back to enemy radar defenses – thus having a low RCS. On the other hand, passenger aircrafts are built to reflect as much signal energy as possible to ground radar systems – thus having a high RCS. In short, the radar cross section is a characteristic of each specific target and its value can be impacted by the size, material and shape of the target.

Continuous-wave radars are applied for determination of the velocity, or movement, of their targets. The radial velocity of a target is obtained from the measurement of the Doppler frequency shift (explained in detials in the next section). That is to say, CW radars are not capable[2] of measuring the range, i.e. distance, to the target. Another possible drawback of continuous-wave radars is the difficulty in signal processing and analysis when there is a large number of targets in the field of view of the radar. In such situations, it might be impossible to acquire information about a specific target.

2.1.2 Doppler effect

In the fields of optics and acoustics, it is well known that if either the source of oscillation or the observer of the oscillation is in motion, an apparent shift in frequency will result. In the case of continuous-wave radars, the radial velocity of a target produces a phase-shift on the received signal. Such effect is known as the Doppler effect, or Doppler shift, and is the basis of the CW radar functionality. In other words, the Doppler effect is caused by a relative movement between the radar and reflecting objects, identical to acoustics when there is a velocity difference between the hearer and the sound

---

[1] An isotropic antenna is an antenna that, in theory, would radiate power with the same intensity and uniformly in all directions. The concept of an isotropic antenna is used as reference for measurements of the gain and directivity of real antennas. This means that, if a real antenna has a high gain, it radiates more power into the target direction, i.e. has a high directivity. If an antenna has a low gain, it means that it has a broad radiation area and consequently less power into the target direction, i.e. low directivity.

[2] Range measurement with CW radar can be achieved in very special cases, over the range of uniqueness of the signal, i.e. half the wavelength of the transmitted signal, as seen in [15].

source [15], e.g. when a police or ambulance passes by with its siren on. In Figure 4, it is shown an illustration of a radar detection. Below, the Doppler effect will be explained in details.
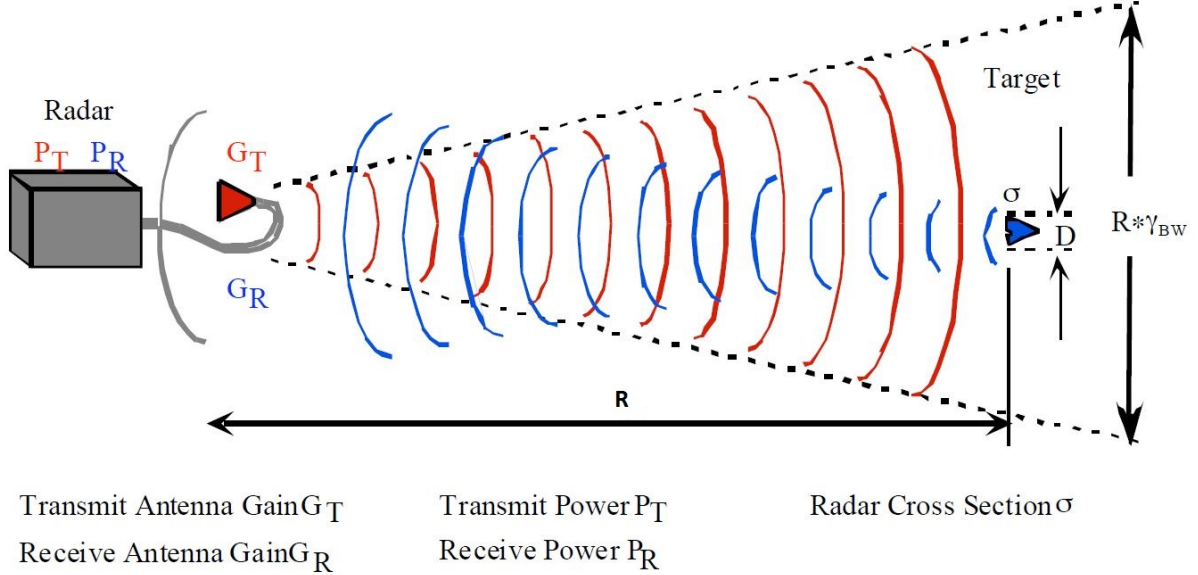
Figure 4 – Illustration of the radar principle [15].

As seen in [12], if R is the distance from the radar to target, the total number of wavelengths λ contained in the two-way path between the radar and the target is $2R/\lambda$. The distance R and the wavelength λ are assumed to be measured in the same units. Since one wavelength corresponds to an angular excursion of 2π radians, the total angular excursion ϕ made by the electromagnetic wave during its transit to and from the target is $4\pi R/\lambda$ radians. If the target is in motion, R and the phase ϕ are continually changing. A change in ϕ with respect to time is equal to a frequency. This is the Doppler angular frequency ω_d, given by:

$$\omega_d = 2\pi f_d = \frac{d\phi}{dt} = \frac{4\pi}{\lambda}\frac{dR}{dt} = \frac{4\pi v_r}{\lambda} \; , \tag{2.2}$$

where f_d = Doppler frequency shift and v_r = relative (radial) velocity of target with respect to radar.

And the Doppler frequency shift is:

$$f_d = \frac{2v_r}{\lambda} = \frac{2v_r f_o}{c} \; , \tag{2.3}$$

where f_o = transmitted frequency and c = velocity of propagation $\approx 3 \times 10^8 m/s$.

Hence, when the target is in motion with a relative velocity v_r, it causes the frequency shift $\pm f_d$ in relation to the transmitted frequency f_o. If the distance between target and radar is decreasing (approaching target), the Doppler frequency f_d is positive ($+$) and the received signal frequency is greater than the transmitted signal frequency. Alternatively,

if the distance between the target and radar is increasing (receding target), the Doppler frequency f_d is negative $(-)$ and the received signal frequency is lower than the transmitted signal frequency.

The received echo signal at a frequency $f_o \pm f_d$ enters the radar via the receiving antenna and is mixed with a portion of the transmitter signal f_o to produce a Doppler beat note of frequency f_d. In this process, the sign of f_d can be lost [12].

In Figure 5, it is shown a simplified CW radar schematic.
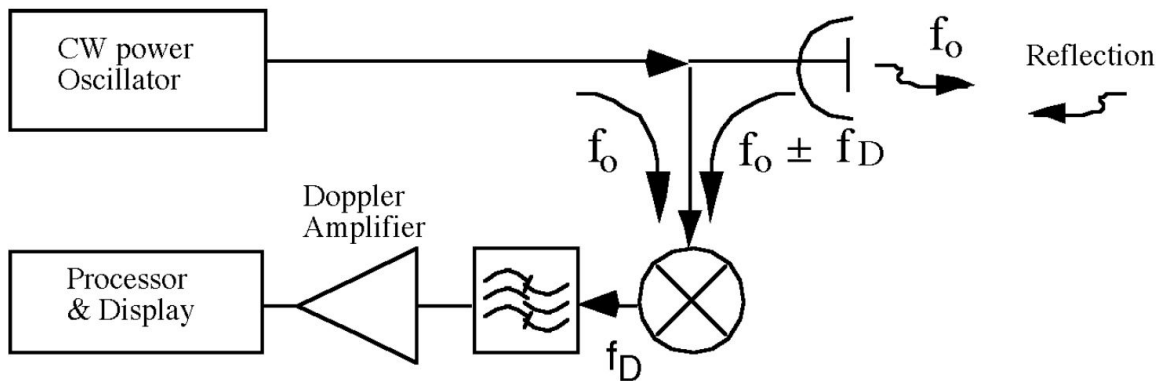
Figure 5 – Simplified schematic of the Doppler frequency detection [15].

The purpose of the Doppler amplifier, seen in the above figure, is to eliminate echoes from stationary targets and to amplify the Doppler echo signal to a level where it can operate an indicating device [12]. The power oscillator, also known as local oscillator (LO), is the part of the radar which is used to generate the transmitting signal at a certain defined frequency f_o.

When two mixers are applied, instead of only one, the sign of f_d and the information about the direction of movement of the target can be maintained. Such approach is known as quadrature modulation, and will be better explained in the next section.

2.1.3   Radar I and Q signals

For the sign of the Doppler frequency to be evaluated and therefore to acquire the direction of movement of the target, a process of quadrature modulation is applied. In quadrature modulation, two mixers are employed with a phase difference of 90° for the output signal of the oscillator. In Figure 6, a simplified schematic of a quadrature demodulator is shown.

A quadrature demodulator, or I/Q-Demodulator, determines the allocation of the receiving signal, which is indicated with reference in-phase (I) or quadrature (Q) – with quadrature meaning perpendicular [15], as shown in Figure 7.
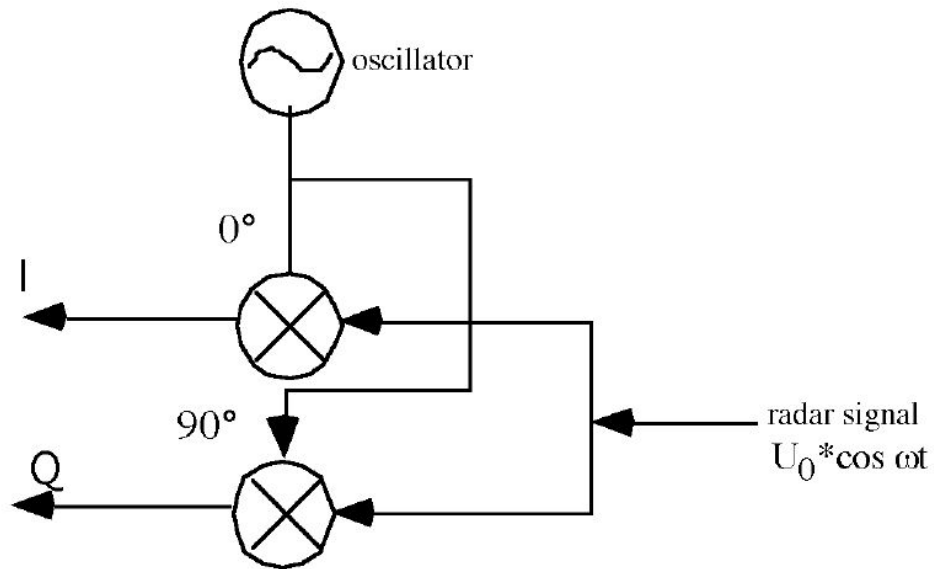
Figure 6 – Quadrature demodulator [15].
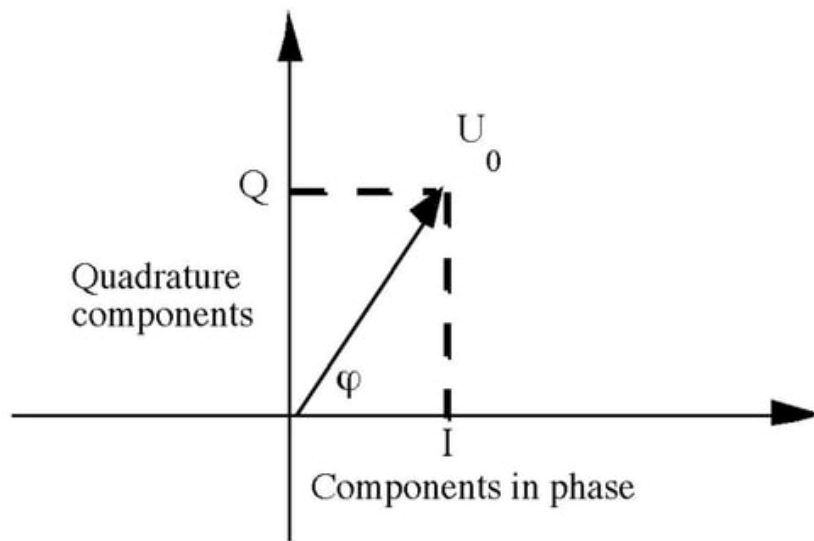
Figure 7 – Quadrature signal [15].

Where,

$$U_0 = \sqrt{I^2 + Q^2} \ , \qquad\qquad (2.4)$$

$$\varphi = arctan\frac{I}{Q} \ , \qquad\qquad (2.5)$$

$$f_d = \frac{d\varphi}{2\pi dt} \ . \qquad\qquad (2.6)$$

After processing the I and Q signals, the information about the direction of movement of the target can be retrieved. For a departing target, the Doppler frequency f_d will be

negative, while for an approaching target, f_d will be positive. In the complex domain, the I and Q radar signals describe a circle for a single moving target [16]:

$$y_I(f_o, t) = U_0 \cdot \cos\left(\frac{2 \cdot \pi \cdot f_o \cdot 2 \cdot R(t)}{c}\right) , \tag{2.7}$$

$$y_Q(f_o, t) = U_0 \cdot \sin\left(\frac{2 \cdot \pi \cdot f_o \cdot 2 \cdot R(t)}{c}\right) . \tag{2.8}$$

In short, the amplitude of the moving circle, or phasor magnitude, U_0, is equal to the amplitude of the receiving radar signal and is related to the radar cross-section (RCS) and proximity of the target to the radar.

The rotation of the vector represents the change in the Doppler frequency. If the vector rotates clockwise, φ decreases, meaning that the Doppler frequency is negative and that the target is approaching the radar. If the vector rotates counterclockwise, φ increases, meaning that the Doppler frequency is positive and that the target is receding.

The rate of change in the phase angle φ, i.e. the speed in which the vector rotates in the plane, is what gives the information about the speed of the target. The higher the speed or rate of change of the phase angle, the higher the speed of the target. The lower the rate of change of the phase angle, the lower the speed of the target.

In this thesis, the radar I and Q signals will be constantly mentioned. During the development of this project, all the information acquired from the radar was through processing and analysis of these signals. In Chapter 3, the radar device used in the project and the extraction of the I and Q signals will be explained with more details.

2.2 Accelerometer basics

In this section, it will be presented an introduction about accelerometers and, more specifically, about the type of device used in this project. Great part of the information introduced here has been extracted from accelerometer manufacturers [17–21], where more detailed information can be found about other accelerometer modules as well.

Accelerometers are devices that measure acceleration, which is the rate of change of the velocity of an object. They measure in meters per second squared (m/s^2) or in G-forces (g). A single G-force for us here on planet Earth is equivalent to 9.8 m/s^2, but this does vary slightly with elevation – and will be a different value on different planets due to variations in gravitational pull. Accelerometers are useful for sensing vibrations in systems or for orientation applications.

There are many different types of accelerometer devices available on the market. The accelerometer used in this project is an electromechanical device that senses either static or dynamic forces of acceleration. Static forces include gravity, while dynamic forces can include vibrations and movement. Also, accelerometers can measure acceleration on one, two, or three axes simultaneously (see Figure 8). Due to a decrease in cost of development, 3-axis units are becoming more and more common. In this project, 3-axis accelerometers are used.

Generally, electromechanical accelerometers contain capacitive plates internally. Some of these are fixed, while others are attached to minuscule springs that move internally as acceleration forces act upon the sensor. As these plates move in relation to each other, the capacitance between them changes. From these changes in capacitance, the acceleration can be determined. In Figure 9, an illustration shows, in a simplified way, the working principle of a two-axis accelerometer. For a three-axis accelerometer, one additional set of capacitors and springs should be added in the z-axis, omitted for better visualization of the system.

Regarding the acquisition of the signals, accelerometers usually communicate over an analog, digital, or pulse-width modulated connection interface. Accelerometers with an analog interface show accelerations through varying voltage levels, which is the case of the module used in this project. The voltage values generally fluctuate between ground and the supply voltage level. Analog types are also usually less expensive than digital accelerometers.

The specifications and detailed information about the accelerometer model used in this project will be shown later in Chapter 3.
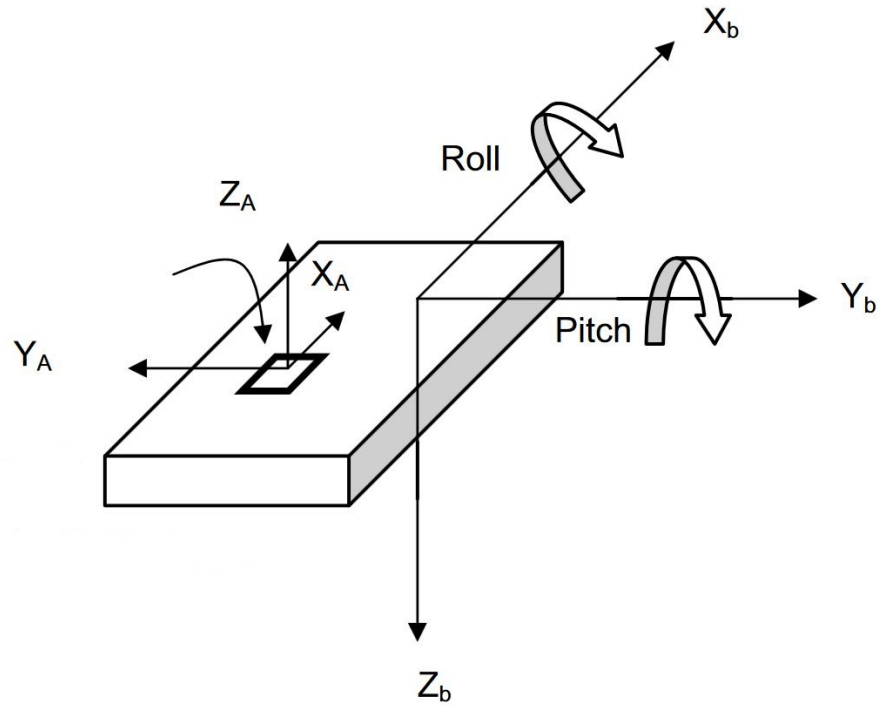
Figure 8 – Axes of measurement for a triple-axis accelerometer [20].
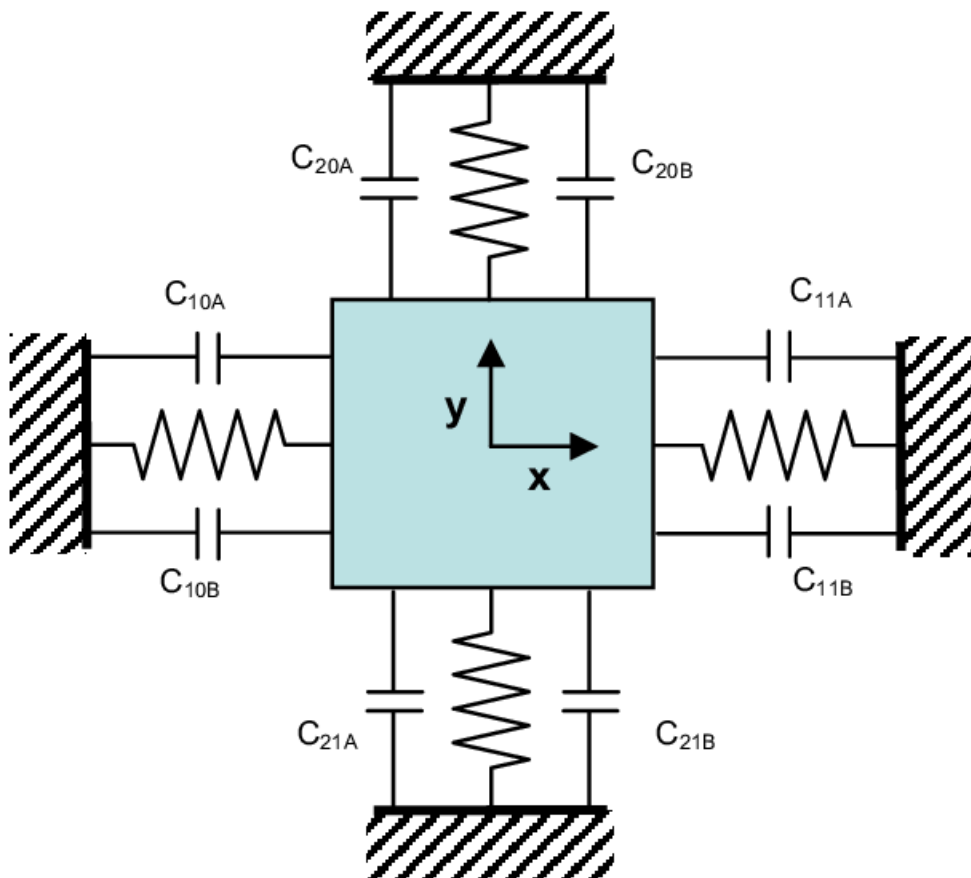
Figure 9 – Working principle of a dual-axis electromechanical accelerometer [22].

3 Project Development: Hardware

While still in the planning phase of the project, two main work divisions already could be clearly distinguished: the hardware and the software. Following this, the same distinction has been brought to this thesis to better describe the overall development. The hardware share in the project development comprises the preparation of the radar (Section 3.1) and accelerometer (Section 3.2) devices, the junction of the radar and an accelerometer into one single device (Section 3.3), elaboration of accelerometer belts (Section 3.4), preparation of the data acquisition device (Section 3.5) and all the necessary connectors and wiring (Section 3.6) to attach the project's components together.

Each following section will describe the purposes of each component of the project, as well as cover all the steps that have been realized in order to achieve the final setup required.

3.1 Radar device

The preparation of the radar first started with the understanding of the hardware functionality and its most relevant signals. Part of this understanding has been approached in Chapter 2, with an introduction to radar theory. In this chapter, the approach will be taken into the radar device itself, its specifications and the information that is relevant to this project.

The sensor used in this project is a classical continuous-wave Doppler radar system with optimized antenna characteristics in order to illuminate the whole rear bench area of a vehicle. The radar works in the 24 GHz ISM-band[1] and uses low-power radio technology to detect occupants based on their movement or breathing, even if they are sleeping [3]. The radar device acts as a radio-frequency motion detector based on the Doppler shift – a detailed description of the Doppler shift has been already presented in Chapter 2. Inside the car, the radar is placed behind the headliner, thus making it unnoticeable for the passengers. In Figure 10, it is shown pictures of the radar device and its radome[2]. In Figure 11, it is shown an illustration of the radar placement inside the vehicle.

The radar front end – or RF front end – can also be seen in Figure 10. The RF front end is where the antenna arrays for radio transmission and reception are located.

Before the application of a radar device for passenger detection, other technologies were investigated by IEE. As exposed in [3], passive 2D camera-based systems are able to classify human contours by looking top-down, but fail in situations where children are

---

[1] Frequency band designated for industrial, scientific and medical (ISM) applications [23].

[2] A radome, an acronym coined from radar dome, is a cover or structure placed over an antenna that protects the antenna from its physical environment and minimizes RF reflections [24].
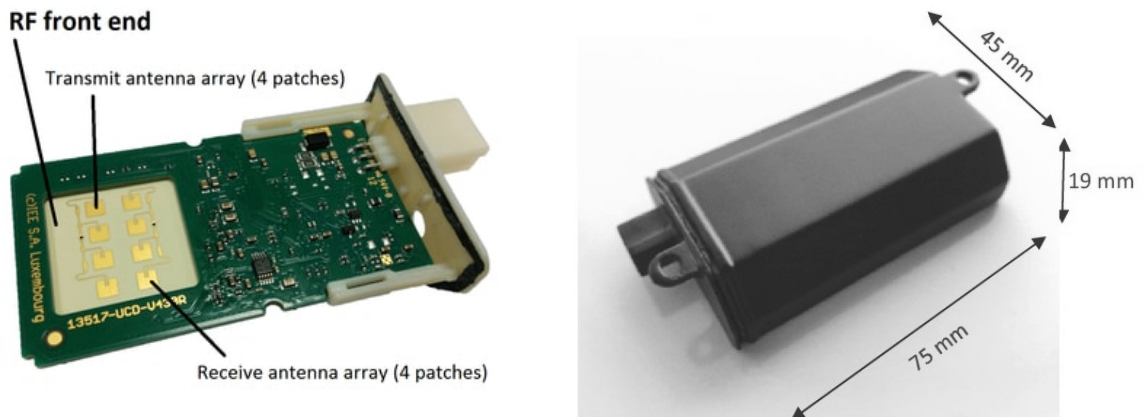
Figure 10 – Pictures of the radar device (left) and radome (right).

Figure 11 – Illustration of the radar device positioning in the vehicle's interior [2].

covered by cloth, e.g. child restraint systems (CRS) sunscreens, or when the environment is too dark. Due to the body heat, infrared cameras are able to detect passengers at night, but human bodies could not be detected when the car interior is already heated, e.g. in summer period. Piezoelectric foils are sensitive enough to detect even heart beats in noise-clean environments, but are very susceptible to vibrations. Breathing measurements with piezoelectric sensors integrated in the seating area are also very difficult to implement, as tests in the IEE R&D department have shown. Compared to other systems, the radar is robust against false detections and benefits from a vehicle-based integration, being connected to the vehicle's infrastructure and keeping the final user away of the responsibility of correct installation and/or activation of the radar.

As seen in Figure 11, the radar is placed under the roof of the vehicle and behind the headliner. In Figure 12, the field of view of the radar is illustrated. Its area of illumination, with a 3dB drop in power, comprises an angle of 76.5° in azimuth and 35.5° in elevation. The angles of illumination can be seen in the antenna diagram in Figure 13, where the red lobe represents the power transmitted (dB) in the vertical angular direction (elevation), and the blue lobe in the horizontal angular direction (azimuth).
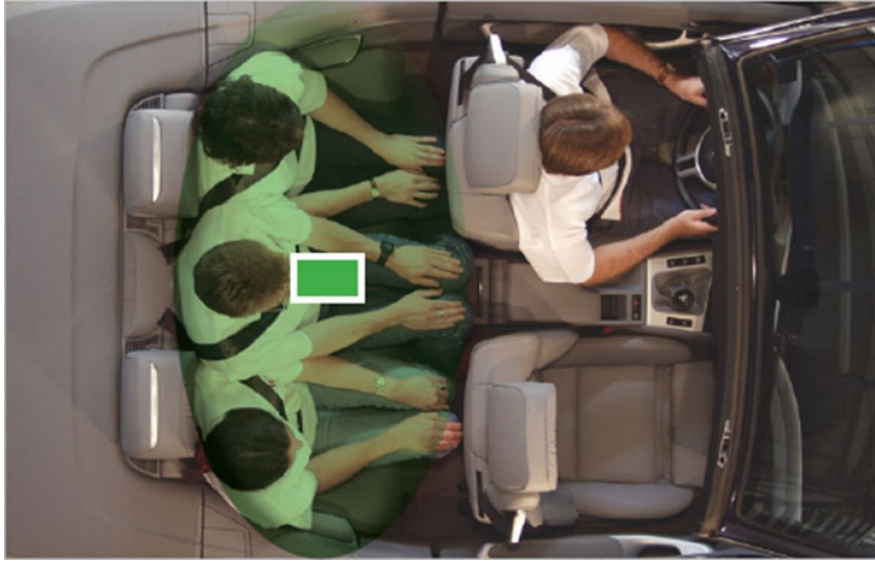
Figure 12 – Field of view of the radar covering the whole rear bench area [2].
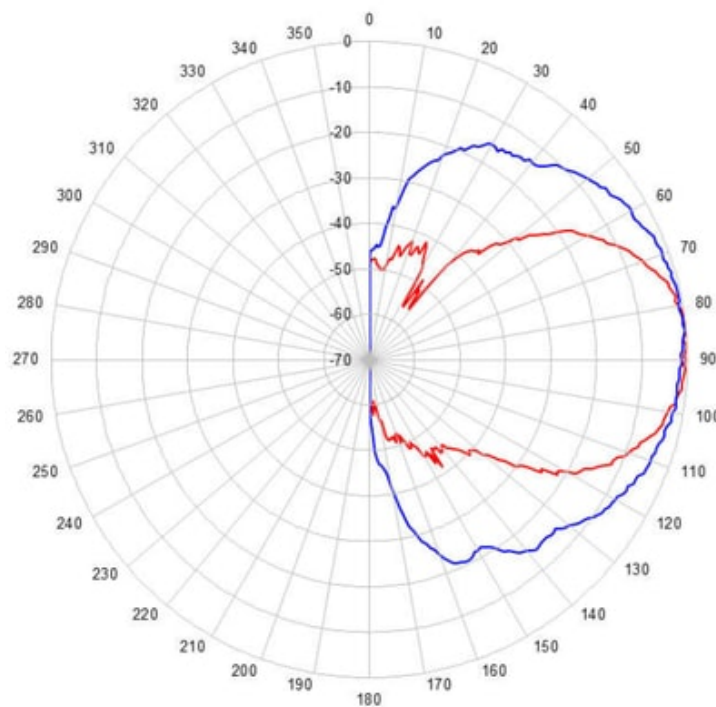
Figure 13 – Radar antenna diagram.

The radar device has been developed to connect to the vehicle's built-in network through the LIN bus. LIN (Local Interconnect Network) is a concept for low cost automotive networks, which complements the existing portfolio of automotive multiplex networks [25]. The LIN connector, besides connecting the radar device to the LIN interface, also provides power and ground connections to the radar. In this project, however, the radar does not benefit from the vehicle network and the communication through the LIN bus is therefore suppressed. The LIN connector, shown in Figure 14, is still attached to the device for powering purposes only.

Table 1 – Pin information for the LIN connector.

Pin	Signal
1	Voltage input (12V DC)
2	Ground
3	LIN bus (not used)
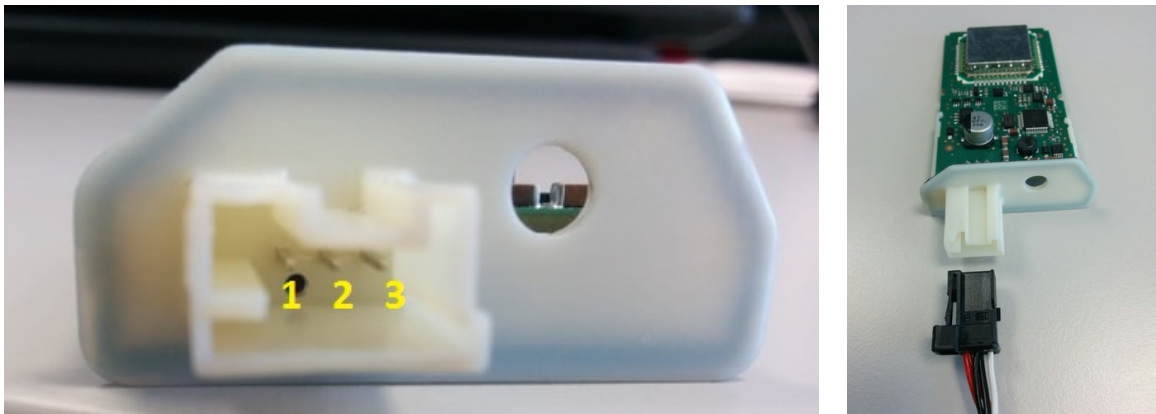
Figure 14 – LIN connector.

The built-in microcontroller in the radar device holds code to auto-initialize the radar operation. Accordingly, as soon as the radar device is powered up, it is already possible to extract its signals without any additional action required.

3.1.1 Identification and extraction of the radar signals

In order to acquire the signals from the radar, it was necessary to go through the radar circuit schematics (fragment shown in Figure 15). A detailed study of the radar circuitry has been performed to identify the placement of the radar components in its printed circuit board (PCB) and, subsequently, identify the extraction points of the desired signals. In Figure 16, it is shown the placement of the radar components in its PCB.

As seen in Chapter 2, the radar signals that carry information about the target movements (i.e. vehicle occupants) are the I and Q signals. For the extraction of these signals,
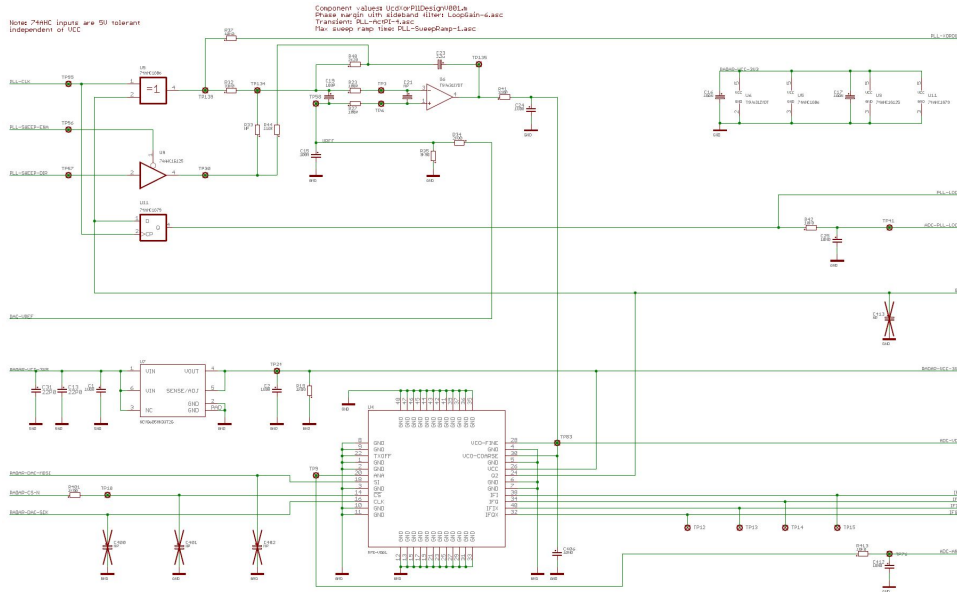
Figure 15 – Fragment of the radar circuit schematics.
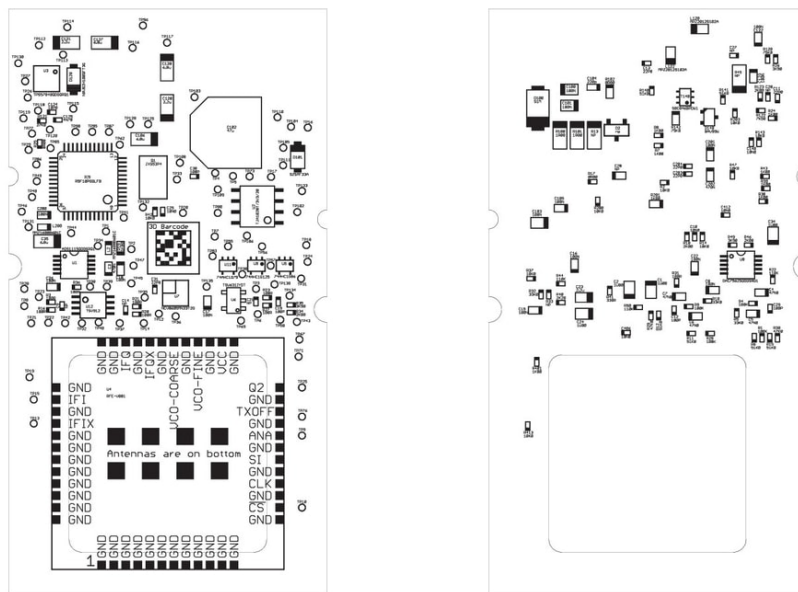
Figure 16 – Radar PCB schematic: top view (left) and bottom view (right) of the PCB.

wires had to be soldered on specific points directly on the radar PCB. Such points are also know as test points of the PCB.

Test points are locations on electronic circuits that are used to monitor the state of the circuitry or to inject test signals. Test points are primarily used during the manufacturing to verity that the newly assembled device is working properly or used after market for necessary repairs to the device. In the case of this project, test points of the PCB were used to extract the I and Q radar signals.

The test points of the radar circuitry are named and defined in a confidential schemat-

ics document. If given access to the document, it is possible to identify the test points
and desired signals. In Figure 17, a picture shows the colored wires soldered on the PCB,
and in Table 2, the identification of the extracted signals.

Table 2 – Signals extracted from radar device.

Wire color	Signal	PCB Ref.
White	I	TP44
Yellow	Q	TP45
Black	Ground	C26
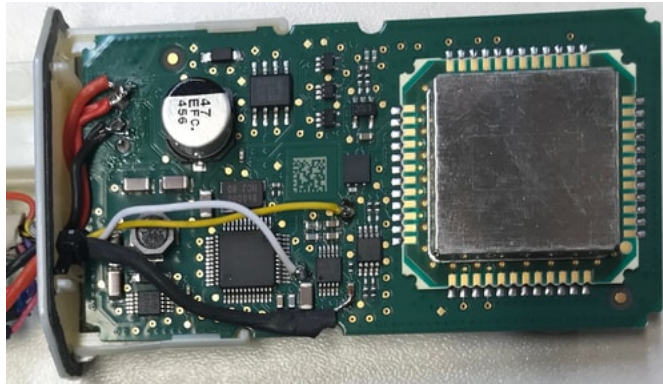
Figure 17 – Wires soldered directly on the PCB of the radar.

Later, in Section 3.5 and Section 3.6, it will be explained how the wires, soldered on
the radar, are connected to a data acquisition device for obtainment and processing of its
I and Q signals. In the next section, it is presented the accelerometer used in the project
and, in Section 3.3, it will be presented the combination of the radar and accelerometer
into one single device.

3.2   Accelerometer device

After preparation of the radar device and successful extraction of the desired signals,
it was necessary to join an accelerometer to it. In Chapter 2, an introduction to the
accelerometer functionality was provided. In this section, details of the accelerometer
model used will be presented. In Section 3.3, the radar and accelerometer integration is
shown.

The accelerometer device used in the project is the model ADXL330, a microelec-
tromechanical system (MEMS) manufactured by Analog Devices. The sensor is a polysil-
icon surface micromachined structure built on top of a silicon wafer. Polysilicon springs
suspend the structure over the surface of the wafer and provide a resistance against accel-
eration forces. Deflection of the structure is measured using a differential capacitor that
consists of independent fixed plates and plates attached to the moving mass. The fixed

plates are driven by 180° out-of-phase square waves. Acceleration deflects the moving mass and unbalances the differential capacitor resulting in a sensor output whose amplitude is proportional to acceleration. Phase-sensitive demodulation techniques are then used to determine the magnitude and direction of the acceleration.

The ADXL330 is a complete 3-axis acceleration measurement system on a single monolithic integrated circuit (IC). The ADXL330 has a measurement range of $\pm 3g$. It contains a polysilicon surface micromachined sensor and signal conditioning circuitry to implement an open-loop acceleration measurement architecture. The output signals are analog voltages that are proportional to acceleration. The accelerometer can measure the static acceleration of gravity in tilt sensing applications as well as dynamic acceleration resulting from motion, shock, or vibration [19]. In Figure 18, the circuit schematic of the ADXL330 is shown.
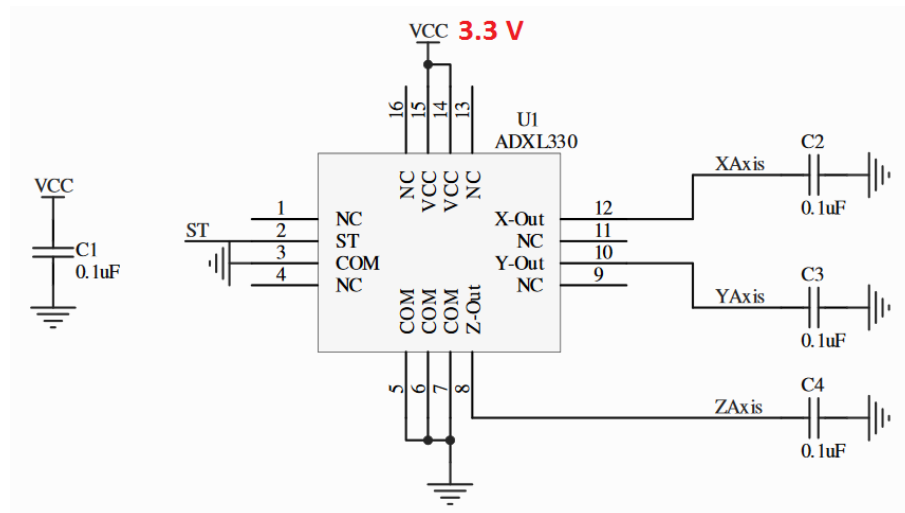
Figure 18 – Circuit schematic of accelerometer ADXL330 [19].

The accelerometer ADXL330, however, is not applied alone. It is integrated in a module with a voltage regulator, shown in Figure 19. The voltage regulator, model 78L33A, is powered by V_{in} (Figure 19) and provides output voltage (V_{cc}) regulated at $3.3V$ for the ADXL330 (Figure 18). The voltage regulator requires an input voltage in the range $6V <= V_{in} <= 30V$ to guarantee the $3.3V$ at V_{cc}. In this project, the LIN connector provides $12V$ supply for the module, thus keeping the input voltage in the required range. The voltage regulator can deliver up to $100mA$ output current for the ADXL330. Appropriately, the accelerometer device is a low-power system, with typical current consumption of only $320\mu A$. In Figure 19, top and bottom views of the accelerometer module are shown, with its pin information on its bottom surface.

Generally, the user selects the bandwidth of the accelerometer using $C2$, $C3$ and $C4$ capacitors at the X_{out}, Y_{out} and Z_{out} pins of the ADXL330 (Figure 18). However, capacitors of $0.1\mu F$ are already placed on the accelerometer module, providing a filtered bandwidth of 50 Hz. For other capacitor values, the respective filtered bandwidth can be
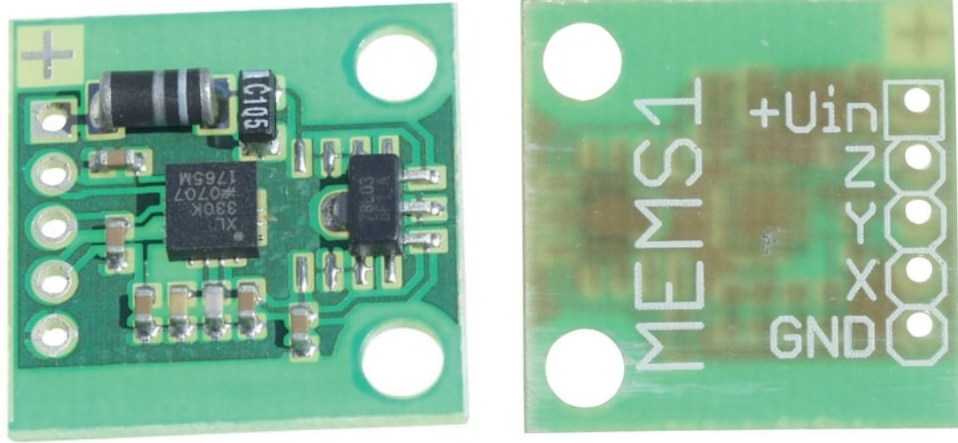
Figure 19 – Accelerometer module: top view (left) and bottom view (right) of the module.

seen in [19]. The capacitor $C1$, also of $0.1\mu F$, is placed close to the ADXL330 supply pins to adequately decouple the accelerometer from noise on the power supply.

The ADXL330 output is ratiometric, it means, the output sensitivity varies proportionally to the supply voltage. In the case of this project, the supply voltage is constant at 3.3V and the sensitivity of the accelerometer is equal to 330 mV/g, nominally 1/10 of V_{cc}. Tests have been performed at IEE and have proven the sensitivity value for the X, Y and Z axes. The *zero g* output is also ratiometric and equals to $V_{cc}/2$. As $V_{cc} = 3.3V$, the zero g output equals to $1.65V$. Below, some examples of outputs in the measurable acceleration range are provided:

$$
\begin{aligned}
\text{for acceleration} &= -3g, & -3g \times (0.330V/g) + 1.65V &= 0.660V \ , \\
\text{for acceleration} &= -2g, & -2g \times (0.330V/g) + 1.65V &= 0.990V \ , \\
\text{for acceleration} &= -1g, & -1g \times (0.330V/g) + 1.65V &= 1.320V \ , \\
\text{for acceleration} &= 0g, & 0g \times (0.330V/g) + 1.65V &= 1.650V \ , \\
\text{for acceleration} &= 1g, & 1g \times (0.330V/g) + 1.65V &= 1.980V \ , \\
\text{for acceleration} &= 2g, & 2g \times (0.330V/g) + 1.65V &= 2.310V \ , \\
\text{for acceleration} &= 3g, & 3g \times (0.330V/g) + 1.65V &= 2.640V \ .
\end{aligned}
$$

The general equation for the accelerometer output voltage V_{out} (in volts), with the acceleration α (in g) as input, is:

$$
V_{out} = \frac{V_{cc}}{10} \cdot \alpha + \frac{V_{cc}}{2} \ .
$$

Simplified, it is:

$$
V_{out} = \frac{V_{cc} \cdot (\alpha + 5)}{10} \ ,
$$

where V_{cc} = accelerometer voltage supply. With $V_{cc} = 3.3V$, the following is found:

$$
V_{out} = 0.33 \cdot \alpha + 1.65 \ . \tag{3.1}
$$

Inverting the Equation (3.1), it is found the equation for the acceleration α (in g) with the output voltage V_{out} (in volts) as input:

$$\alpha = \frac{V_{out} - 1.65}{0.33} \ . \tag{3.2}$$

With the Equation (3.2), it is possible to obtain the acceleration value in g for all three axes as soon as the accelerometer output voltage is acquired.

In Figure 20, the axes of acceleration sensitivity of the ADXL330 are shown. In Figure 21, the output response of the accelerometer is correlated to the orientation of the device to gravity.
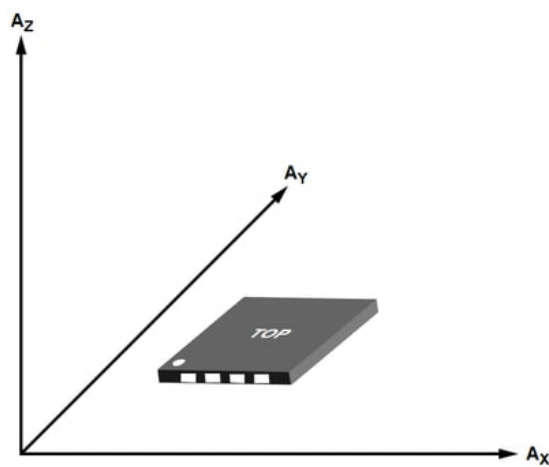
Figure 20 – Axes of sensitivity of the accelerometer [19].
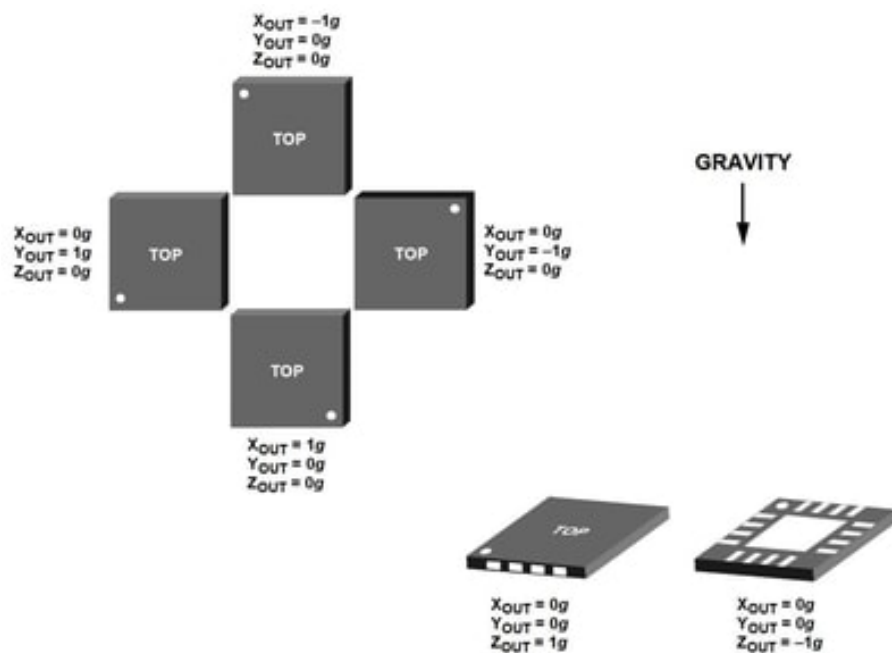
Figure 21 – Output response vs. accelerometer orientation in relation to gravity [19].

3.3 Fusion of radar and accelerometer

As shown in Section 3.1, the radar is attached to the vehicle's structure, placed under the roof and behind the headliner. Consequently, any movements (e.g. acceleration) performed by the vehicle are equally performed by its structure and the radar device. Therefore, for the accelerometer to measure the motion of the radar and of the vehicle, the accelerometer and the radar had to be merged into one single device. With this in mind, the housing of the radar was used as the base for the accelerometer mounting. Holes were drilled on the surface of the housing and the accelerometer module was screwed onto it, as shown in Figure 22. In Section 3.6, the connector between the radar and accelerometer will be detailed.
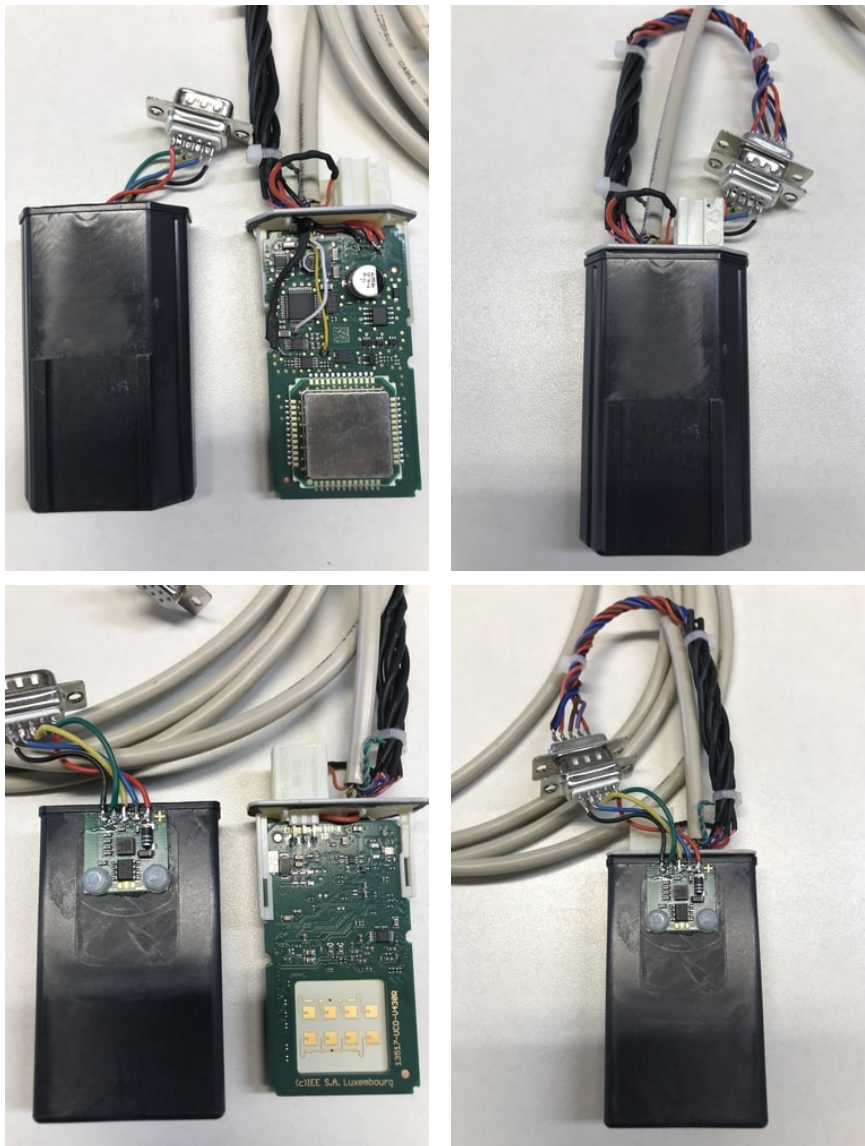
Figure 22 – Top view of the housing and radar (top left); top view of the radar enclosed into the housing (top right); bottom view of the radar and accelerometer attached to the housing (bottom left); bottom view of the radar enclosed into the housing with the accelerometer (bottom right).

3.4 Accelerometer belts

After attachment of an accelerometer module onto the radar, three additional accelerometer modules were used to craft three accelerometer belts. The purpose of the first accelerometer belt is to measure the acceleration – and movement – of the passenger's head. The belt has a fabric strap to allow comfortable placement around the head on the level of the forehead, with a strap adjuster to properly fix it. The second accelerometer belt is similar to the first one, but wider, for placement around the passenger's chest/abdomen. The third accelerometer belt is for measurement of the seat displacement. Therefore, it is placed directly under the passenger's body and on top of the seating area. The passenger is able to sit on top of the device without causing any damages to it.

All three accelerometer belts include a sufficiently long cable for later integration inside a vehicle. In Figure 23, pictures of the accelerometer belts are presented.

(a) Belt for the passenger's head.

(b) Belt for the passenger's chest.

(c) Belt placed on the vehicle's seat.

Figure 23 – Three accelerometer devices were placed on belts to measure the acceleration of the passenger's body (a)(b) and of the vehicle (c).

3.5 Data acquisition device

To acquire the analog signals from the radar and accelerometer devices, a data acquisition device (DAQ) is used. The DAQ used in this thesis is fabricated by National Instruments, model NI-9220. It has 16 analog input (AI) voltage channels and provides differential voltage measurement through a positive and a negative pin for each of the channels. Its maximum voltage measurement range is $\pm 10V$, with a resolution of 16 bits per sample acquired. In Figure 24, it is shown an illustration of the data acquisition device with its pinout information.
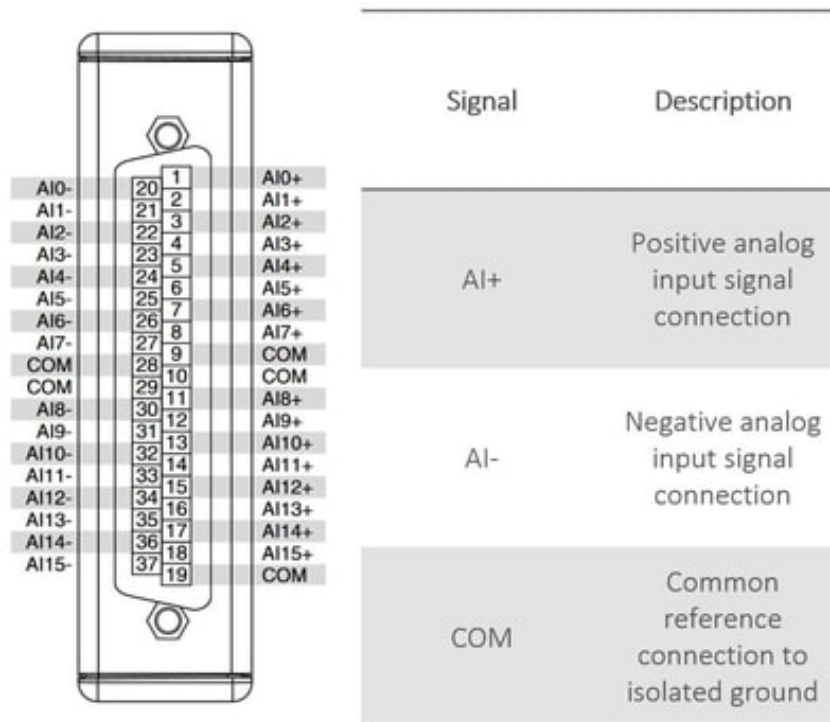
Figure 24 – NI-9220 pinout and signal descriptions [26].

The maximum rate or sampling frequency (F_s) of the DAQ is equal to 100,000 samples per second per channel. Input signals acquired by each channel are stored in an internal buffer of the DAQ and sampled by an analog-digital converter (ADC) as requested. As each AI channel provides an independent signal path and ADC, it is possible to sample all channels simultaneously [27].

As the resolution of each sample is of 16 bits, it is possible to find the maximum size of the output data:

$$resolution = 16 \; bits/sample \; ,$$

$$number \; of \; channels = 16 \; channels \; ,$$

$$max. \; sampling \; frequency = 100,000 \; samples/second/channel \; .$$

Then,

$$max.\ data\ size = 16\ bits/sample \times 16\ channels \times 100{,}000\ samples/s/channel\ ,$$

$$max.\ data\ size = 25{,}600{,}000\ bits/s\ .$$

As 8 bits = 1 Byte, it is found:

$$max.\ data\ size = 3{,}200{,}000\ \text{Bytes/s} = 3.2\ \text{MB/s}\ ,$$

which corresponds to the value of 3.2 MB/s informed in the DAQ datasheet [27].

In this project, however, only 14 channels of the 16 available are used: 2 channels for the I and Q signals of the radar; 3 channels for the accelerometer device (one channel for each axis) attached to the radar; 3 channels for the accelerometer belt attached to the passenger's head; 3 channels for the belt attached to the passenger's body; and 3 channels for the accelerometer module placed on the vehicle's seat.

Additionally, the maximum value for the sampling frequency F_s is not needed. As seen in Section 3.2, the accelerometer module has a built-in low-pass filter at 50 Hz. The radar device components also provide low-pass filtering for higher frequencies which are not interesting for the analyses. Therefore, for this project, a sampling frequency of 100 Hz was already sufficient for an alias-free signal sampling. This was also interesting to maintain the record files of the tests in a reasonable size. For example, for a road test of 30 minutes at a sampling rate of 100 Hz, a record file is typically 25 MB in size.

For this project, the DAQ NI-9220 is placed into a chassis from National Instruments, model cDAQ-9174. The cDAQ-9174 is a Compact DAQ USB chassis designed for small, portable sensor measurement systems. The chassis provides the simplicity of a USB for fast and easy connection of the DAQ with a PC-based setup. The chassis has four available slots, but only the first slot – with the NI-9220 – is used. In Figure 25, both the chassis and the data acquisition device are shown.

Figure 25 – Data acquisition device NI-9220 and chassis NI cDAQ-9174.

3.6 Connectors

To allow proper integration of the devices in this project, specific connectors were needed. For the fusion of the radar and the accelerometer, presented in Section 3.3, it was applied a D-sub connector type DE-9. D-sub connectors are common electrical connectors with a characteristic D-shaped frame. Among its main advantages, the family of D-connectors ensures correct orientation of the coupling. In Figure 26, a picture of the DE-9 connector is shown.

Figure 26 – D-sub connector type DE-9.

D-sub DE-9 connectors have, in total, 9 pins arranged in two rows. In this project, 5 of the 9 pins were used for the fusion of the radar and the accelerometer. One of the pins was used to power the accelerometer with the same input voltage of the radar device, i.e. the 12V from the LIN bus. Another pin was used to couple the radar device and the accelerometer to the same ground reference. And the other three remaining pins were used to carry the X, Y and Z accelerometer outputs over the same long wiring cable that connects the radar to the DAQ device. The advantage of joining the radar signals (I and Q signals) and the accelerometer signals (X, Y, Z outputs) into the same wiring cable was to simplify the connection with the data acquisition device; after all, there is only one DAQ being employed and it should receive the signals of all the devices used in this project.

D-sub DE-9 connectors were also used for the coupling of the three accelerometer belts. The accelerometer belts were presented in Section 3.4 and, in Figure 23, it is possible to note the DE-9 connectors at the end of the cables. The logic behind the connection of the belts is similar to the logic of the connection between the radar and

accelerometer described above. However, instead of connecting the DE-9 of the belts to the radar device, the accelerometer belts are connected directly to the data acquisition device, through another type of D-sub connector that will be described below.

For the data acquisition device, as it can be seen by the shape of the DAQ in Figure 24 and Figure 25, a D-sub connector type DC-37 is needed. A picture of the D-sub connector and its pin information are shown in Figure 27 and Figure 28, respectively.

Figure 27 – D-sub connector type DC-37.
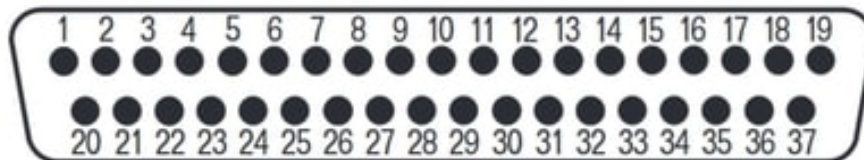
Figure 28 – Pin numbering of the DC-37.

With the DC-37, it is possible to connect the wires from the radar and accelerometer devices to the data acquisition device. Each pin of the DC-37 connects directly into one of the pins of the DAQ NI-9220. Ultimately, all the signals of the radar and accelerometer modules are connected to the DC-37, and the DC-37 is the only connection made directly to the data acquisition device. This construction makes it possible to easily plug and unplug the radar system to the DAQ device.

In Figure 29, it is possible to observe the radar connected to its accelerometer module through a DE-9 connector. In the same figure, the long wiring cable with a DC-37 connector in its extremity is shown in details. In Figure 30, it is shown the connection of the DC-37 connector to the DAQ NI-9220. The three DE-9 connectors that are shown loose in the figures are the connectors for the three accelerometer belts.
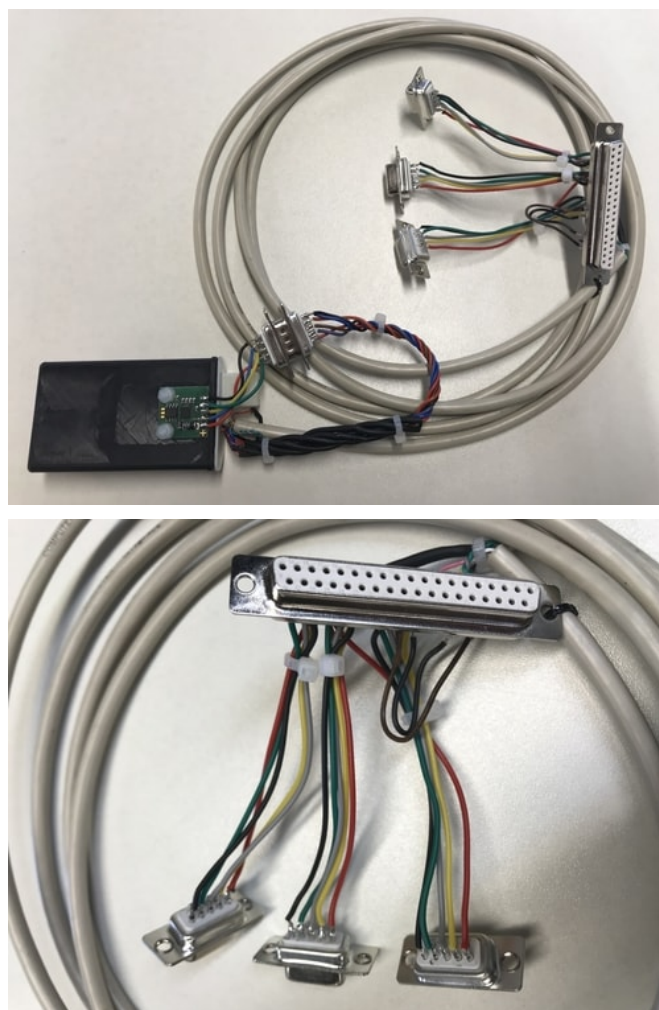
Figure 29 – Picture of the radar and wiring to the D-sub connectors (top); picture of the D-sub DC-37pin connector for the radar and three additional D-sub DE-9pin connectors for each of the accelerometer belts (bottom).
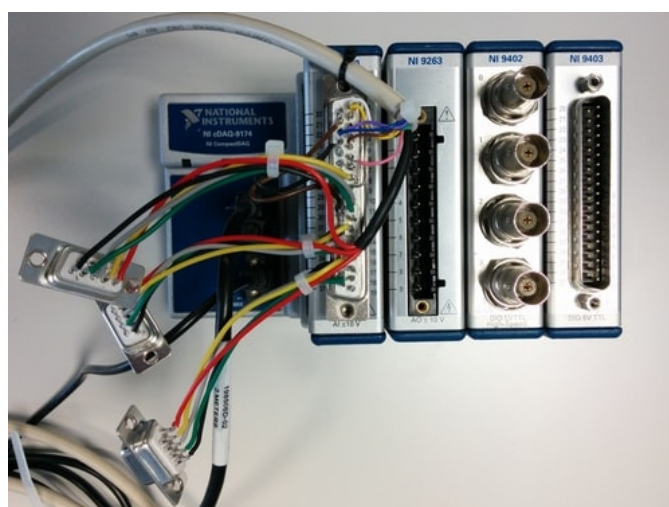
Figure 30 – Data acquisition device and D-sub connectors for analog input of radar and accelerometer signals.

Each pin number of the DC-37 connector corresponds to the same pin number on the NI-9220 DAQ device. For example,

Pin 1 *of the* DC-37 *connects to Pin* 1 *of the* DAQ ,

Pin 2 *of the* DC-37 *connects to Pin* 2 *of the* DAQ ,

$$\vdots$$

Pin 37 *of the* DC-37 *connects to Pin* 37 *of the* DAQ .

Therefore, in Table 3 it is shown the pin numeration of both the DC-37 connector and the NI-9220 device in correspondence with the pin name and the signal connected to each pin.

Table 3 – Pin information of the DAQ and the signals acquired.

Pin #	Pin Name	Signal Acquired	Pin #	Pin Name	Signal Acquired
1	AI0+	Radar I signal	20	AI0-	LIN Ground
2	AI1+	Radar Q signal	21	AI1-	LIN Ground
3	AI2+	Not used	22	AI2-	Not used
4	AI3+	Acc. Radar X-axis	23	AI3-	LIN Ground
5	AI4+	Acc. Radar Y-axis	24	AI4-	LIN Ground
6	AI5+	Not used	25	AI5-	Not used
7	AI6+	Acc. Radar Z-axis	26	AI6-	LIN Ground
8	AI7+	Acc. Head X-axis	27	AI7-	LIN Ground
9	COM	LIN Ground	28	COM	LIN Ground
10	COM	Not used	29	COM	Not used
11	AI8+	Acc. Head Y-axis	30	AI8-	LIN Ground
12	AI9+	Acc. Head Z-axis	31	AI9-	LIN Ground
13	AI10+	Acc. Chest X-axis	32	AI10-	LIN Ground
14	AI11+	Acc. Chest Y-axis	33	AI11-	LIN Ground
15	AI12+	Acc. Chest Z-axis	34	AI12-	LIN Ground
16	AI13+	Acc. Seat X-axis	35	AI13-	LIN Ground
17	AI14+	Acc. Seat Y-axis	36	AI14-	LIN Ground
18	AI15+	Acc. Seat Z-axis	37	AI15-	LIN Ground
19	COM	Not used			

For acquisition and analysis of the signals described above, a complete software with graphical user interface was developed in this project. In Chapter 4, the software will be presented.

4 Project Development: Software

The goal of the software is to acquire and process the radar and accelerometer signals. For that to be possible, an interface between the computer – i.e. MATLAB – and the data acquisition device (DAQ) had to be programmed. As explained in Chapter 3, the data acquisition device used in this project is from National Instruments (NI), model NI-9220. Therefore, it was required to use the drivers provided by NI to successfully communicate with the DAQ.

The necessary driver, NI-DAQmx, is provided on National Instruments' website [28] for download. NI-DAQmx provides support for customers using NI data acquisition and signal conditioning devices. It includes a manual [29] and a library [30] of C-coded functions which were used in the development of this project.

The NI-DAQmx driver was necessary not just to develop the program, but it is also required for the software to run smoothly, enabling communication with the DAQ. Another requirement is MATLAB, version 2018b [31], with its Digital Signal Processing (DSP) System Toolbox installed.

4.1 Introduction to DAS: Data Acquisition Software

Data Acquisition Software (DAS), as its name suggests, is a program to acquire and process analog signals through a data acquisition device. In this project, it is used for acquisition of radar and accelerometer signals, but its development enables its application in any system that requires acquisition of analog (e.g. voltage) signals. DAS has been developed in the MATLAB environment, making use of C-coded functions from the NI-DAQmx library and MATLAB App Designer for the graphical user interface (GUI) development.

The main functions of the program were divided into three distinct groups, in relation to their objectives in the application. The groups are represented by the *Configuration* functions, the *Data Acquisition and Recording* functions and the functions for *Visualization and Analysis* of the data.

The structure of folders and files of the software can be seen in Appendix A. To start the software, the file *main.mlapp* must be executed. In the following sections, the functionality of the software will be depicted, along with a guide to the GUI.

4.2 Graphical user interface

After execution of the *main.mlapp* file, the software starts running. The GUI is loaded and a series of messages are updated and shown to the user. There are four initial steps in which DAS loads configuration files and resets the data acquisition device.

In the first step, a *Loading App Files* message is displayed to the user while the software loads the program code and all the necessary configuration files. The software configuration will be better described in Section 4.2.1. In step two, a *Searching for DAQ Device* message is displayed while a suitable data acquisition device is searched for. At this stage, the USB cable of the DAQ chassis has to be already plugged into one of the USB ports of the PC. If DAS finds a suitable device, it goes to step three. In step three, the data acquisition device is reset and a *Resetting DAQ Device* message is displayed. In step four, DAS configures the input/output channels of the data acquisition device. In this project, only analog input channels are configured. After successful completion of all four stages, the software enters in its *Idle* mode, waiting for the user to start using the program. In Figure 31, all fours initial steps plus the idle state are shown.
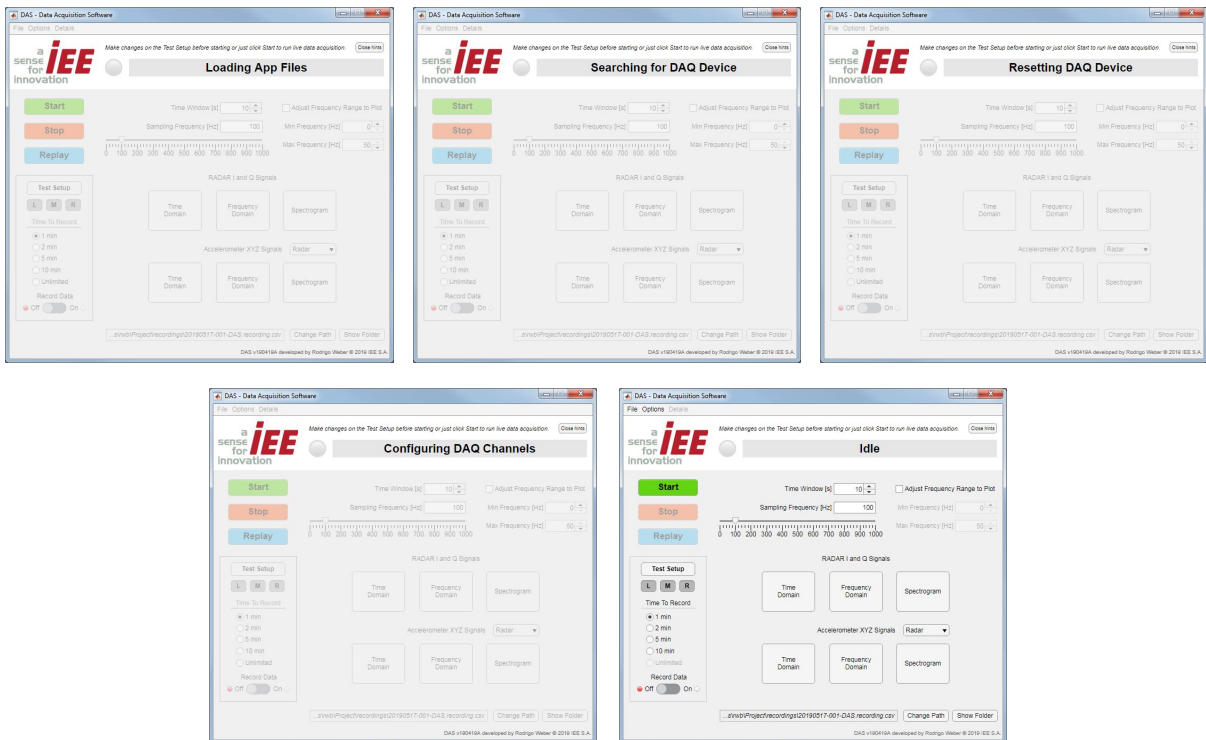
Figure 31 – Initial states of the GUI.

In step two, when DAS looks for a suitable data acquisition device, it is possible that none is found. This can happen in many cases, for example, if the user has not connected the data acquisition device to the computer, if the device is turned off, or if the NI-DAQmx library and/or driver are not properly installed. In these cases, an error message will be displayed to the user and a *Restart* button is shown in the GUI. If the

data acquisition device is simply turned off, the user can turn the device on and click on the *Restart* button. DAS will then restart itself and re-run its initial configuration steps without any other user interaction needed. In Figure 32, a picture of the error message is shown.
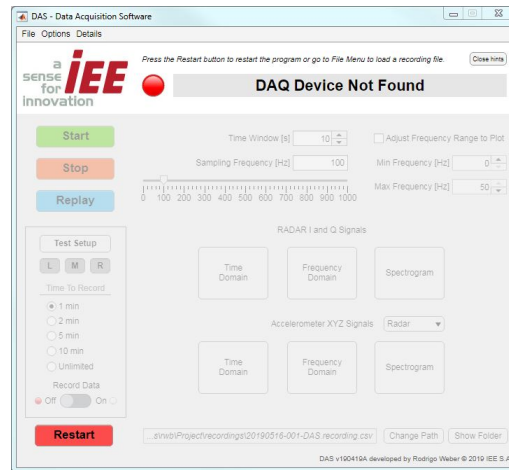
Figure 32 – Error message shown after no DAQ device has been found.

After successful completion of the initial DAS loading steps, the program reaches its *Idle* state.

4.2.1   Configurations

In its *Idle* state, the software enables access to its top menu bar. The top menu bar has two main submenus: the *File* menu and the *Options* menu. In the *File* menu, the user has access to recording and replay settings: the recording can be set to on/off, the recording file location can be changed, or a recording file can be loaded for the replay functionality. In Figure 33, a picture of the software showing its *File* menu and sub-list is presented.
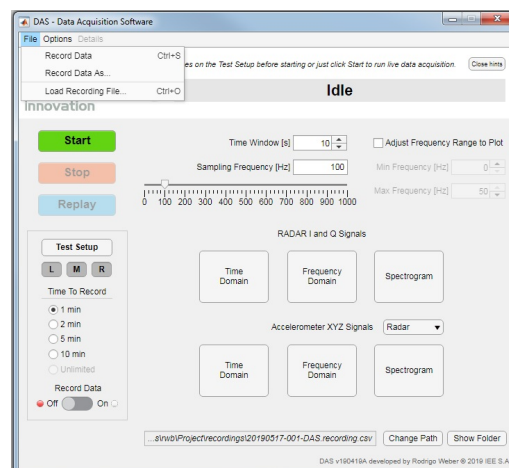
Figure 33 – File menu.

In the *Options* menu, the user has access to the software's *Startup Preferences* and the *Test Setup* options. The *Options* menu is shown in Figure 34.
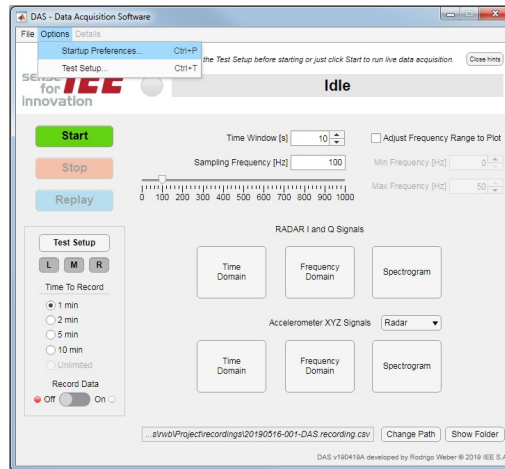
Figure 34 – Options menu.

Selecting the *Startup Preferences* option, the user has access to the software configurations. A new window will open, allowing the user to customize the preferences as wanted. The options for customization, shown in Figure 35, are the following:
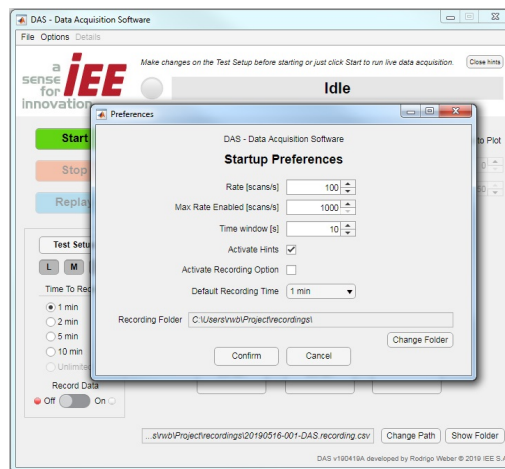
Figure 35 – Startup preferences: DAS loads them during its initialization.

- Rate – sampling frequency for the DAQ, in samples per second per channel;

- Max Rate Enabled – maximum rate value enabled/allowed for the DAQ, in scans per second per channel;

- Time Window – time window value, in seconds, for use in the analysis with FFT windowing;

- Activate Hints – enables/disables hint messages in the GUI;

- Activate Recording Option – enables/disables the option to record acquisition data into a file;

- Default Recording Time – adjusts the default time to record;

- Recording Folder – the folder path in which the recording files should be saved.

Also in the *Options* menu, the user can select and change the *Test Setup*. If selected, a new window will open, as shown in Figure 36. The *Test Setup* window allows the user to change the parameters for a data acquisition test. A data acquisition test can, for example, include information about which car the test is being performed in, and the number of occupants inside the vehicle. All the information is later saved in the header of the recording file, if the recording option is selected.
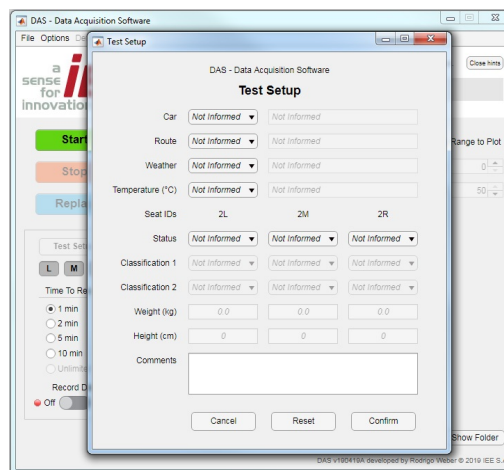
Figure 36 – Test setup: parameters and information of the data acquisition test.

The complete list of *Test Setup* parameters can be seen below:

- Car – test car in which the data acquisition test is going to be performed in;

- Route – predefined route in which the test is going to run on;

- Weather – weather at the time of the test;

- Temperature – ambient temperature at the time of the test;

- Seat Status – status of the vehicle seats (occupied/empty);

- Classifications – classifications for the seat occupancy (e.g. person, CRS, object);

- Weight – weight of the occupant or object;

- Height – height of the occupant or object;

- Comments – miscellaneous information to be saved in the recording file.

In Figure 37, a selection of parameters for the *Test Setup* is shown. Depending on the selection of the status of the vehicle seats, the GUI is updated with the seats information: green color indicator for occupied seats and grey color indicator for non-occupied (empty) seats. The updates on the GUI indicators are shown in Figure 38.
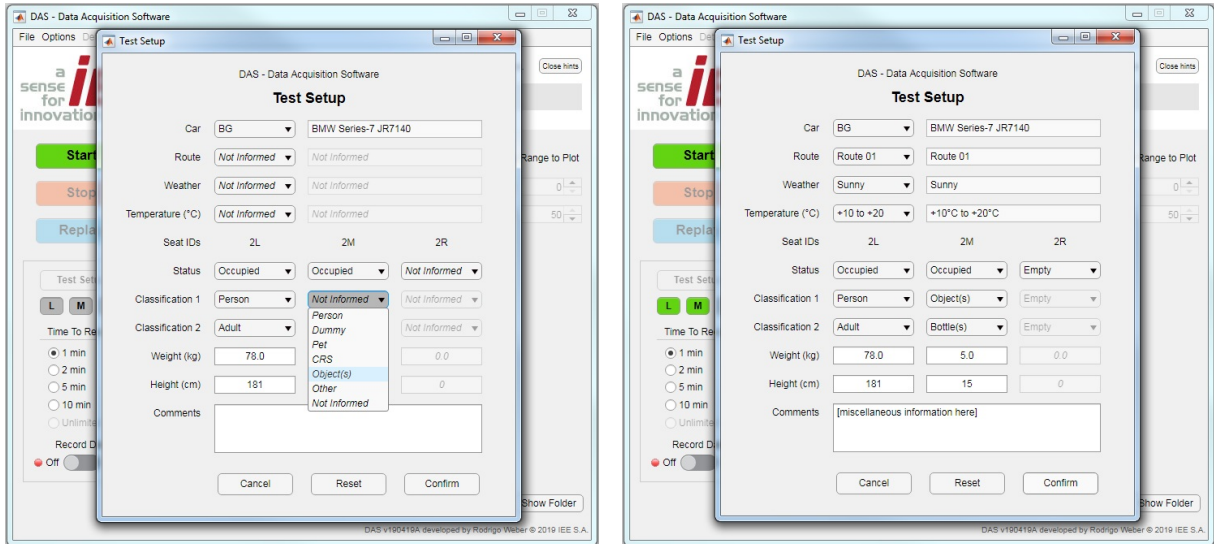
Figure 37 – Selection of parameters for the Test Setup.
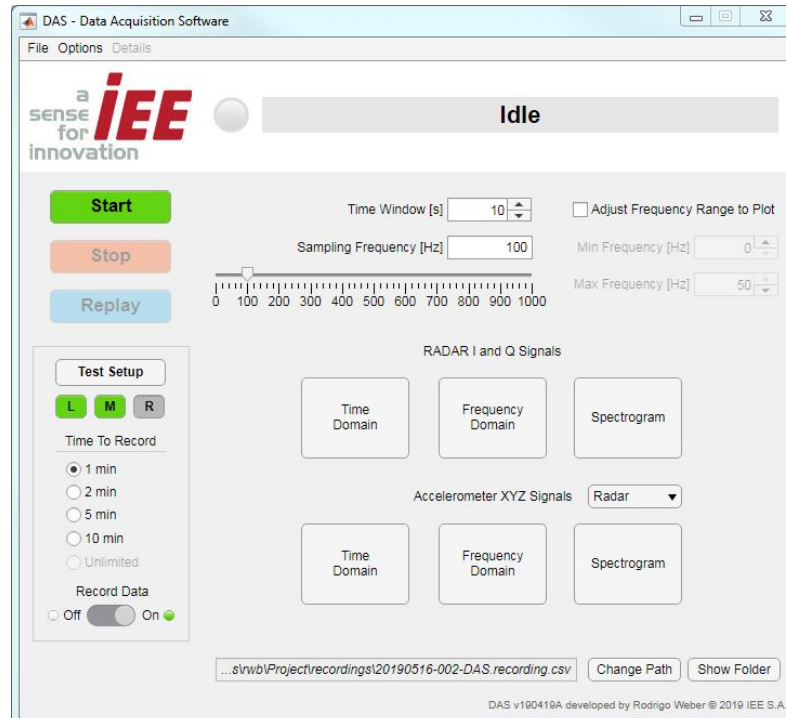
Figure 38 – GUI indicators are updated after confirmation of test setup parameters.

After confirming the alterations on the *Test Setup* parameters, DAS saves the information internally and later transcribes them to the header of the recording file. In the next section, it will be explained how to run live data acquisition and recording.

Note: additional channel configurations can be made directly into the code of the *main.mlapp* file. For this project, the hard-coded channel configurations should never be changed, since the data acquisition device used is always the same, and a defined number of analog input channels had to be used. However, if the software is to be used for a different project or system, such channel configurations can be changed. A fragment of code from *main.mlapp*, in which the configuration can be seen, is displayed below:

```
1    properties (Access = private)
2
3        (code supressed ...)
4
5                    % Data Acquisition Settings
6        vmins = -10;  % the minimum voltage that you expect to measure
7        vmaxs = +10;  % the maximum voltage that you expect to measure
8
9        channelPorts = {'Mod1/ai0','Mod1/ai1','Mod1/ai3','Mod1/ai4','Mod1/
    ai6','Mod1/ai7','Mod1/ai8','Mod1/ai9','Mod1/ai10','Mod1/ai11','Mod1/ai12
    ','Mod1/ai13','Mod1/ai14','Mod1/ai15'};
10
11       channelNames = {'I','Q','RadarX','RadarY','RadarZ','HeadX','HeadY
    ','HeadZ','ChestX','ChestY','ChestZ','SeatX','SeatY','SeatZ'};
12
13       (code supressed ...)
14
15   end
```

4.2.2 DAS modes: live, recording, and replaying

In this section, it will be presented how to run the software's data acquisition in its live and recording modes, as well as its replay feature.

In a live data acquisition, the software acquires radar and accelerometer signals, processes the data, but does not save it. The data can also be visualized and analyzed during live acquisition mode. A more detailed view of the data visualization and analysis tools will be presented in Section 4.2.3.

For the user to start a live acquisition, the software must be in its *Idle* state. After pressing the *Start* button, the data acquisition is immediately started. In Figure 39, the transition from *Idle* to *Live Acquisition* mode is shown. After entering the live acquisition mode, the user can no longer access and change the *Test Setup* parameters, e.g. route, passengers information, etc. Depending on the DAS configuration, the user also cannot change some of the recording settings, e.g. time to record and/or sampling frequency. The purpose of this behavior is to force the settings to be specified before the test and to avoid unintentional changes to important parameters while running tests.
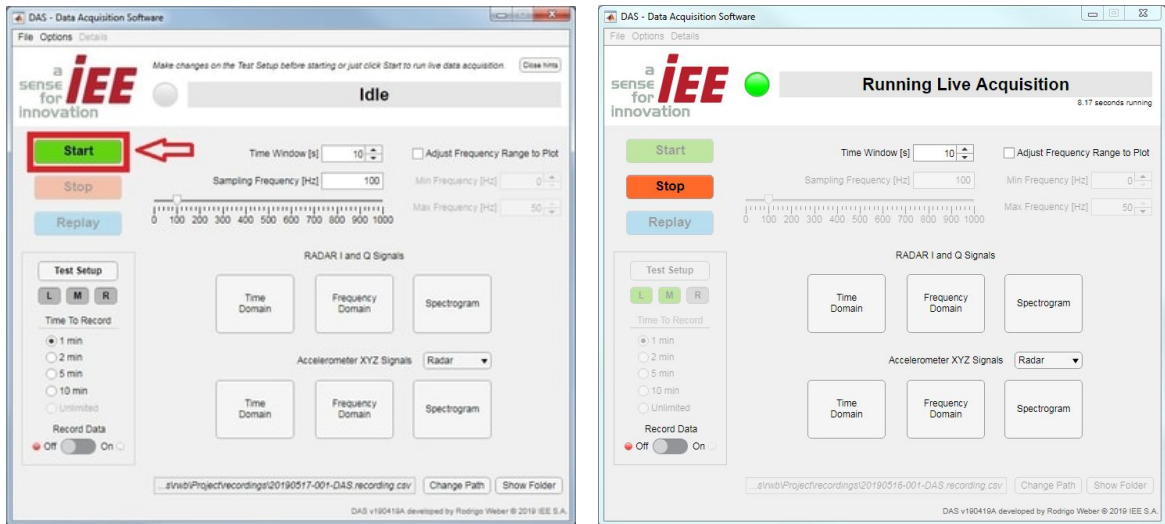
Figure 39 – Starting live acquisition.

During live acquisition mode, the user can stop the data acquisition at any moment. After pressing the *Stop* button, the data acquisition is immediately stopped. In Figure 40, the transition from a *Live Acquisition* to *Stopped* state is shown. Once the live acquisition is stopped, the user can again change the *Test Setup* parameters and recording settings in the same way that in the *Idle* state.
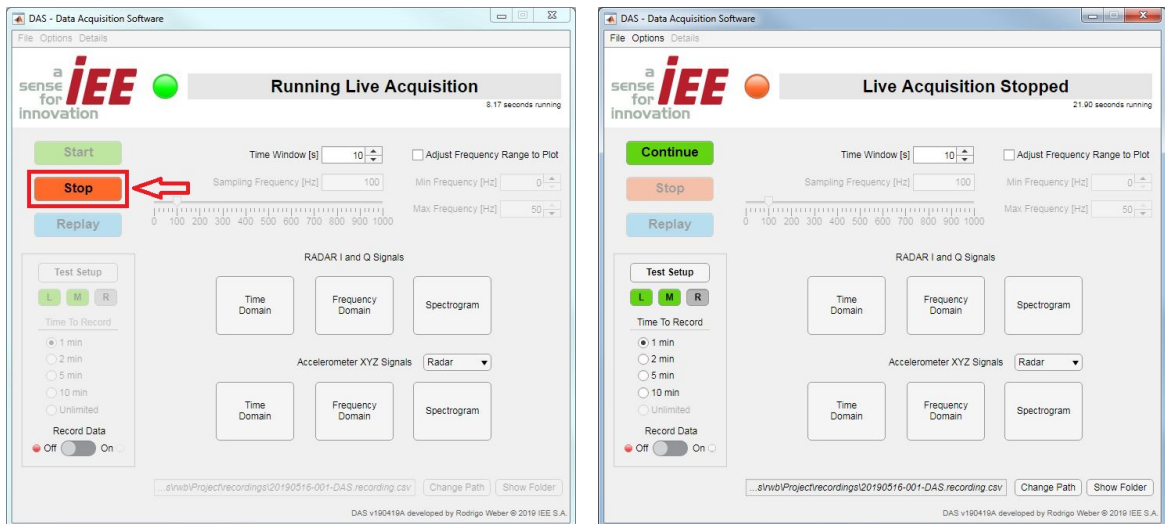
Figure 40 – Stopping live acquisition.

While in live acquisition mode, it is also important to note that the user can, at any moment, enable the recording of the acquired data into a file. In fact, there are two ways to enable the recording of the acquired data: one way is to enable it while in *Live Acquisition* mode, another way is to enable it while DAS is in its *Idle* state. For this, it is only needed to push the *Record Data* switch, on the lower left corner of the DAS screen.

If the *Record Data* switch is activated during *Live Acquisition*, the software immediately enters in its *Acquiring and Recording* mode. If the switch is activated while in *Idle*

state, the user still has to press the *Start* button to initiate the acquisition and recording. In Figure 41, the transition from live acquisition to recording state is shown.
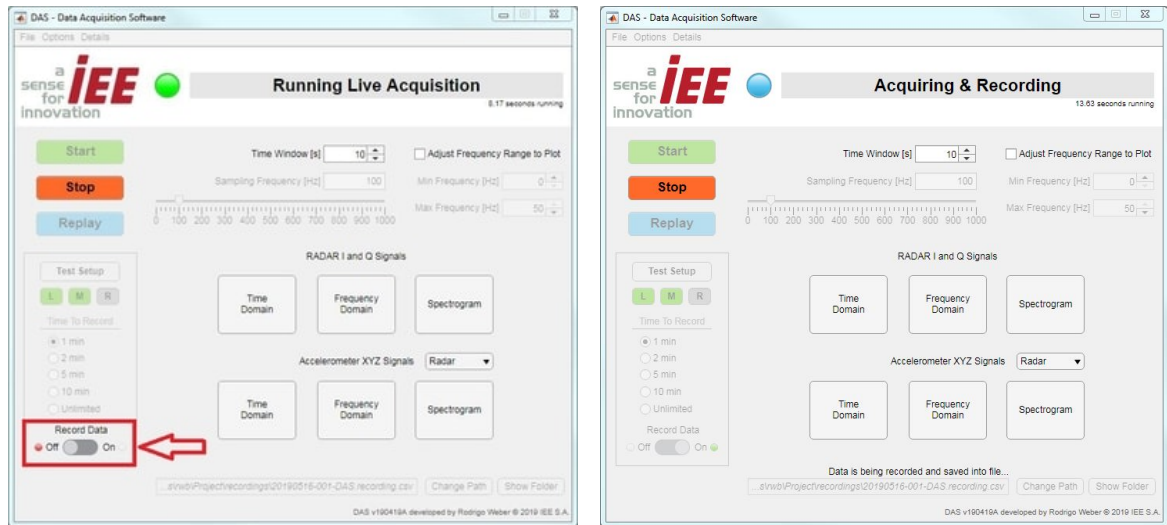
Figure 41 – Transition to recording mode.

With recording mode activated, DAS creates a CSV[1] file in the folder path previously selected by the user. In the header of the recording file, DAS saves all the *Test Setup* parameters and recording settings. As the recording file is saved in CSV format, it is possible to open it in Excel, as shown in Figure 42.

Figure 42 – Recording file opened in Excel.

---

[1] CSV, which stands for comma-separated values, is a open file format used to store structured data, e.g. as in a table. Many spreadsheet programs are able to open and edit such files, including Microsoft Excel, Apple Numbers, Google Sheets, etc.

In Section 4.2.1, Figure 37, it was shown an example of *Test Setup* parameters selected by the user. In addition to these selected parameters, DAS also saves supplementary information into the recording file header. The header includes the version of DAS that was used to create the recording file, the exact initial time (HH:MM:SS) and the date (DD/MM/YYYY) of the recording.

In the recording file, the acquired data is saved under the header while the program is running. Each data line is saved as soon as the data is acquired, increasing the file size as long as more data samples are received from the data acquisition device. There are 17 columns per data line, and each data line contains one sample of each signal acquired by the DAQ. The list below describes each of the columns of the acquired data in the recording file:

- Sample – number of the sample acquired by the DAQ;

- Time – time stamp of the sample, in seconds (s), calculated since the beginning of the recording;

- Rate – selected sampling rate, or sampling frequency, of the data acquisition device (in samples per second per channel);

- I and Q – raw I and Q signals acquired from the radar device (in volts);

- RadarX, RadarY and RadarZ – acceleration signals acquired from the accelerometer module attached to the radar device (in volts);

- HeadX, HeadY and HeadZ – acceleration signals from the accelerometer belt attached to the passenger's head (in volts);

- ChestX, ChestY and ChestZ – acceleration signals from the accelerometer belt attached to the passenger's chest (in volts);

- SeatX, SeatY and SeatZ – acceleration signals from the accelerometer belt attached to the vehicle's seat (in volts).

During recording, data is acquired from the sensors and is continuously saved into the recording file. If the user presses the *Stop* button while in recording mode, DAS immediately stops the acquisition and properly closes the recording file. All the data acquired until then is safe and can be accessed by opening the respective file.

Otherwise, if the user does not press the button to stop the recording, DAS automatically stops it once the selected time to record is reached. There are 5 options available for the recording time: 1 minute, 2 minutes, 5 minutes, 10 minutes, or unlimited. If the unlimited option is chosen, the user will have to manually stop the recording at some point. In Figure 43, it is shown the transition from recording to stopped state, after reaching the selected recording time of 1 minute.
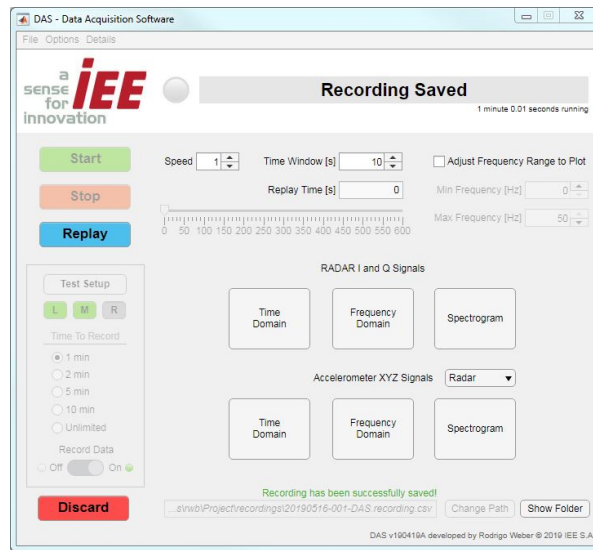
Figure 43 – Recording is finished when the selected recording time is reached.

When the recording mode is finalized, DAS enters in *Recording Saved* state and enables the replay of the newly created recording file. To replay the recorded data, it is necessary to press the *Replay* button. In Figure 44, it is shown the transition from *Recording Saved* to *Replaying* state after the press of the *Replay* button.
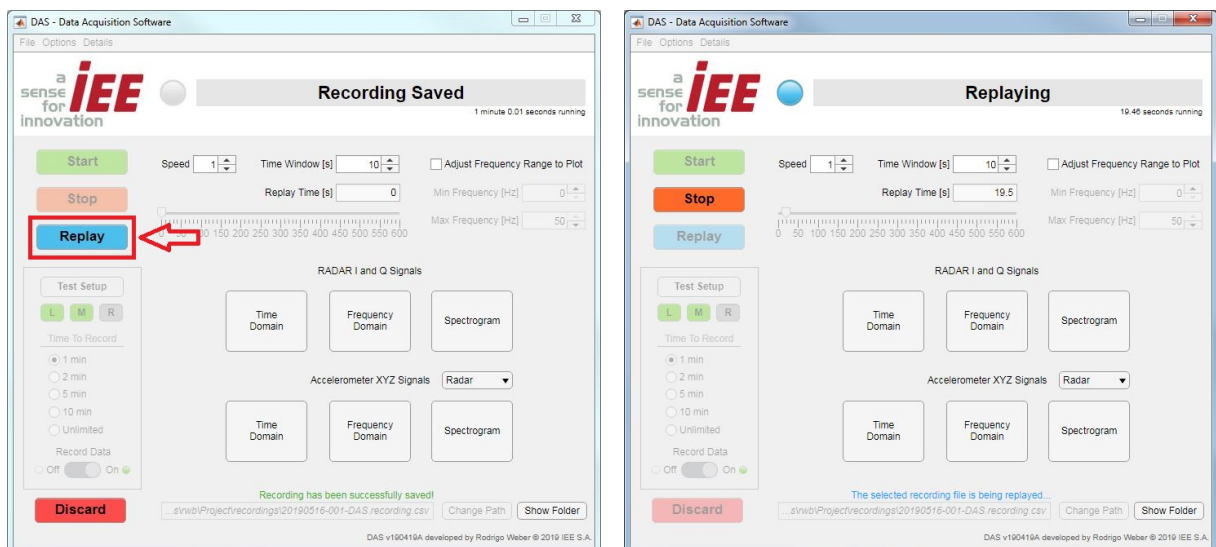
Figure 44 – Starting replay mode.

Replay can be activated as soon as a recording is finished. The user also has the option of loading any DAS recording file from the *File* menu in the top menu bar.

While in replay mode, the user has the option of stopping the replay at any moment. If stopped or if the recording file has reached its end, the recording can be discarded. In Figure 45, the options to stop and to discard the recording are displayed.

Pressing the *Discard* button only makes the software available for further usage, i.e. DAS enters its *Idle* state. The recording file is not deleted from the disk and it can be

reloaded to the software for replaying again, if needed. In Figure 46, the *Discard* button is pressed and the transition to *Idle* state is shown.
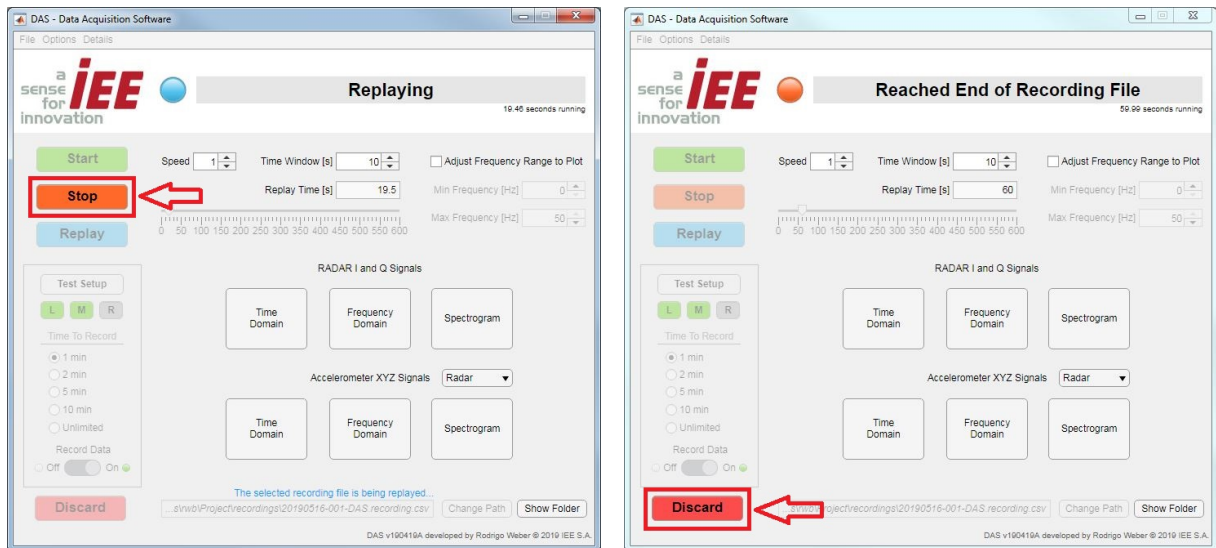
Figure 45 – Options to stop or to discard replay.
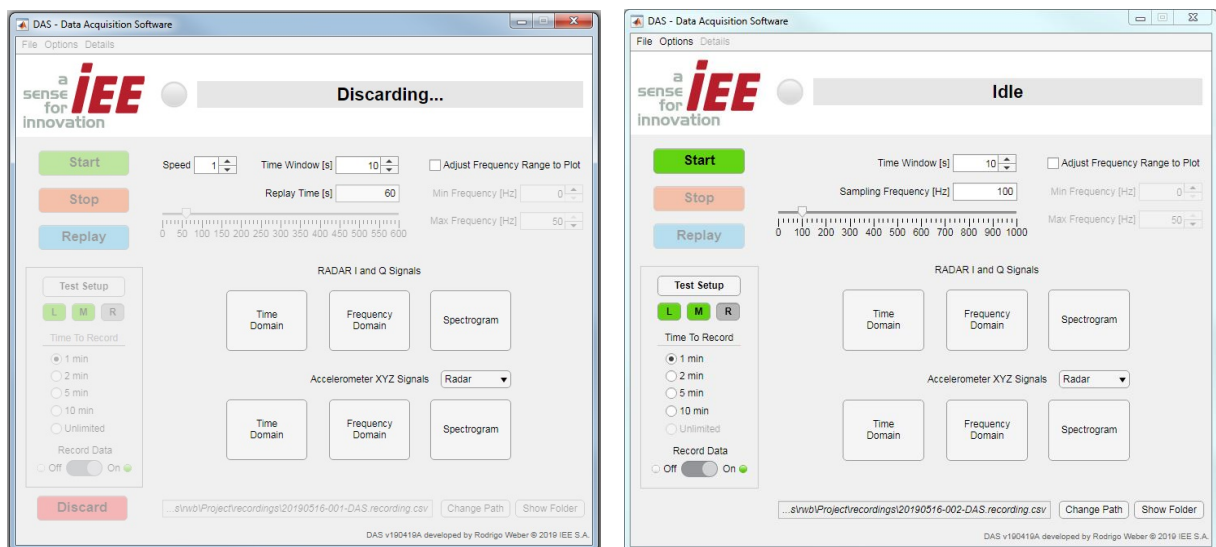
Figure 46 – Discarding a recording file and returning to idle state.

In the next section, the software tools developed for data visualization and analysis will be introduced.

4.2.3   Data visualization and analysis

One of the main goals of the software was to acquire and record analog voltage signals received through the data acquisition device. Another main goal was to develop tools to enable the software to visualize and analyze the data acquired.

Such tools were separated in two distinct panels in the DAS screen, as seen in Figure 47.
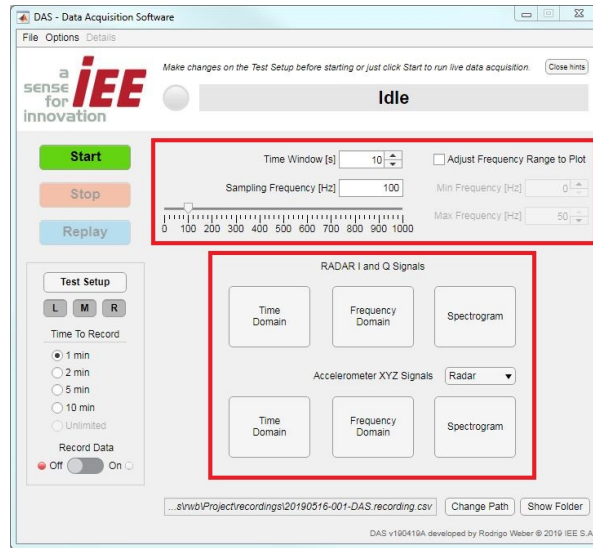
Figure 47 – Distinct panels for data visualization and analysis.

The first panel, on top, has tools for adjusting the settings for the data analyses and plots. The panel is shown in details in Figure 48. It includes the following list of adjustable settings:

- Time Window – time value, in seconds, for the duration of the data in the time domain plots. In the frequency domain plots, the value represents the data length used for the FFT calculations;

- Sampling Frequency – sampling frequency for the DAQ, in hertz or samples per second per channel;

- Frequency Range to Plot – if the box is checked, it enables the selection of a frequency range for plotting of the signals in the frequency domain. Simply put, it enables zooming in/out in the frequency domain;

- Min. Frequency – minimum frequency, in hertz, to show in the plot figures;

- Max. Frequency – maximum frequency, in hertz, to show in the plot figures, with the maximum frequency allowed equal to the Nyquist frequency[2].
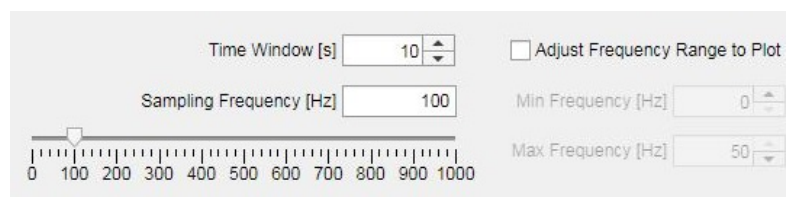
Figure 48 – Panel with buttons for data visualization and analysis.

---

2   The Nyquist frequency is given by half the selected sampling rate, and represents the highest frequency that can be coded at the given sampling rate in order to be able to fully reconstruct the signal.

The second panel, on the bottom, has two rows of buttons for visualization of the acquired signals. Each button opens one or more plots of a respective group of input signals. The buttons on the upper row relate to the I and Q signals acquired from the radar device. The buttons on the bottom row relate to the accelerometer signals in the X, Y and Z axes. As seen in Figure 49, it is possible to select which of the accelerometer devices the user wishes to analyze.
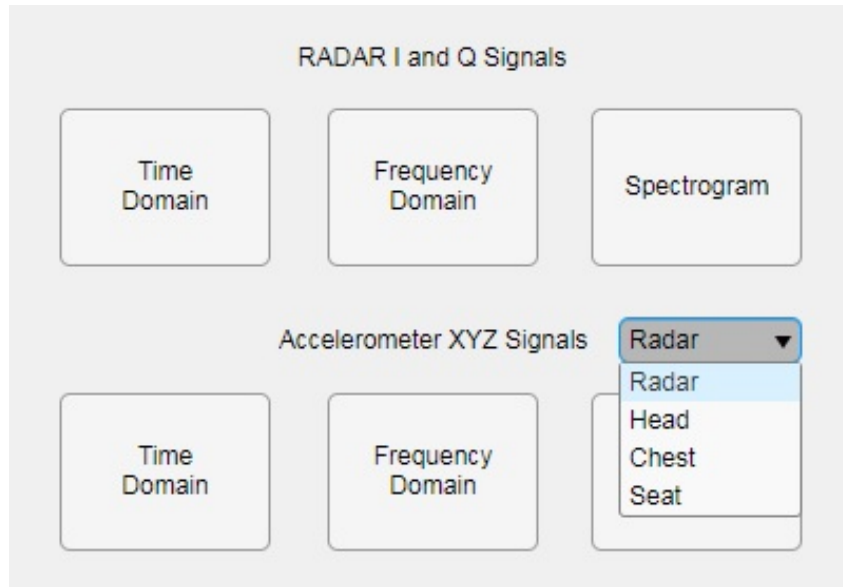
Figure 49 – Panel with buttons for data visualization and analysis.

The first button on the left of each row is for visualization of the signals in the *Time Domain*. The second button of each row is for visualization in the *Frequency Domain*. The third button opens a *Spectrogram* for visualization of the frequency range over time.

In Figure 50, a example of radar detection is shown. A radar corner reflector was positioned in the field of view of the radar and was manually moved to produce such signals. From top to bottom, it is possible to identify the three different types of plots (Time Domain, Frequency Domain and Spectrograms). In Time Domain, it is possible to observe a sequence of sinusoids of different frequencies. The frequencies of the sinusoids correspond to the Doppler frequency seen from the motion of the corner reflector. The amplitude of the sinusoids correspond to the strength of the signal, and it is impacted by the distance of the radar device to the target, as seen in Chapter 2. In the Frequency Domain and Spectrograms, it is possible to observe the power spectrum of the vibrations, with higher power in frequencies between 0 and 5 Hz.

The objective of this section was to present the software capabilities and the tools developed for data visualization and analysis. In Chapter 6, tests and analyses of both the radar and accelerometer signals will be explained in details. In the next chapter, the integration of the hardware of this project into a real vehicle system will be presented.
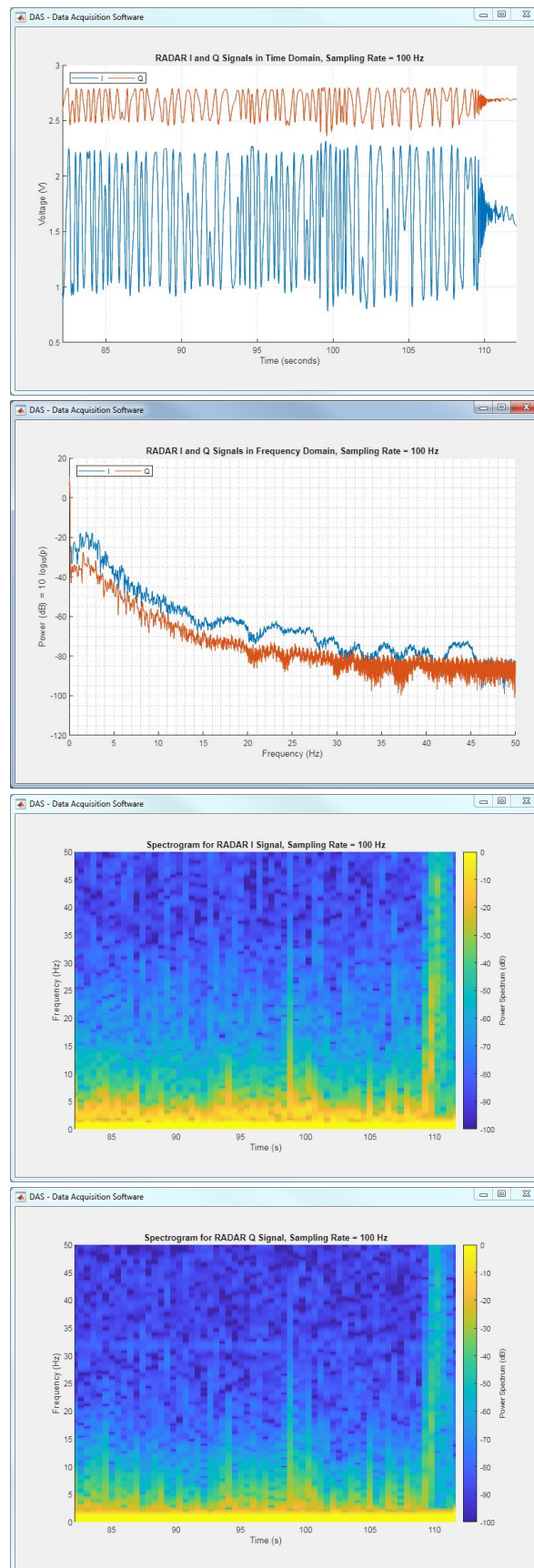
Figure 50 – Detection of movements from a radar reflector, from top to bottom: radar I and Q signals in time domain, in frequency domain and spectrograms.

5 Project Integration

In Chapter 3, it was presented the hardware components of this project: the radar device, the accelerometer modules, the accelerometer belts, the data acquisition device and the connectors. Such components had to be integrated into an unique system in order to run the required tests. In Chapter 4, it was presented the software developed to control the communication of the components in the system, a key factor to enable the devices to work together.

As seen in Chapter 1, among the goals of the system is to acquire the radar signals in relation to the movements of a vehicle. Therefore, to enable the tests to be performed, the entire system had to be integrated into a real vehicle structure, being able to work independently of the outside world. It means that the power for the components and the control of the operations of the devices should be done from within the vehicle.

In section Section 5.1, the real vehicle system will be presented. It includes the vehicle setup and the power management system that was developed and included into the vehicle by IEE. In Section 5.2, it will be presented the connection of the project components into the vehicle structure.

5.1 Vehicle and power system

The vehicle used for the tests is a BMW series 7, fifth generation. The car is owned by IEE and has been used for tests of the company's products since its acquisition. In Figure 51, pictures of the car are shown.

Figure 51 – Vehicle used for system integration and testing.

In the car's trunk, it was placed a system that is responsible for powering and controlling the installed devices and products for tests. The power control system is adapted for tests and makes use of an additional battery, other than the vehicle's standard built-in battery. The system has a voltage control feature that provides an output voltage of 12V for the devices connected to the vehicle's structure, e.g. through the LIN bus. In Figure 52, it is shown pictures of the power control system.

Figure 52 – Power control system built-in into the vehicle's trunk.

In this project, the power control system is used only for the purpose of providing power for the LIN bus. As explained in Chapter 3, Section 3.1, the communication through the vehicle structure is suppressed for simplification reasons.

In this project, the entire communication and control are done through a laptop. More details about the laptop and the communication between the devices will be provided in Section 5.2.

5.2 Embedding the project devices

As seen in the previous section, the vehicle is adapted for tests and has a built-in power control system. In this section, it will be presented the connection of the project devices into the vehicle structure.

The section is divided into four subsections. In Section 5.2.1, it is explained the connection and powering of the radar with the accelerometer module. In Section 5.2.2, the integration of the data acquisition device is shown. In Section 5.2.3, it is described the placement and connection of the accelerometer belts. Lastly, the integration of the Data Acquisition Software for communication and control of the devices is shown in Section 5.2.4.

5.2.1 Integration of the radar

In Chapter 3, Section 3.1, illustrations of the radar positioning inside the vehicle were shown. Below, in Figure 53, it is shown pictures of the real system setup and the positioning of the radar in its mounting base, behind the vehicle's headliner.

Figure 53 – Positioning of the radar behind the vehicle's headliner (top) and closer view of the radar in its mounting base (bottom).

The radar is fixed on a sliding base and its LIN connector is connected directly to a LIN bus located under the roof. As seen in Figure 53, the long wiring cable of the radar is fixed to the vehicle's headliner with tapes, preventing the cable to be swinging around in the detection zone of the radar. The radar wires are directed towards the front of the vehicle because of the placement of the data acquisition device.

5.2.2 Integration of the data acquisition device

The NI-9220 DAQ was placed in the front area of the vehicle to facilitate connections and disconnections of the devices. As seen in Chapter 3, Section 3.6, the radar and all three accelerometer belts have a direct connection to the DAQ. The placement of the DAQ in front of the passenger's seat enables the pilot/co-pilot to have easy access to the device while running the tests. Another reason for the placement choice of the DAQ is regarding its power supply location. Unlike the radar and accelerometer belts, the DAQ is not powered by the LIN bus. The data acquisition device uses a special DC-AC inverter[1] that is connected to the vehicle's 12V socket, also known as the cigarette lighter. In this project, the inverter is connected to the 12V socket and provides 220V AC output for the data acquisition device.

In Figure 54, it is shown pictures of the DC-AC inverter used in the project. The inverter has a switch that enables the driver or co-pilot to easily turn on/off the data acquisition device.

Figure 54 – DC-AC inverter used to power the data acquisition device.

---

[1]   A power inverter is an electronic device that converts direct current (DC) power to alternating current (AC) power at a specified frequency and voltage output.

In Figure 55, it is shown pictures of the DAQ and inverter placements under the front passenger's seat. It is also possible to observe the connection of the power inverter to the 12V socket of the vehicle. In the picture, the 12V socket is divided into two connectors, one being used for the power inverter and the other one being used to power the laptop with the DAS program.

Figure 55 – Data acquisition device fixed on the feet area of the front passenger's seat.

Both the data acquisition device and the power inverter are fixed on the vehicle's floor with strong double-sided tapes. The tapes prevent the devices from moving around during execution of tests. All the wires that connect the DAQ to the radar and accelerometer belts are also fixed with tapes. The connections are very robust and are placed away from the movement area of the occupants.

5.2.3   Integration of the accelerometer belts

As seen in Chapter 3, Section 3.4, accelerometer belts were developed to measure the acceleration of a passenger's body in the back seat of the vehicle. Therefore, it was necessary to provide an accessible connection between the accelerometer belts and the device to acquire and process its signals. Considering the placement of the data acquisition device at the front passenger's seat area, it was decided to place the accelerometer belts in the seating position behind the front passenger's seat. This seating position is also known as position 2R – 2 for the second row of seats, R for the right side[2] of the car.

In Figure 56, it is shown a picture of the accelerometer belts placed on the position 2R. It is possible to see one of the accelerometer belts fixed on top of the seat and used

---

[2]   The side orientation in relation to the vehicle is taken from its direction of movement, i.e. seen from the back of the vehicle.

to measure the acceleration of the vehicle's seat when the passenger is sitting on top of it. The other two belts are not fixed and are used to measure the acceleration of the passenger's body. In the picture, these accelerometer belts are seen hanging on the seat backrest.

Figure 56 – Positioning of the accelerometer belts on the back right seat of the vehicle: one belt attached to the seat and two belts to be placed on the passenger.

Due to the long cables of the accelerometers belts, it is possible for the passenger to stand outside of the vehicle while adjusting the belts on the body. The wider belt is for placement around the passenger's chest/abdomen. The smaller belt is for placement around the head. Both belts are made of a fabric strap with strap adjusters, thus allowing them to be placed on passengers of all ages, from small kids to adults.

Above the seat, a piece of cloth is placed in order to cover the accelerometer module fixed on the seat. The cloth makes it more comfortable for the passenger to seat on the device, while also protecting the device from possible damages, e.g. getting caught by pants pockets, being displaced during the seating movement, etc.

Similarly to the radar wiring cable, the wires from the accelerometer belts are also fixed to the floor and sidelines of the vehicle. The wires are kept away from the feet area to prevent damages to the cable, only leaving enough length for the passenger to adjust the belts outside of the vehicle.

5.2.4   Connection to DAS

The wires from the radar and accelerometer belts are connected to the data acquisition device, as explained in details in Chapter 3. In the vehicle integration, the DAQ receives the analog voltage signals from the devices and is connected to a laptop through a USB cable.

The laptop, seen in Figure 57, has the Data Acquisition Software installed and serves as the control platform for starting/stopping the system, i.e. acquisition, recording, etc. It is placed either on top of the front passenger's seat, or on the central armrest of the car (as shown in the picture below).

Figure 57 – Computer setup for running data acquisition software (DAS).

The laptop uses an adapter for connection to the 12V socket of the vehicle. When plugged on the power supply, it can be charged by the vehicle battery while running the tests.

An additional webcam was later connected to the laptop as well. The USB webcam was used to video record some of the passenger tests – provided that they accepted the recording. Images of the video recordings or other pictures are not included in this thesis for privacy related purposes. The images, however, can be used in future analyses by IEE.

6 Tests and Results

This chapter presents some of the tests performed in this thesis. Some of the tests were performed even before the integration of the project into the vehicle's structure. These pre-tests, realized on a lab, or workstation, had the purpose of calibrating and validating the functionality of the project devices and the Data Acquisition Software (DAS).

In the early development of the project, many of the tests had to be realized on the hardware devices. During the studies on the radar device, for example, it was necessary to perform tests in order to identify the extraction points of the desired signals – as explained in Chapter 3. Later on, after the soldering of the wires and connectors for extraction of the signals had been finalized, more tests were necessary to verify if the signals were being correctly acquired. The same applies for the fusion of the radar and the accelerometer module, and for the conception of the accelerometer belts, where the solder contacts and wiring connections had to be consistently tested.

During and after the development of DAS, for example, it was necessary to perform communication tests between the program and the data acquisition device to validate the acquisition of the analog signals. The software functions of live data acquisition, recording and replaying also went through intensive testing and reformulations. The software was maintained in development until the end of the vehicle integration stage, with constant implementation of adjustments and addition of features to the program.

After conclusion of the integration of the project components into the vehicle, tests on real road environments could be performed. For the tests, different test scenarios were defined, including selection of routes and test subjects.

In Section 6.1, tests performed at laboratories will be presented. In Section 6.2, it is presented some of the tests that were executed in the vehicle, as well as all the test scenarios that were previously defined.

6.1 Lab tests

Tests in laboratories and on workstations were performed to validate the operation of the hardware devices, as well as their communication with the Data Acquisition Software. Such tests were also needed to have an understanding of the signals expected from the radar and accelerometers.

6.1.1   Radar in an empty environment

In the first test, the radar device was placed on an empty environment, without any person or moving object in its field of view. The radar was connected to the DAQ, and the DAQ to the software (PC) through an USB cable. In the software, the data acquisition was set with a sampling frequency of 100 Hz.

In Figure 58, it is shown plots of the radar I and Q signals in the time domain (top left), frequency domain (top right) and spectrograms (bottom).
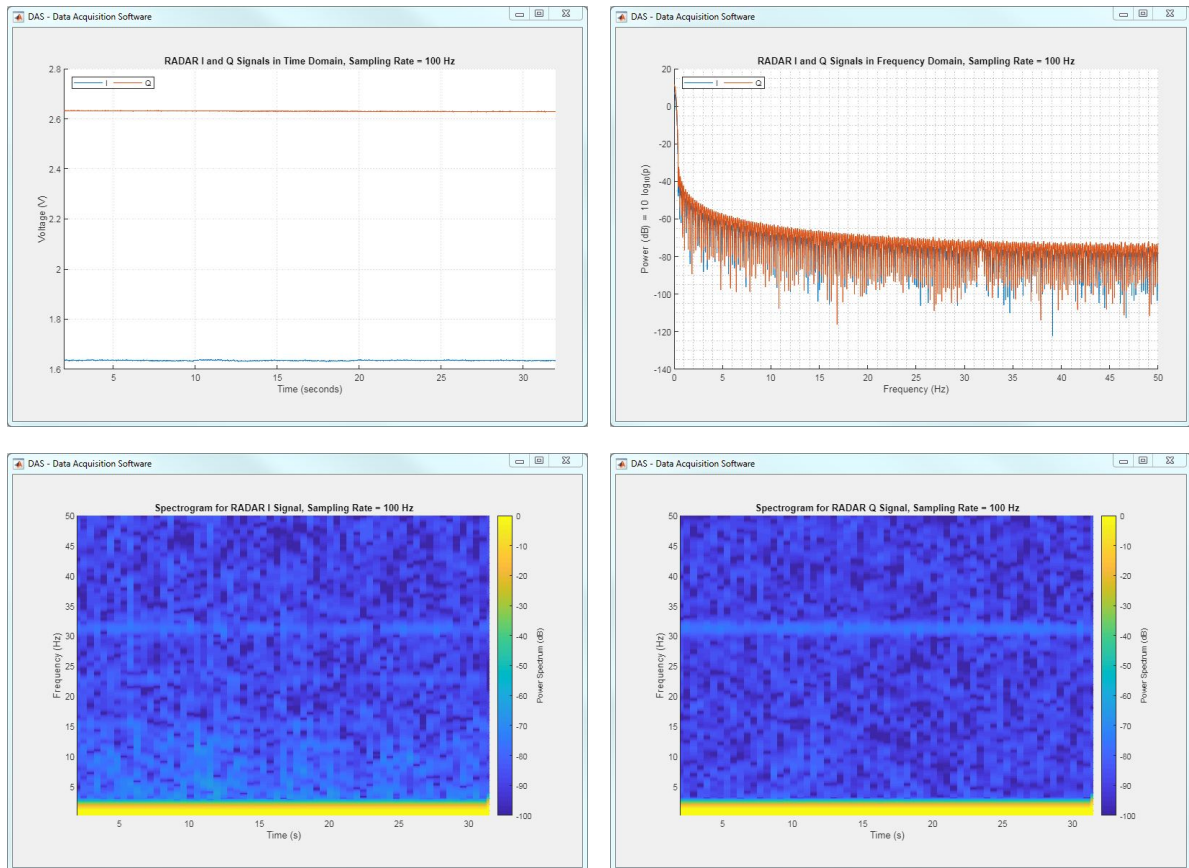
Figure 58 – Measurement of the radar I and Q signals, with the radar in an empty/static environment.

With an empty environment, no movement should be detected by the radar. This is corroborated by the signals in the time domain with constant behavior and no apparent oscillation. The frequency domain analysis and both the spectrograms also do not show any major power influence in the frequency range observed (0–50 Hz).

In this test, it was important to understand the radar response without any excitation caused by a target. The constant signal in time domain and the absence of high energy frequency components in the frequency domain are also used as basis for comparison with other tests. It was proven that, if no target is seen by the radar, there is no perceptible oscillation in the output.

6.1.2 Detection of breathing in laboratory

Another test with radar was performed to extract the vital signs of a person. Similarly to the first test, the connections between the radar, DAQ and software were made, and the data acquisition was set with a sampling frequency of 100 Hz.

In the field of view of the radar, a test person was placed sit and still. The test person did not perform any movements other than the chest movement caused by breathing.

In Figure 59, it is again shown plots of the radar I- and Q-signals in the time domain (top left), frequency domain (top right) and spectrograms (bottom).
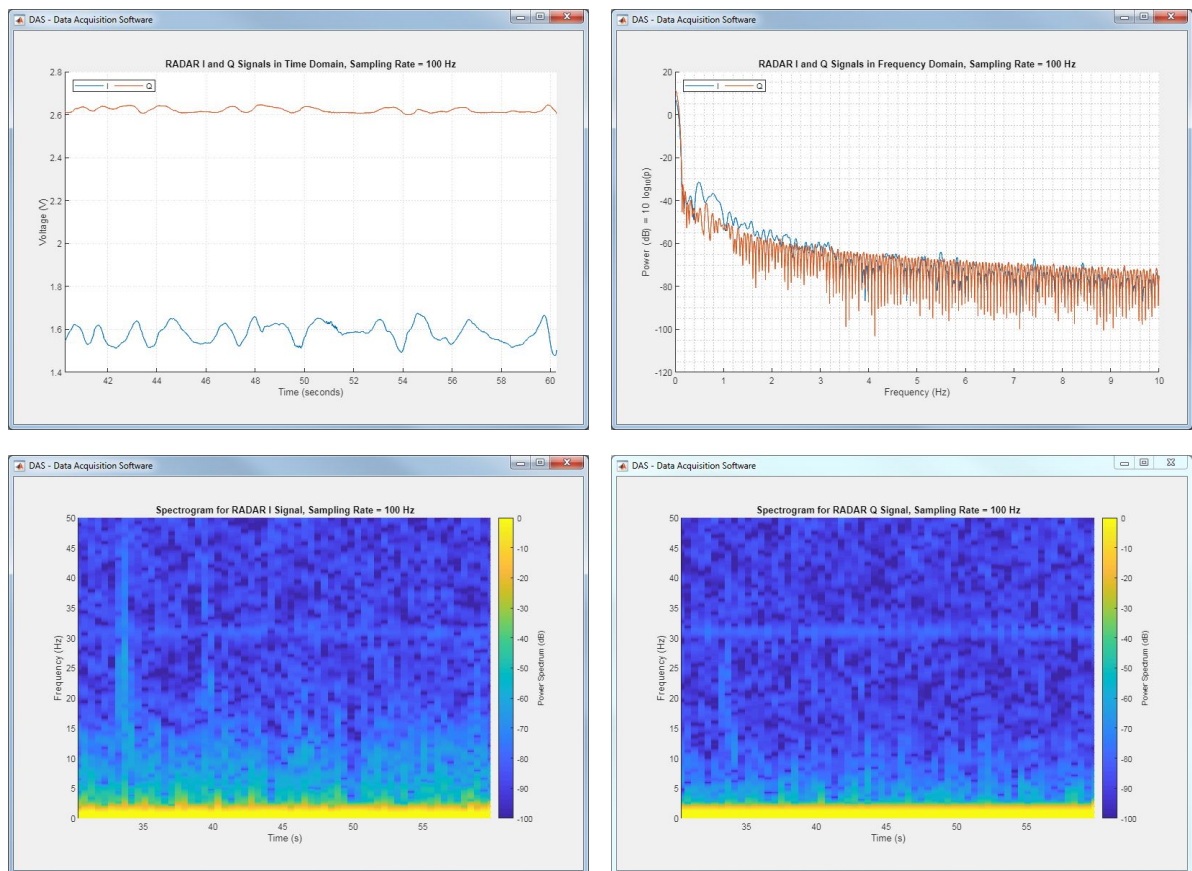
Figure 59 – Radar detecting breathing.

The differences in the signal from this test in comparison with an empty environment are clearly visible. In the time domain, now it is possible to observe well defined oscillations caused by the chest displacement while breathing. In the frequency domain, spikes can be seen between 0.2 and 0.7 Hz. In the spectrograms, it is also possible to observe higher power in the low frequency range.

With this test, it was important to observe how the breathing movement is detected by the radar and how the form of the output signals. This test also validated the software and the acquisition and processing of the radar signals.

6.1.3   Accelerometer in a movement-free environment

To understand the output of the accelerometer module, tests were first performed in an environment without perturbations. The accelerometer module was fixed on a table free of movements and vibrations that could disturb the measurement. The accelerometer module was connected to the DAQ and software, with sampling rate of 100 Hz.

In Figure 60, it is shown pictures of the accelerometer output in time and frequency domain.
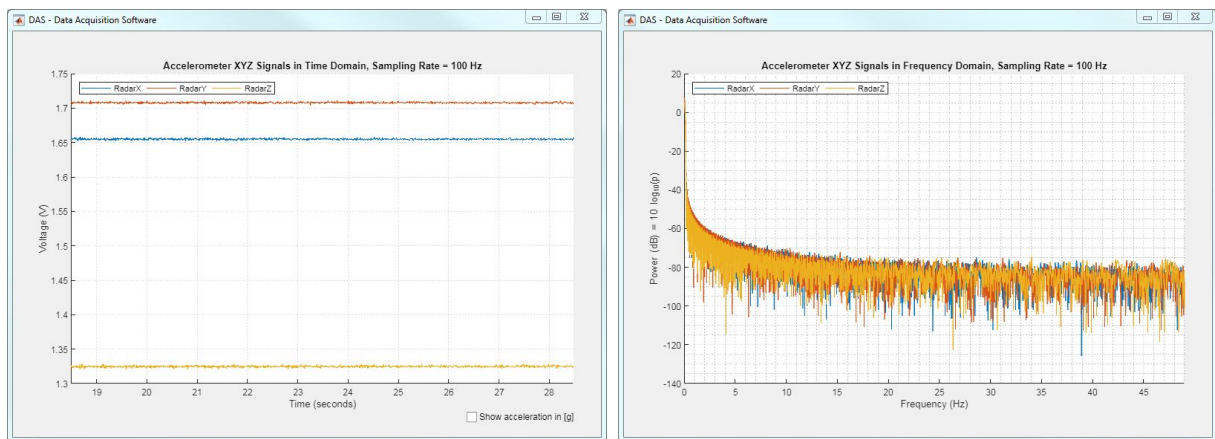
Figure 60 – Accelerometer test: no perturbation, in time and frequency domain.

In the time domain, the voltage value of each signal represents the acceleration being measured in each of the three axes. The behavior – or form – of the signal, in this case constant, is what gives the information about the movement. The signals with constant values indicate that no dynamic acceleration is being measured in any of the three axes; static accelerations – e.g. gravity – are measured but are not relevant for this analysis. The changes in the mean voltage value of each signal represent the measurement of the gravity force (static acceleration) and are impacted by changes in the orientation of the accelerometer module in space. In the frequency domain, as it is shown, the power value is not relevant in any of the frequencies in the frequency range – not considering the DC component at 0 Hz.

Considering that the accelerometer module was placed on a table free of movements, the analysis is correct and the acquisition of the accelerometer signals is being successfully processed. No acceleration or movement is perceived by the sensor, and only the gravity is measured – impacting the mean value of the constant signals. Therefore, the output of accelerometer in a free-movement environment can be taken as standard for comparisons with the subsequent tests. Any other behavior or movement should be detected after analysis of this test.

6.1.4 Accelerometer sensibility to finger touches

The second test with the accelerometer module was to verify its sensibility to minor movements. It was again fixed on a table free of movements or vibrations. The module was connected to the DAQ and DAS for signal acquisition, with sampling rate of 100 Hz.

To show the sensibility of the accelerometer even to minor movements, the module was touched with a single finger. In Figure 61, it is shown pictures of the accelerometer response in the time domain (left) and frequency domain (right).
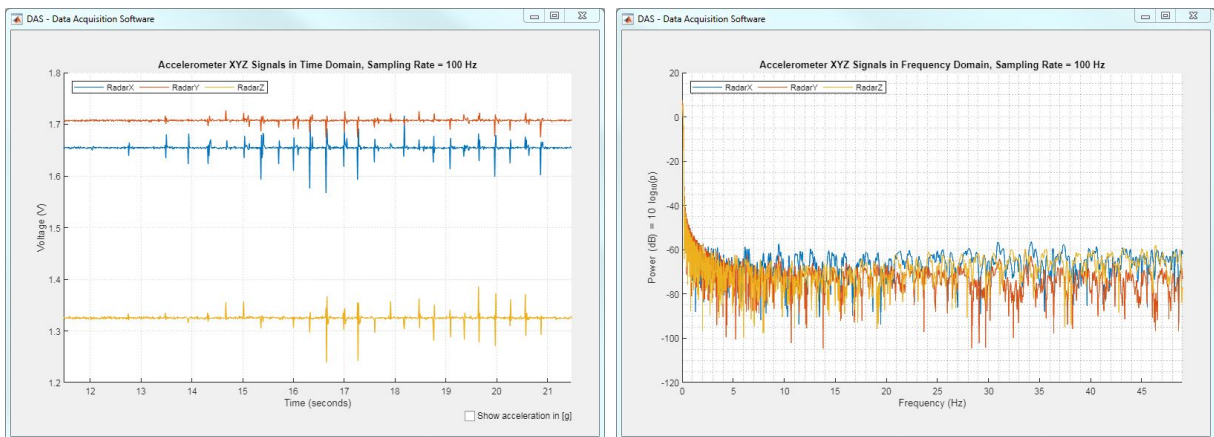
Figure 61 – Accelerometer sensibility to a single finger touch.

In the time domain, it is possible to observe a sequence of spikes. The sequence of spikes is the output response of a sequence of finger touches, with each spike corresponding to a single touch.

In the frequency domain, it is shown that the finger touches do not cause any major power influence in the frequency range observed.

With this test, it is possible to prove that even minor movements or vibrations will be detected by the sensor. The finger touch does not cause any perceptible displacement of the module, but it is still easily differentiated from a signal of the module in a movement-free environment.

6.1.5 Accelerometer agitated in axes X, Y and Z

In the third and last accelerometer test in the laboratory, the accelerometer was agitated in each of its three axes of measurement (X, Y and Z). The accelerometer module was placed on a support tool to be able to move it in an unidirectional manner. The module was connected to the data acquisition device and the software DAS was set with an acquisition rate of 100 Hz for the test.

In Figure 62, it is shown pictures of the accelerometer output in the time domain (left) and frequency domain (right).
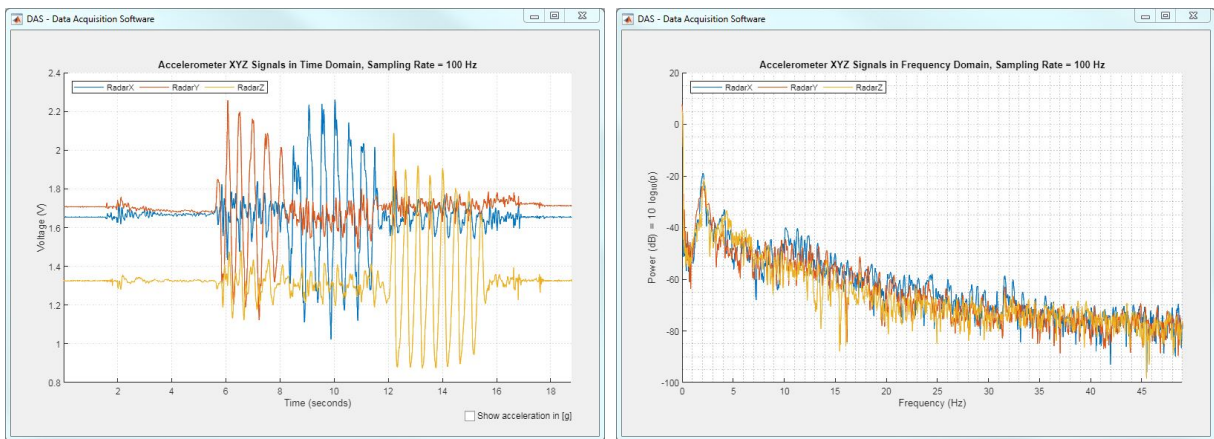

Figure 62 – Accelerometer being agitated in its three axes X, Y and Z.

In the time domain, it is possible to see oscillations in each of the three axes of measurement. The oscillations are alternated between the axes, corresponding to the movements performed by the accelerometer module. As each of the three axes are represented by one different color, it is easy to differentiate which movement is occurring and in which axis. It is also possible to observe that, during the movement in one respective axis, some minor oscillations can also be seen in the other axes. These secondary oscillations are due to minor changes in the accelerometer orientation during its movement. If the movement could be made in a perfect unidirectional manner, secondary oscillations should not be perceptible.

In the frequency domain, now it is possible to observe higher power influence in the frequency range of 2 Hz. Such influence is seen due to the periodic movement performed in the three axes.

With this final lab test, it was possible to observe the response of the accelerometer module in each of its axes separately. The periodicity of a signal can also be seen in the frequency analysis, thus proving that the software is capable of displaying patterns in the acceleration seen by the accelerometer module.

6.2 Vehicle tests

In this section, it will be presented some of the tests performed on real road environments. As discussed and seen in the previous sections, many lab tests were done during the development of the project. After integration of the project devices into the vehicle structure, it was necessary to go a step further and start testing the system on the road.

As the first step, the test scenarios and routes for the tests were defined. One of the goals of the road tests was to validate the functioning of the system and to demonstrate its successful operation while integrated to the vehicle and during the vehicle's movement. After validation of the system, another goal was to collect maximum amount of data with as many test subjects – or test persons – as possible. For the data collection to be maximized, all the characteristics and test setup parameters of the DAS software (seen in Chapter 4) were informed and saved in the recordings.

The definition of the test scenarios included information about the parameters of the tests in order to make each scenario unique. For the first and second scenarios, it was defined that the car should be parked and its seat should be empty. The difference between them was the engine, with one test having the engine off and another having it on. The goal of these first two tests was to have a definition of the signal when the system (radar and vehicle) is not undergoing any influences of occupants. The differentiation of the engine being on or off was to observe possible impact of vibrations in the output signals.

The third and fourth tests scenarios were very similar to the two above. The difference was, instead of having the seat empty, a water gallon of 20L was placed on the seat with the accelerometer belts attached to it. Water gallons or bottles are common radar test objects because their reflection rate of the electromagnetic waves of the radar is approximate of what would be from a human body – explained by the fact that the majority of a human body composition is made of water. Accordingly, the third scenario had the water gallon sit still and the vehicle's engine off, while the fourth scenario had the engine on in order to see, again, possible influences caused by the engine vibrations.

In the fifth scenario onward, the tests were performed while the vehicle was moving. For these driving tests, short and long test routes were defined. The short route (1,8 km) was defined around the former IEE headquarters, in Contern. Its objective was to enable easy comparison between the behavior of the output signals of different test subjects. On the other hand, the goal of the long route (25,6 km) was to incorporate different road profiles, including uphills and downhills, highways, curvy paths, low-speed and high-speed sections, etc. The different road profiles in the same route should cause different impacts on the movement of the car and passenger, thus maximizing and diversifying the collected data. In Figure 63 and Figure 64, the short and long routes are shown.
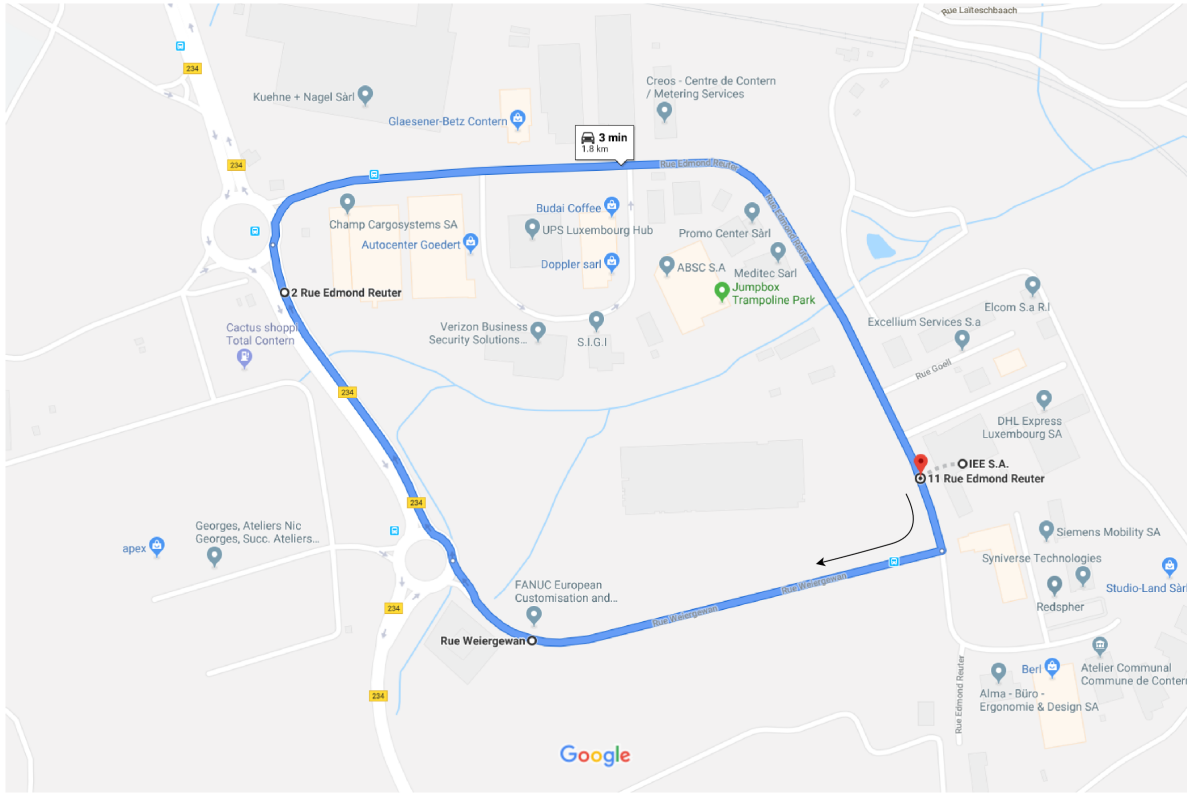
Figure 63 – Short route[1].

Figure 64 – Long route[1].

---

[1] https://maps.google.com/.

Proceeding with the presentation of the scenarios, the fifth and sixth test scenarios were performed with the vehicle empty: one in the short route and another in the long route. The ride was done in a loop around the company, while the radar and accelerometer signals were acquired and recorded. The signals of the empty vehicle were collected to be used as comparison in future analyses. Without occupancy of the seat and of the accelerometers belts, it is possible to obtain the motion of the vehicle seat without pressure of any object's or person's weight on top of it.

The seventh and eighth scenarios were performed with the vehicle moving and with a 20L water gallon on top of the rear car seat. The water gallon is attached to the accelerometer belts in the same way explained in the third and fourth scenarios. The purpose of this test was to observe the behavior of the acquired signals with a movable object (water) on the back seat.

The two last scenarios, the ninth and tenth, were performed with adult test persons sit on the rear seat of the vehicle. For these test scenarios, some volunteers were invited to participate as the test subjects. In total, 9 persons participated, 5 men and 4 women, with ages in the range between 25 and 35 years old.

During the tests, the test subjects had to sit on the rear bench of the vehicle while wearing accelerometer belts. As seen in Chapter 3, three accelerometer belts were developed. One of the accelerometer belts was placed on top of the seat with a cloth covering it, for the test subjects to sit directly on top of the cloth and of the accelerometer module. The accelerometer on the seat was responsible to acquire the seat acceleration and movement during the test, considering the weight of the test person that was also informed as one of the test parameters passed to the DAS software.

The other two accelerometer belts were placed directly on the body of the passenger or test person: one belt attached to their head and another to their chest/abdomen. The purpose of these belts was to acquire the acceleration of different parts of the test subject's body. Since the tests performed in this thesis had never been performed by IEE before, the movement of a passenger's body in the back seat of a vehicle was not known. Therefore, having two sources of acceleration data (head and chest) seemed the optimal way to collect the body acceleration. Also, as seen in Chapter 3, the radar and the accelerometer belts were already using 14 of the 16 available input channels of the data acquisition device (DAQ), making it impossible to add another accelerometer to the same DAQ (it would require three more channels for three additional axes).

In Figure 65, it is shown pictures of test persons sitting on the position 2R of the vehicle (right rear seat) and wearing the accelerometer belts.

Figure 65 – Test subjects wearing accelerometer belts (head and chest).

During the tests, the test persons could freely move, talk, look around, etc. The only requirement was to remain in the same seat of the vehicle and, obviously, to keep breathing! It is also very important to note that, in the first 10 seconds and in the last 10 seconds of each test, a calibration process was done with each test person. During the calibration period, the test persons had only to breathe and do not perform any other movement. The calibration process was done with the car parked, before and after each of the tests in the short and long routes. The goal of the calibration process was to acquire the vital signs pattern of each individual without interference of the vehicle's movement.

Finally, a summary of all the test scenarios described can be seen in Table 4.

Table 4 – Test scenarios.

Scenario	Seat	Route	Car Status
1	empty	–	parked w/ engine off
2	empty	–	parked w/ engine on
3	full water gallon	–	parked w/ engine off
4	full water gallon	–	parked w/ engine on
5	empty	short	driving
6	empty	long	driving
7	full water gallon	short	driving
8	full water gallon	long	driving
9	test persons	short	parked and driving
10	test persons	long	parked and driving

Considering the number of scenarios and the different test persons that participated, a total of 23 tests were performed, with a record file generated for each test. In these tests, approximately 250 MB of data was collected, with one single file holding up to 3.5 million raw signals acquired from the sensors.

In numbers, it was a considerable amount of data acquired, which is a good outcome of this project. Consequently, the data had to be filtered in order to present only the most relevant results here in this thesis. In the next subsections, three different test results will be presented.

In Section 6.2.1, it will be presented some of the signals extracted from the calibration process done with the test persons. In Section 6.2.2, it will be presented the results on the extraction of a respiratory pattern while the vehicle is moving. In Section 6.2.3, a preliminary analysis on the extraction of heartbeat signals will be presented.

6.2.1   Detection of breathing in a parked vehicle

Prior to the start of the road tests, each test person was submitted to a calibration process. The intention of this calibration period was to acquire the respiratory pattern of each individual, in order to compare with the signals later extracted during the movement of the vehicle. As stated previously, the duration of each calibration period was of minimum 10 seconds, done one time before and one time after the execution of the road tests.

In this section, the procedure of a calibration process will be shown in details, along with its results. For the extraction of the signals presented, the test person was placed still on the rear bench of the vehicle. The person was oriented to not perform any movements other than the ones caused by the breathing motion. The radar, as shown in Chapter 3, is integrated on the vehicle headliner and its field of view comprehends the whole rear bench area of the vehicle. The test person, sitting on the right rear seat (position 2R), is in the field of view of the radar and any movements performed will be detected by the sensor.

For the acquisition of the sensors' data inside the vehicle, a laptop was used (as seen in Chapter 5). The laptop is connected to the data acquisition device (DAQ) and has the Data Acquisition Software (DAS) installed. In the software, the sampling frequency is set to 100 Hz.

The expectation was that the respiratory pattern should be easily visible when analyzing the I- and Q-signals acquired from the radar. Such expectations were confirmed after analysis of the acquired data, with the radar Q-signal showing a nearly perfect sinusoidal wave. As shown in Figure 66, there are approximately 3.5 sinusoidal breathing cycles in the 10 seconds observed, corresponding to approximately 21 breathes per minute. In normal conditions, as studies show [32, 33], the respiratory rate (RR) of human adults can be observed in the range of 12-26 breathes per minute. This information reaffirms the validity of the data acquired, as well as of the devices and software developed for this thesis.

Interesting to note is that the accelerometer belt placed on the passenger's chest also reproduces the breathing movement, although with much more noise information. In the Figure 67, it is presented the acceleration signal obtained from the Z-axis of the accelerometer belt attached to the test person's chest.

Both the Q-signal and the acceleration signal from the belt are taken in the same time interval. The interval corresponds to the exact first ten seconds of test, when the test subject is under the calibration period.
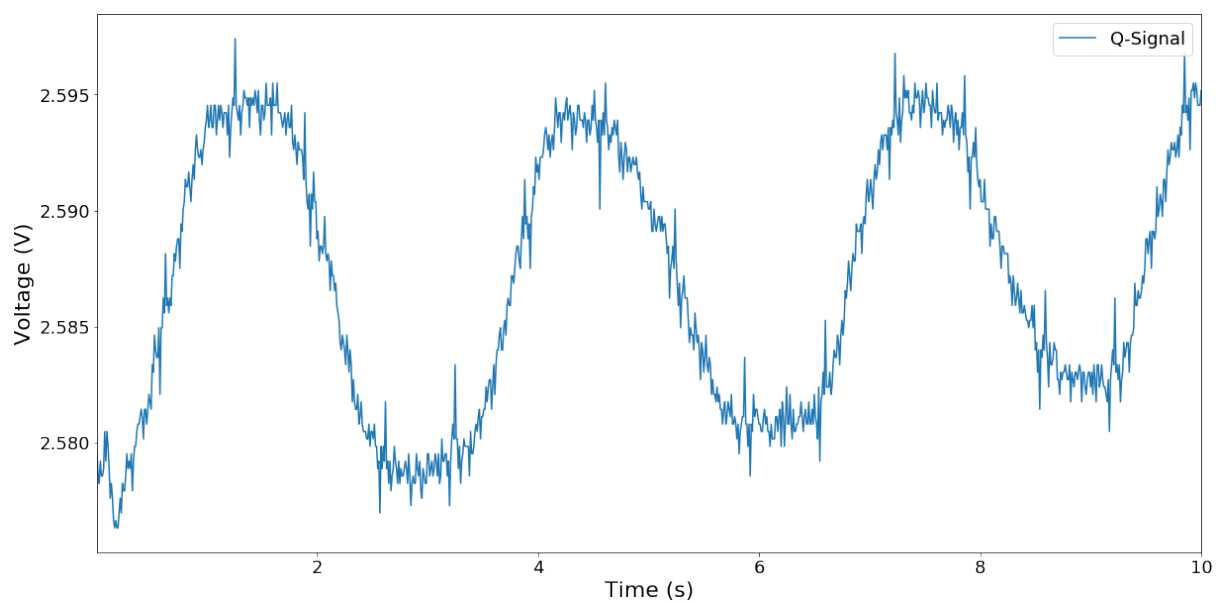
Figure 66 – Radar Q-signal extracted during pre-test calibration: the respiratory pattern of the test subject is clearly visible.
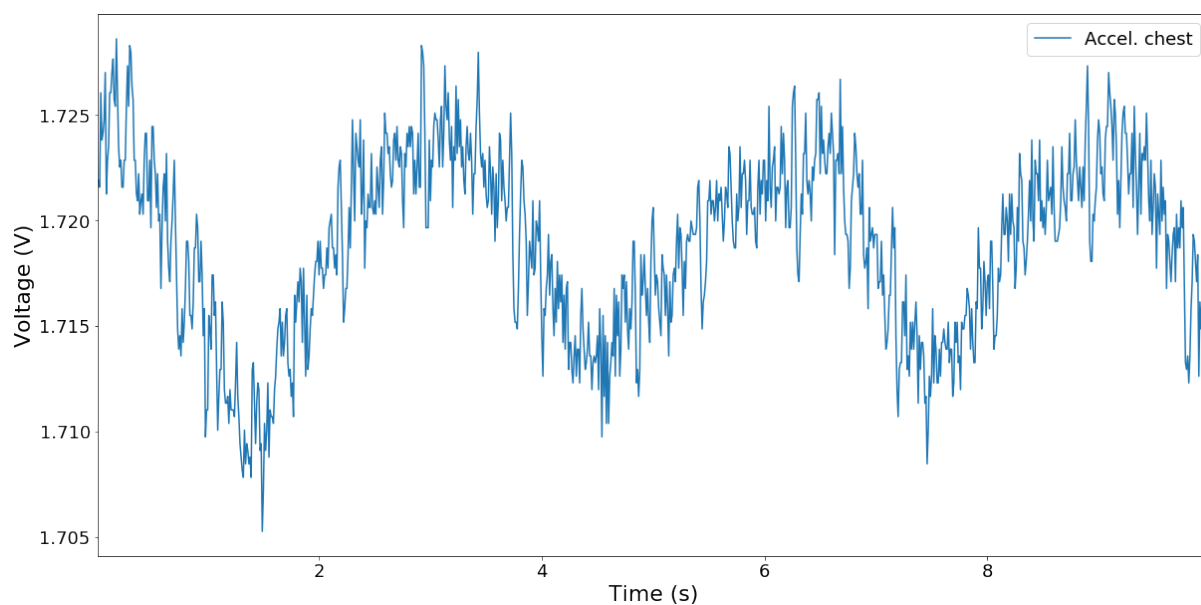

Figure 67 – Signal extracted from the accelerometer belt attached to the passenger's chest: the respiratory pattern matches with the radar.

6.2.2 Detection of breathing in a moving vehicle

As seen in the Introduction of this thesis, one of the main goals of this project was to perform tests with a group of people in real road environments. More than that, one of the goals of this thesis was to acquire the vital signs of passengers with the vehicle in motion.

In the previous section, it was presented a successful extraction of a respiratory movement from a test subject, during the calibration period and while the car was parked. As explained in Chapter 1, the same extraction could be impaired in a situation with a moving vehicle, due to noises caused by the vehicle's movement and relative movements of the passenger.

The test presented in this section had the goal of overcoming these obstacles and, consequently, obtain the respiratory movement of the passenger while both the car and the passenger's body are moving. In the same way that presented earlier, the test subjects were placed sit on the position 2R of the vehicle, with the accelerometer belts attached to the person's body.

In this test, differently from the calibration test, the test persons could freely move their body while not leaving the seat area. During the tests, the test subjects should act normally, being able to have conversations, look around at the landscapes, check their phones, and anything else that they could normally do. The purpose of this test was to successfully acquire respiratory patterns in a normal driving situation, without imposing an artificial behavior.

The acquisition of the signals from the devices was done through the laptop presented in Chapter 5, with the DAS program installed and connected to the data acquisition device. This test was performed with a sampling frequency of 100 Hz as well.

For the analysis of the radar signals here presented, a frame of 10 seconds was again taken from the data acquired. The data frame was taken from a test in the long route, 20 minutes after the driving start point.

In Figure 68, it is shown the acquired radar signal. Analyzing the radar signal and its mean value[2] plotted, it is already possible to observe the pattern resulting from the respiratory movement, despite some noises caused by the road and passenger's movements.

In Figure 69, it is presented the signal extracted from the accelerometer belt attached to the passenger's chest, in the same time frame. Although with much more noise than before, it is also possible to see the movement of the chest reflected in the accelerometer signal. Both the radar and accelerometers are in accordance and reflect the same respiratory pattern, made more visible with the rolling mean functions added to the plots.

---

[2] Rolling mean functions have been applied in Python for analyses of the signals. The rolling mean of a signal, also known as its moving average, is a calculation to analyze a data signal by creating a series of averages of sub-parts of this same signal.

Also interesting to analyze is the signal from the accelerometer attached to the radar device, shown in Figure 70. This specific accelerometer module was attached to the radar, forming one single device, as detailed in Chapter 3. Both the accelerometer and the radar are fixed to the vehicle's structure, and any movements performed by the vehicle are immediately seen in the accelerometer response. In Figure 70, the accelerometer response clearly shows a spike standing out from the rest of the data signal. The spike seen by the accelerometer can be interpreted as a sudden change in the vehicle's movement, possibly caused by a bump, or slope, on the road.

Even more interesting to see is that the irregularity on the road, showed in Figure 70, caused spikes in both the radar signal and the accelerometer attached to the passenger's chest in the same time period (see Figure 68 and Figure 69). Therefore, it is possible to suppose that a road bump caused a specific movement on the vehicle, and that the vehicle's movement was reflected on a passenger's reaction.

With some signal processing and filtering, it should be possible to remove the noises caused by the movements of the vehicle and the passenger, as well as the irregularities of the road. For that, a nine-order Butterworth low-pass filter was designed to be applied on the radar signal. The filter was designed with a cut-off frequency (-3 dB) in 1.5 Hz, in order to maintain only the low frequencies of the breathing and, at the same time, to remove the noises caused by the movements of the car and test person. In Figure 71, it is shown the frequency response for the designed filter. In Figure 72, it is presented the radar signal after applying the low-pass filter, with the respiratory pattern evidenced.

In conclusion, it is possible to affirm that this test was successful in detecting the respiratory pattern of the passenger in a moving vehicle. Irregularities were seen on the road, which caused some interference in the signals seen by the radar and accelerometer. Nevertheless, with signal processing and filtering, it was possible to remove such interference and extract a clean respiratory pattern.
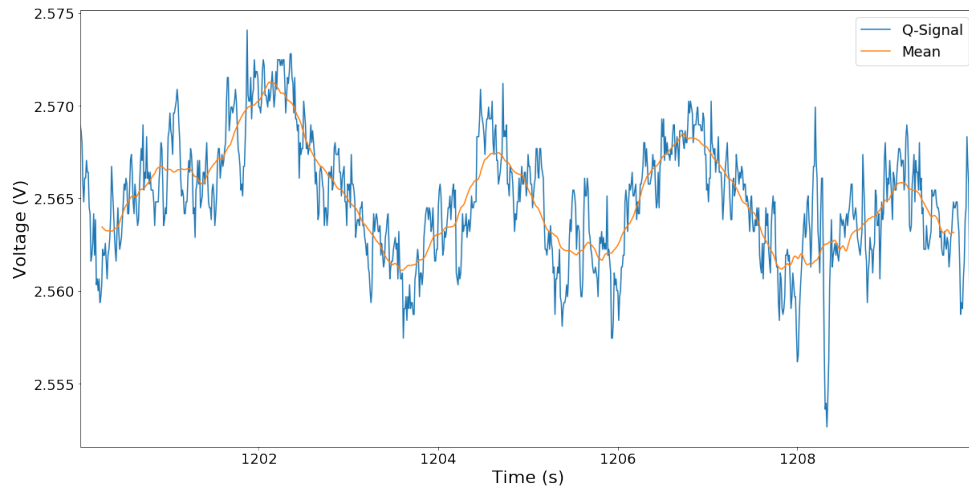
Figure 68 – Detection of a breathing signal in a moving vehicle.

Figure 69 – Signal acquired from the accelerometer belt attached to the passenger's chest.

Figure 70 – Signal acquired from the accelerometer module attached to the radar device.

Figure 71 – Frequency response of the nine-order Butterworth low-pass filter, designed with a cut-off frequency of 1.5 Hz.

Figure 72 – Respiratory pattern evidenced after applying the Butterworth low-pass filter on the radar signal.

6.2.3 Analyses on the detection of heartbeats

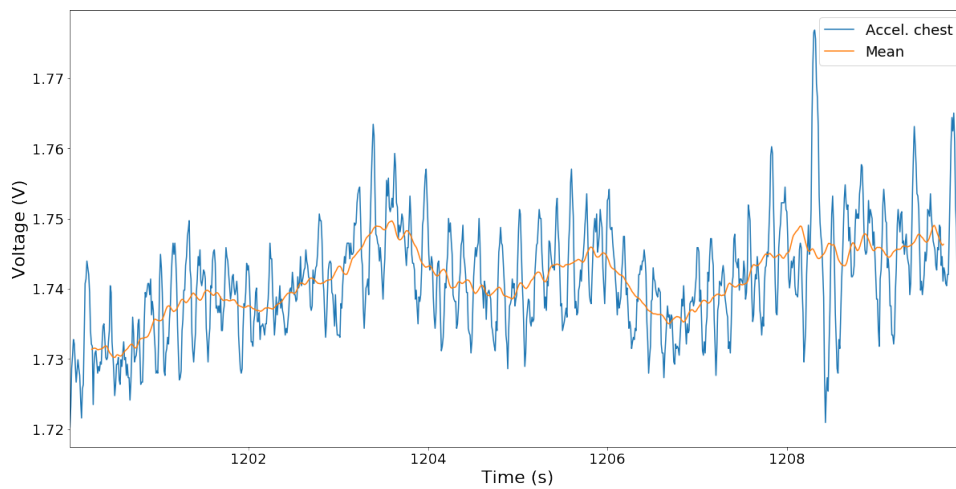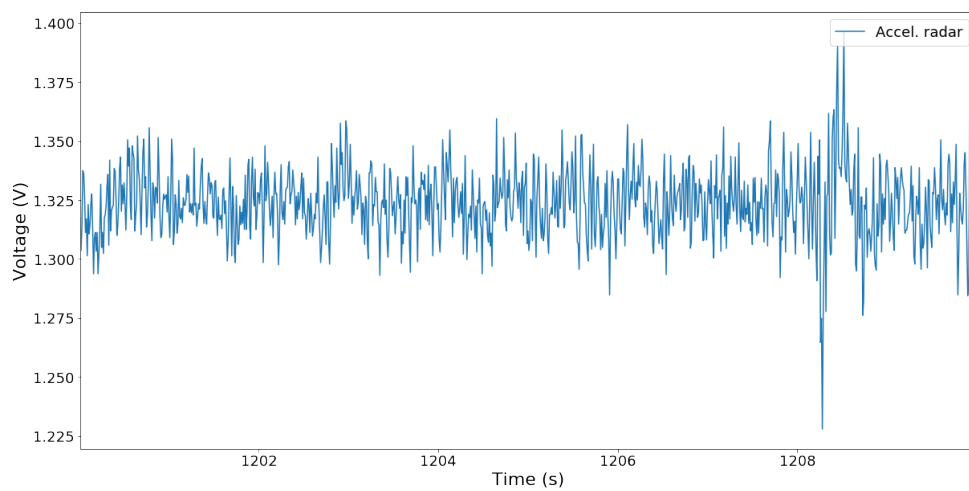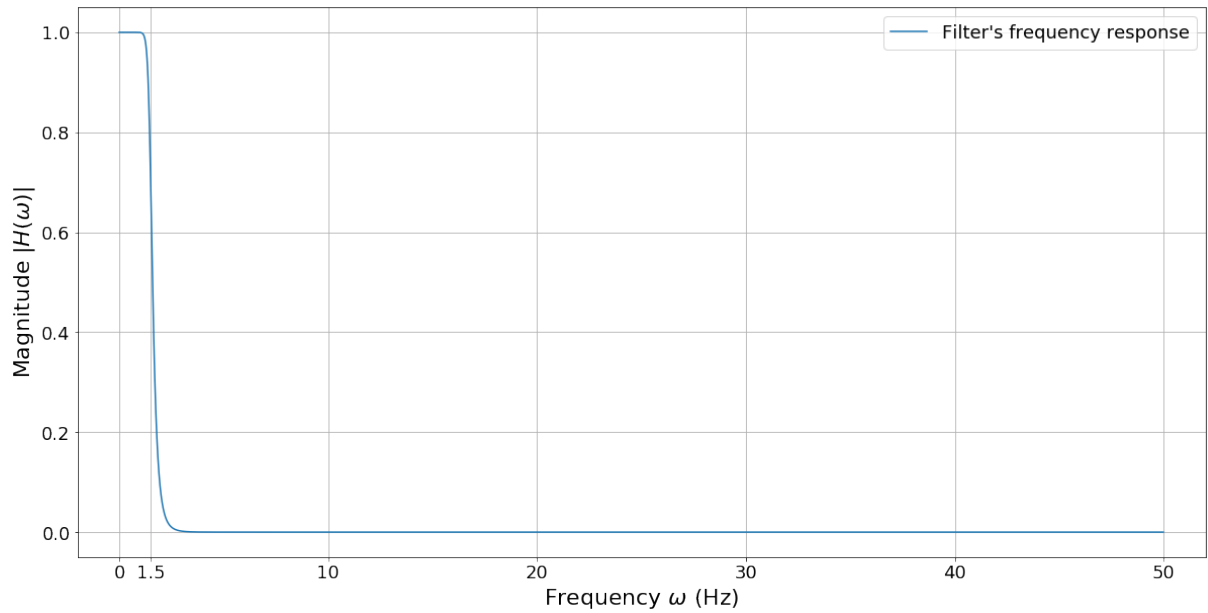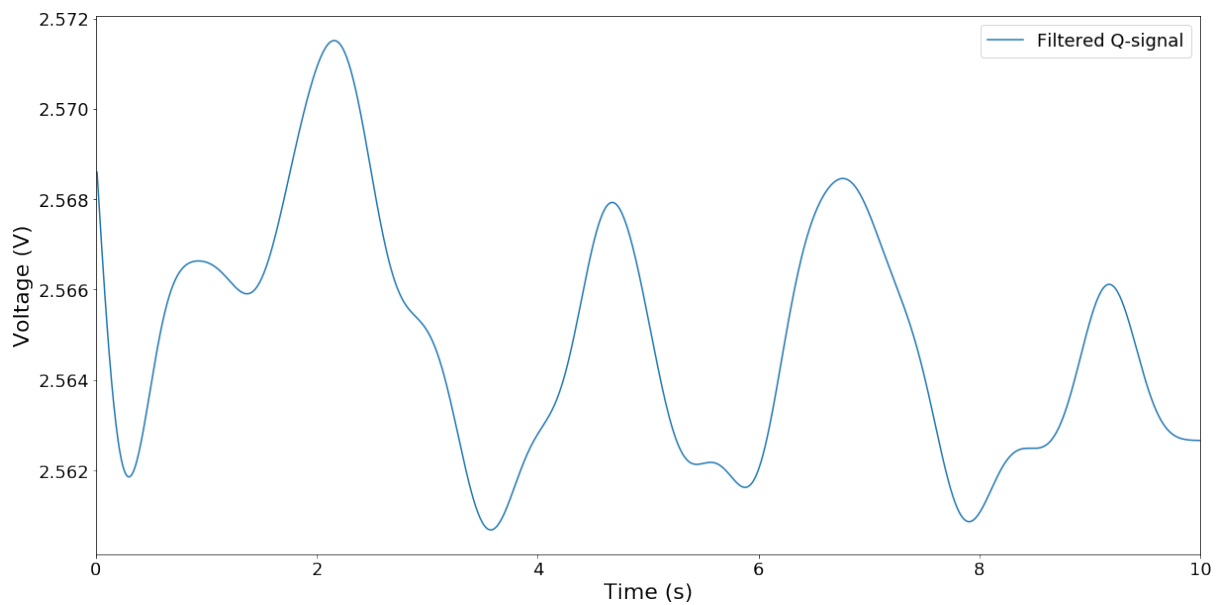In the last two sections, tests have shown that the respiratory pattern of passengers can be acquired from radar signals, with the vehicle in both parked and moving states. The successful extraction of the breathing movement was a great achievement for this project and it opens the possibility for further analyses to be performed on top of the collected data.

After close observation of the breathing data acquired, especially the one shown in Section 6.2.1, questions were raised about the feasibility of the extraction of heartbeat signals of the test subject. The extraction of heartbeat signals of test persons would be another great achievement, a bonus for the results of this project.

Therefore, this section presents preliminary analysis on the collected data, in order to extract information about the heartbeat information of the passenger. In Figure 73, it is shown the data frame collected from the calibration period, while the vehicle was parked. The red arrows in the figure indicate what could be heartbeat signals mixed into the radar signal.
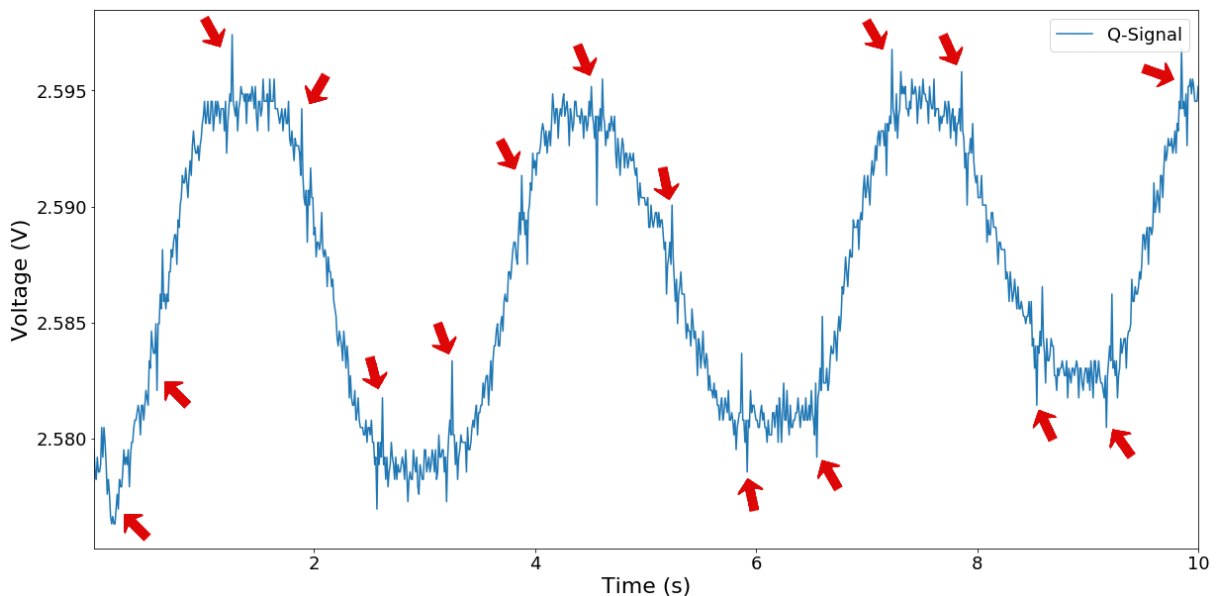
Figure 73 – Heartbeat signals possibly detected in close observation of the radar signal.

The data frame of the Figure 73 corresponds to a period of 10 seconds. In this period, between 15 and 16 possible heartbeats were observed and marked with arrows. However, due to the influence of the breathing and noise, it is not possible to precisely define or characterize the heartbeats as valid data. Signal processing and filtering should be applied to remove the respiratory pattern and noise, enabling analyses to be performed on a cleaner signal.

Also, for comparison and to properly validate the future data as a valid heartbeat signal, it is necessary to evaluate the pattern of known human heartbeats. From studies

performed on fetal [34] and adults [35] heart monitoring, it is possible to see in Figure 74 and Figure 75 what the heartbeat signal should look like after filtering.
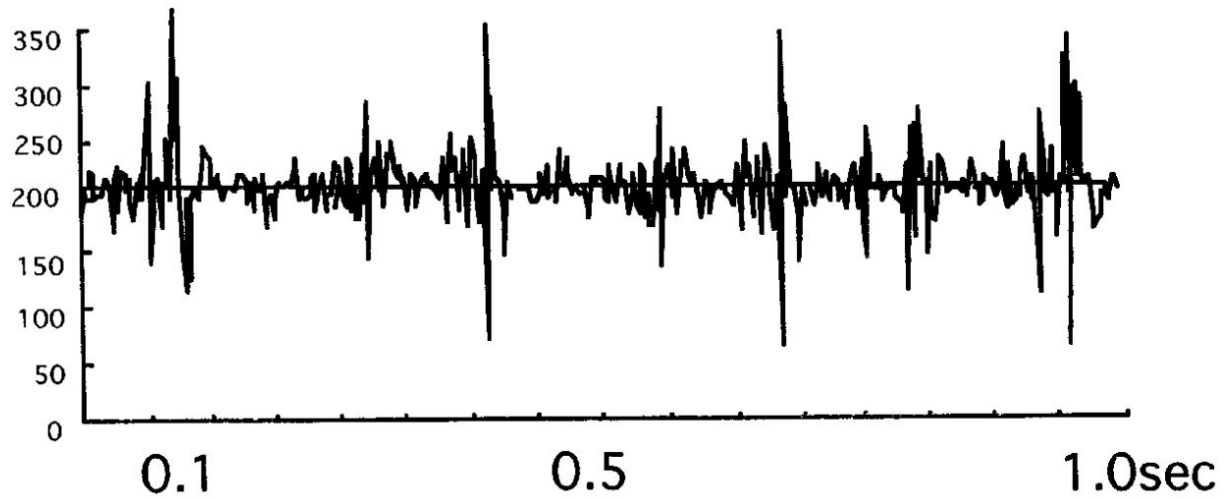
Figure 74 – Ultrasound Doppler signals reflected from a fetal heart [34].
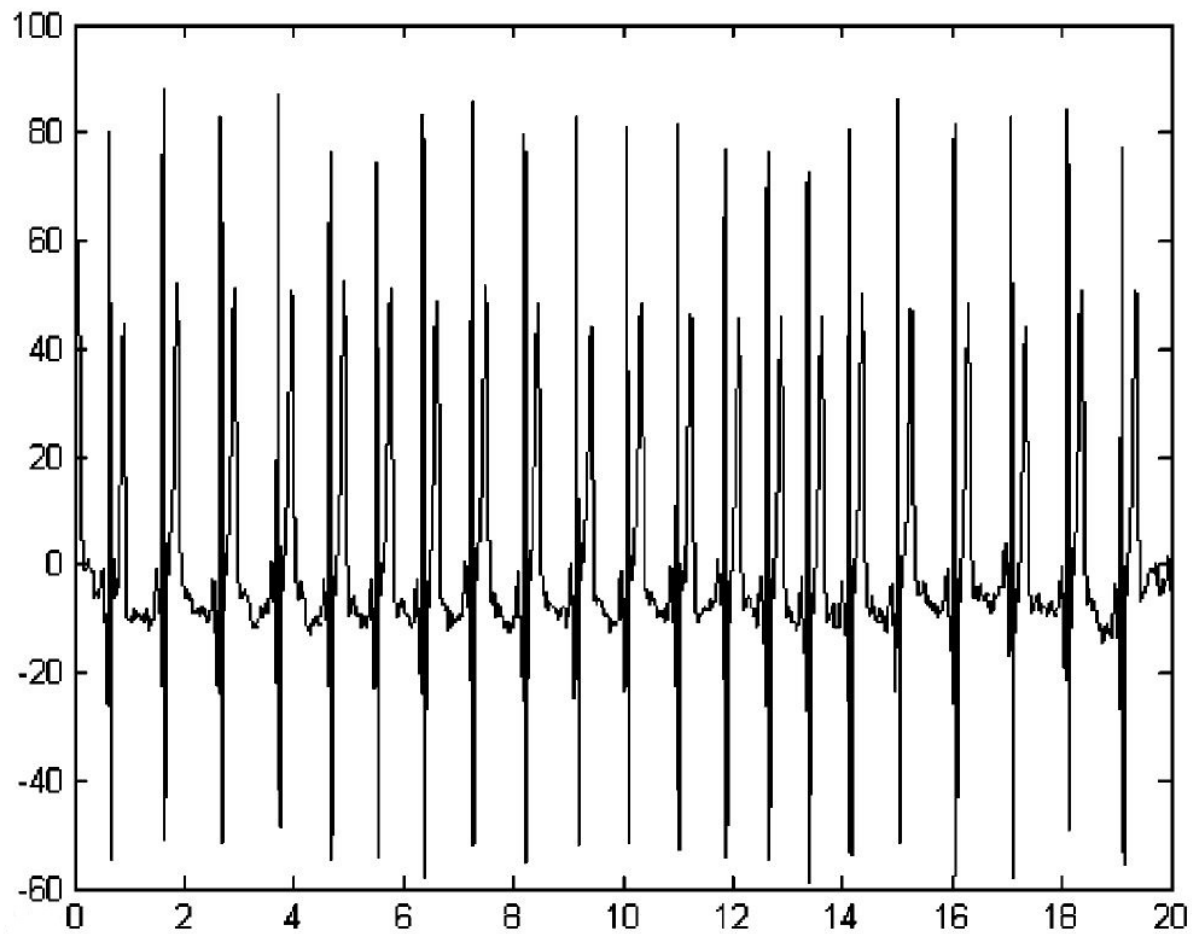
Figure 75 – Raw electrocardiogram data from an adult person [35].

Accordingly, for this analysis, a nine-order Butterworth high-pass filter was designed, with a cut-off frequency (-3 dB) in 10 Hz. After applying the filter, the low-frequency movements – including breathing – should be removed, with the remaining signal showing the high frequency pattern of a heartbeat signal. In Figure 76, it is shown the frequency response of the designed filter. The filter was then applied on the radar signal for extraction of the heartbeats. As a result, the heartbeats of the test person were successfully retrieved. In Figure 77, it is shown the radar signal after applying filtering.
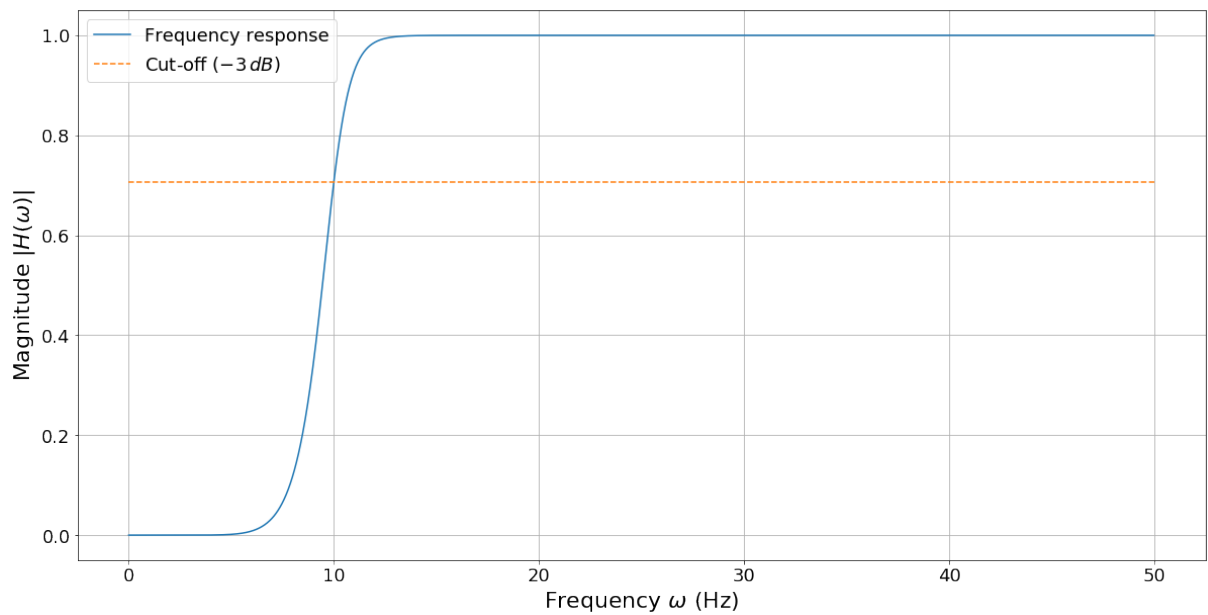
Figure 76 – Frequency response of the nine-order Butterworth high-pass filter, designed with a cut-off frequency of 10 Hz.

Figure 77 – Heartbeat signals shown in details after filtering the radar signal.

Analyzing the Figure 77, it is now possible to clearly identify 15 peaks, corresponding to 15 heartbeats in the data frame of 10 seconds. Thus, for a one minute interval, the heart rate of the test person can be calculated as 90 beats per minute. Such heart rate value, as found in [36], is classified as in the normal heart rate range for a person in a rest state, which comprehends 60 to 100 beats per minute. From the point of view of the test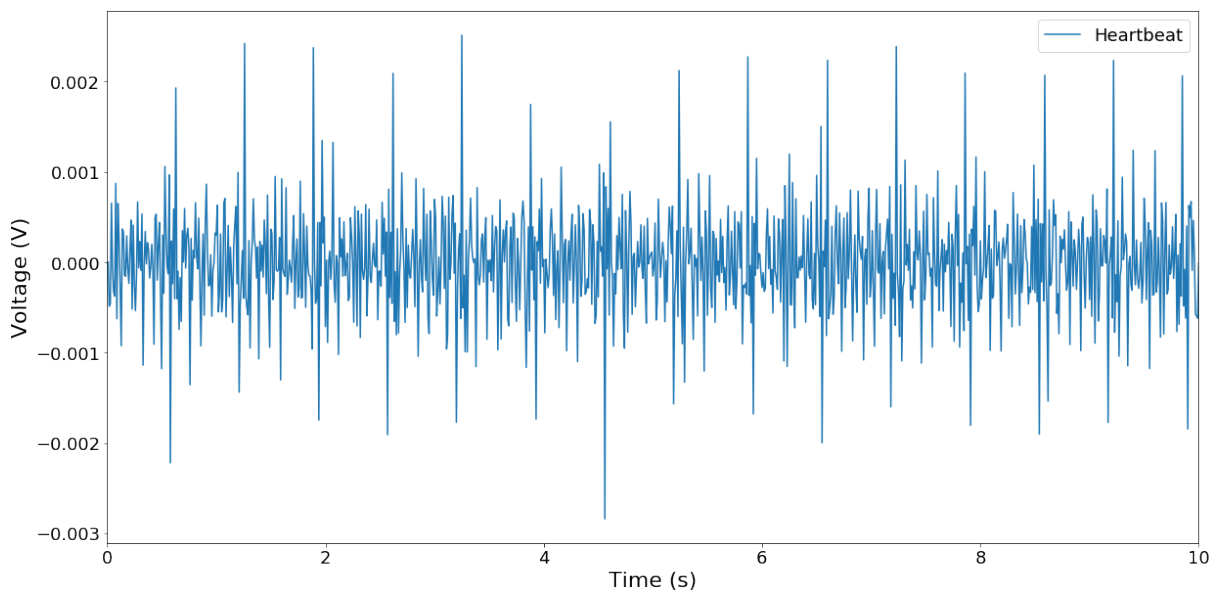, the analysis is consistent, considering that the test person was not undertaking any stress during the calibration period.

Therefore, the information here presented is a step-forward to validate the data and the results found in this thesis, going beyond the extraction of the breathing pattern and consistently acquiring the heartbeat of the test subject.

In Figure 78, it is shown another data frame from the radar signal, this time acquired while driving. In this signal, differently than in Figure 73, it is not possible to observe any indications of heartbeats. Instead, there is a substantial amount of noise caused by the movements of the vehicle and passenger. Consequently, it raises a question: would it still be possible to filter the radar information in such a way that the heartbeat signals could be detected even in a moving vehicle?
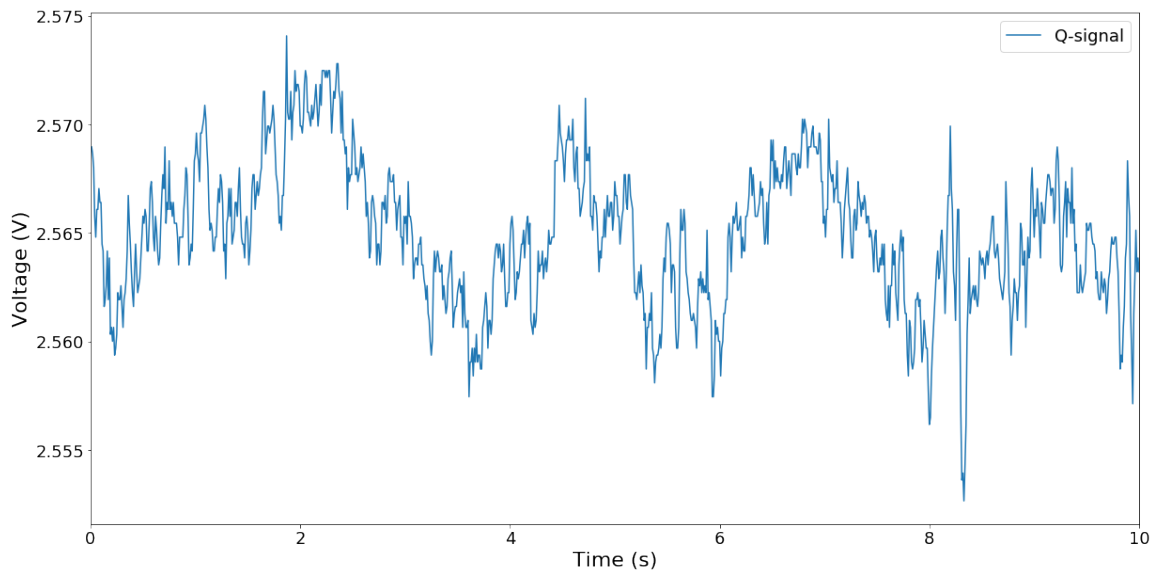
Figure 78 – Radar signal detecting a test person in a moving vehicle.

For this approach, it was first performed an analysis of the filtered heartbeat signal (Figure 77) in the frequency domain. The goal of this analysis was to identify the frequencies with most influence on the heartbeat, and then apply a filter for the frequency band of the desired signal. However, as shown in Figure 79, the power of the heartbeat signal spreads across a high number of frequencies in the frequency domain. The extraction of the heartbeat was not a straightforward task and many filters had to be tested in order to find the best method.
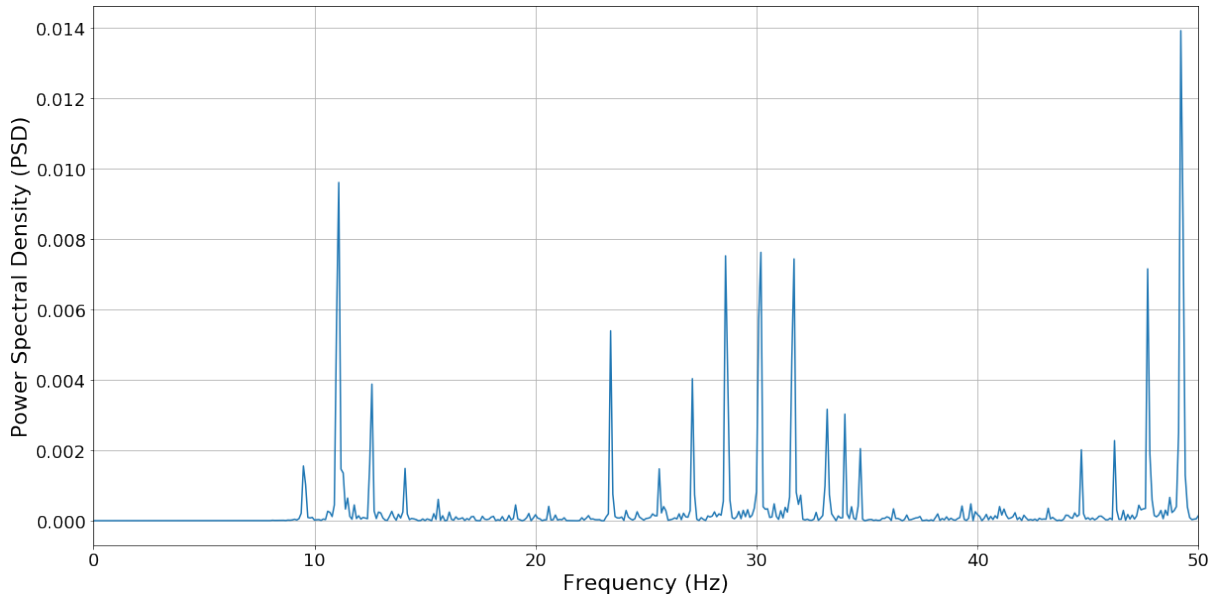
Figure 79 – Power density spectrum of the heartbeat signal shows that the signal spreads across a broad number of frequencies.

In fact, more than ten filters were designed in order to find the best approach for the radar signal filtering. Different filter orders and different cut-off frequencies were tested, with a nine-order Butterworth high-pass filter showing the best results. In Figure 80, it is shown three of the filters designed: the first with a cut-off frequency at 10 Hz, the second with a cut-off at 22 Hz and the third at 37 Hz.
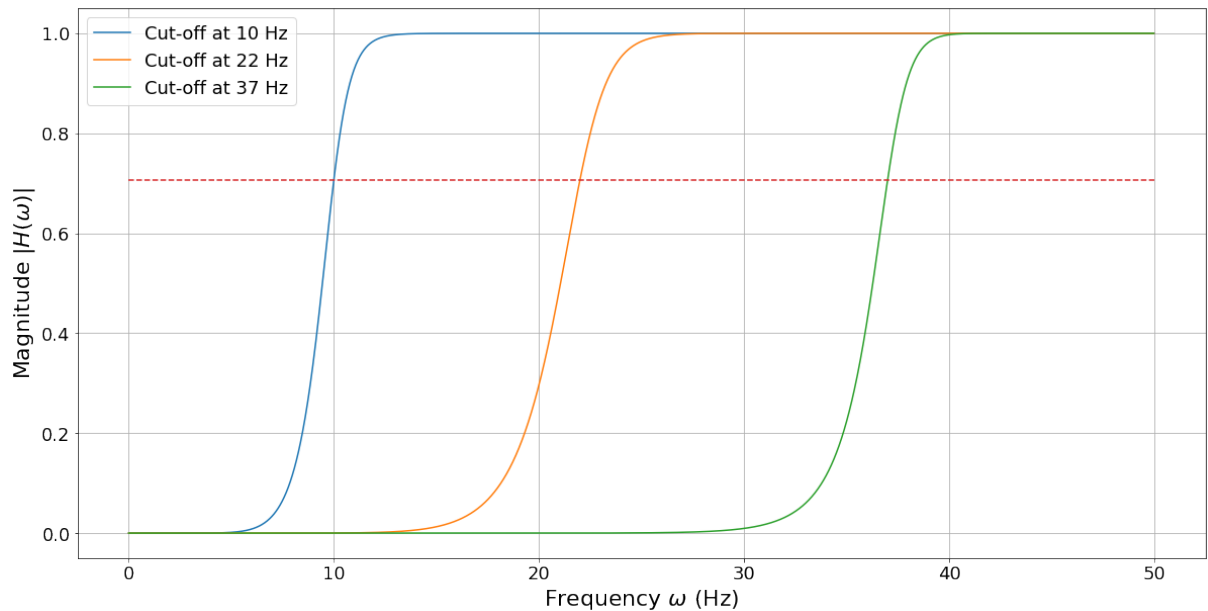
Figure 80 – Nine-order Butterworth high-pass filters designed for extraction of the heart-beats, with cut-off frequencies at 10 Hz (blue), 22 Hz (orange) and 37 Hz (green).

The filters were all applied on the radar signal acquired in the moving vehicle (Figure 78), with the results presented in Figure 81.
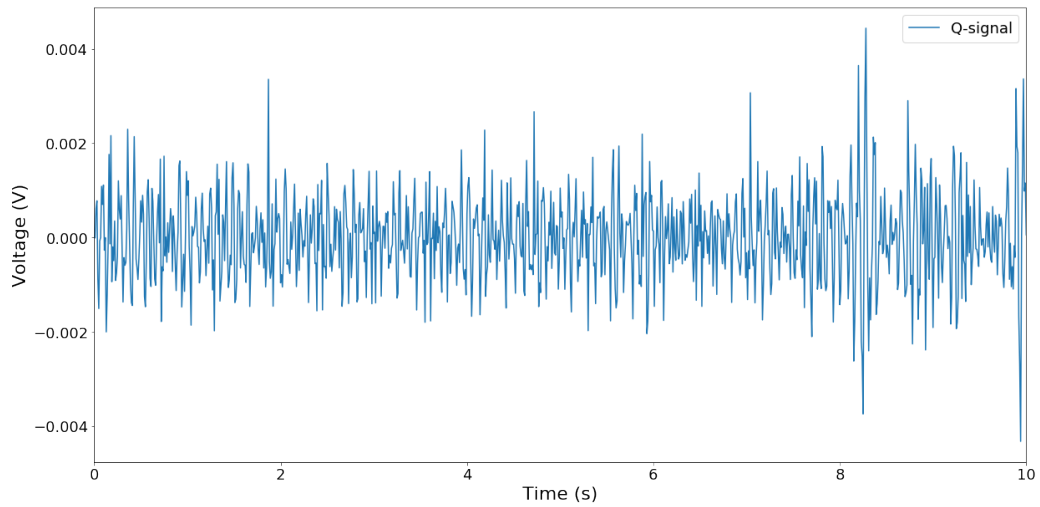
(a) Applying the high-pass filter with a cut-off at 10 Hz, it is not possible to differentiate the heartbeats from noise.
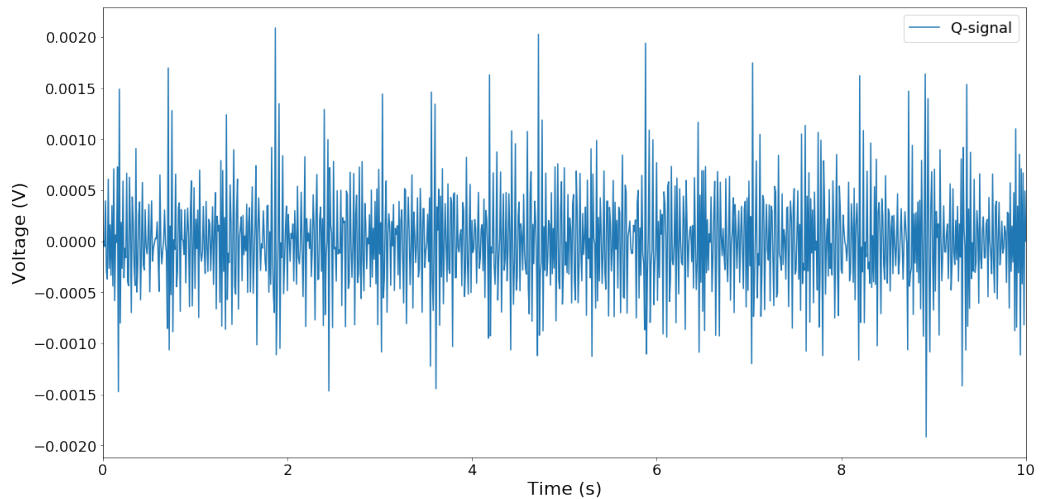
(b) With the cut-off at 22 Hz, some heartbeat patterns can already be seen.
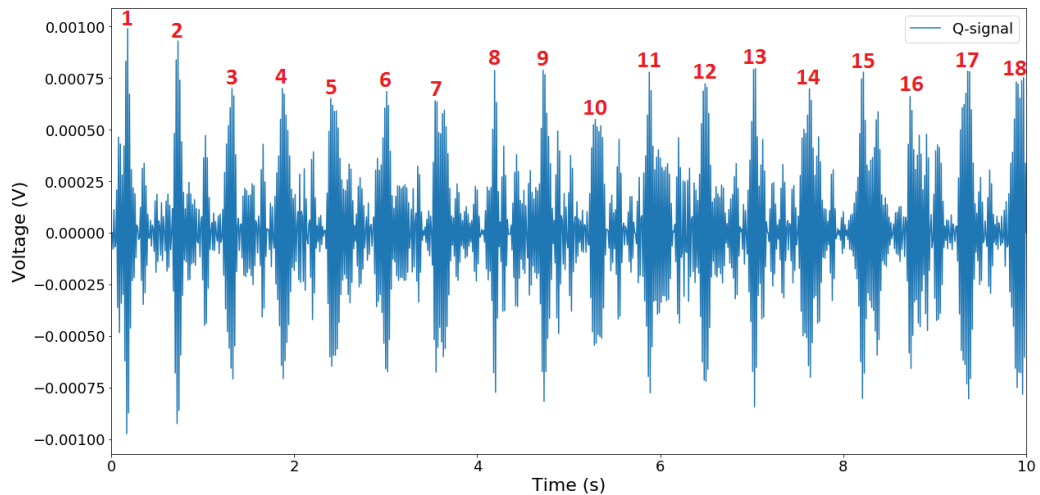
(c) With the cut-off at 37 Hz, the heartbeats are clearly distinguished.

Figure 81 – Radar signal from a moving vehicle, after applying high-pass filters with cut-off frequencies at 10 Hz (a), 22 Hz (b) and 37 Hz (c).

In Figure 81, it is possible to distinctly observe 18 heartbeats in the time period of ten seconds. Calculating for a one-minute interval, the heart rate of the test person can be defined at 108 bpm (beats per minute) for this driving period. Comparing to the previous heart rate, measured at 90 bpm in a steady state, it is possible to assume that the test person was under effects of emotion or stress, with an increased heart rate. Some studies [37, 38] have shown that driving situations can considerably increase the heart rate, possibly caused by the speed of the vehicle, curves and sense of awareness in driving situations. Although the stress can be much more impactful and evident on drivers, with heart rates going from 55-100 bpm while resting to 75-145 bpm while driving [37], anxiety and awareness can possibly impact passengers as well.

Thus, it is reasonable to say that such evidences support the analyses on the detection of heartbeats. Comparing to known heartbeat signals from other studies, in Figure 74 and Figure 75, the pattern is clearly exposed. Such findings can open new possibilities for passenger's detection in moving vehicles, going beyond the acquisition of the respiratory movement only. As a next step, further proofs can be achieved with the aid of proper medical devices for heart rate detection, with a promising outcome on the confirmation of the results found in the radar signal analyses.

7 Conclusion and Perspectives

This thesis presented the project realized at IEE in the fields of radar, software development and data acquisition. The project accomplished all its main goals, which were the preparation of the hardware devices, the development of a complete software with user interface for data acquisition and analysis, and the execution of tests in real road environments. More importantly, the project succeeded in the extraction of vital signs from passengers even in a moving vehicle.

The fusion of the radar and accelerometer has proven its reliable operation, with a successful implementation of the accelerometer belts as well. The integration with the data acquisition device was made after thorough inspection and evaluation of the best methods for hardware integration. The scheme of connectors provided straightforward capabilities for coupling/uncoupling the devices, facilitating the setup of tests and allowing easy replacement of faulty parts.

The acquisition, processing and recording of all the radar and accelerometer signals were done through DAS (Data Acquisition Software), a program uniquely developed for this thesis. Additionally, the software itself was designed to be easily applicable even in other projects. The architecture of the code allows the change of a number of internal parameters, in order to effortlessly adjust the software for the future needs of the company. The software was developed in clean coding, with no warnings at the source code level and no untreated errors shown to the user. The program has redundancies to design out user errors and to provide the best user experience as possible.

The integration of the entire system into the vehicle structure was completed and a broad number of tests were performed, in accordance with a predefined list of test scenarios. With the tests, more than 250 megabytes of raw data were collected, amounting to more than 26 million raw sample points acquired.

With the acquired data, analyses have been made and the results surpassed prior expectations. Breathing patterns from the test subjects were seen in both static and driving conditions. Many filters with different orders and cut-off frequencies were designed to find the best outcome. With further investigations, analyses found promising results even on the detection of heartbeats.

For subsequent projects, there is a vast number of potential investigations to be done on top of the acquired data. Possible analyses include extraction of information from breathing and heartbeats for classification of passengers. Regarding the heartbeat signals, the data can be validated and further investigated with additional tests with radar and a dedicated medical device for measurement of the heart rate. The heart rate, in fact, can be even more interesting than breathing for artificial intelligence systems to detect

the emotional state of drivers and passengers. Further tests can be made with higher sampling frequencies, in order to better analyze the spread of the heartbeat signal in the frequency domain.

For a more precise detection of passengers' movements, a gyroscope sensor could be added to the radar. A gyroscope, which measures angular velocity, would be useful to assist in the approximation of the radar orientation, possibly making the calculations more precise and faster in performance. Future implementations could also use the sensors' data to construct models for the movements of the vehicle and passengers. With a prediction of the movements of passengers, such information can be used for new strategies in the filtering of the radar signal.

More tests and distinguished scenarios can also be performed in future works. It would be interesting to investigate, for example, the response of the radar detection to the presence of two or three passengers simultaneously, or to the addition of vibrating objects next to the passengers.

Nevertheless, it is important to emphasize the contributions of this project and of the already presented data. The perspectives are great on the topics of vehicle security and classification of passengers, with the rapid development of automated driving technologies making everything even more interesting.

The detection of breathing and the preliminary analyses on the detection of heartbeats in moving vehicles are contributions that this project has achieved with much effort. Possibilities are open for applications in passenger detection and classification, for support in the deployment of security systems such as airbags, or in warning systems such as in the detection of forgotten children and seat belt reminders. Outside the automotive field, such radar capabilities can find applications in the areas of medicine, rescue and emergency services, offering detection of persons in steady or moving states. In the medical and veterinary fields, specifically, contactless monitoring of vital signs for human and animals are of much interest, benefiting from non-intrusive options to observe patients. Ultimately, this thesis paves the way for continuing investigations on the relation between vehicle's movements and radar detection capabilities, with much more yet to come.

References

1 DIRECTORATE-GENERAL FOR EDUCATION, YOUTH, SPORT AND CULTURE (EUROPEAN COMMISSION). **ECTS Users' Guide**. Luxembourg: Publications Office of the European Union, 2015. ISBN 978-92-79-43559-1. DOI: `10.2766/87192`.

2 IEE Official Website. Available from: <`www.iee.lu/en`>. Visited on: 22 Mar. 2019.

3 DIEWALD, A. R.; LANDWEHR, J.; TATARINOV, D. et al. RF-based Child Occupation Detection in the Vehicle Interior. In: 2016 17th International Radar Symposium (IRS). Krakow, Poland: IEEE, 2016. ISBN 978-1-5090-2518-3. DOI: `10.1109/IRS.2016.7497352`.

4 ENDER, J. **98 Years of the RADAR Principle**: The Inventor Christian Hülsmeyer. Cologne, Germany, 2002. Available from: <`http://www.design-technology.info/resourcedocuments/Huelsmeyer_EUSAR2002_english.pdf`>. Visited on: 5 May 2019.

5 BAUER, A. **Christian Hülsmeyer and about the early days of radar inventions**. 2005. Available from: <`https://aobauer.home.xs4all.nl/Huelspart1def.pdf`>. Visited on: 5 May 2019.

6 GEBHARD, L. **Evolution of Naval Radio-Electronics and Contributions of the Naval Research Laboratory**. Washington, D.C., USA, 1979. Available from: <`https://apps.dtic.mil/dtic/tr/fulltext/u2/a084225.pdf`>. Visited on: 5 May 2019.

7 CHILD Vehicular Heatstroke Fatalities by Year (1990-2018): Involving U.S. Children Age 14 and Under. Available from: <`www.kidsandcars.org/wp-content/uploads/2019/04/heat-calendar-EN-19.pdf`>. Visited on: 13 May 2019.

8 TRENDS and Patterns in Pediatric Vehicular Heatstroke Deaths, 1998-2018. Available from: <`www.noheatstroke.org/Heatstroke_Trends_2018.pdf`>. Visited on: 13 May 2019.

9 LU-DAC, M.; DI MARIO-COLA, P.; TATARINOV, D. et al. **Method and system for unattended child detection**. 24 Sept. 2015. PCT/EP2015/056017.

10 CRUZ, S. D.; BEISE, H. P.; SCHRÖDER, U.; KARAHASANOVIC, U. Detection of Vital Signs in Presence of Car Vibrations and RADAR-Based Passenger Classification. In: 2018 19th International Radar Symposium (IRS). IEEE, June 2018. DOI: `10.23919/IRS.2018.8447952`.

11 CRUZ, S. D.; BEISE, H. P.; SCHRÖDER, U.; KARAHASANOVIC, U. A Theoretical Investigation of the Detection of Vital Signs in Presence of Car Vibrations and RADAR-Based Passenger Classification. In: IEEE Transactions on Vehicular Technology. IEEE, Apr. 2019. p. 3374–3385. DOI: `10.1109/TVT.2019.2898512`.

12 SKOLNIK, M. **Introduction to Radar Systems**. 3. ed.: McGraw-Hill, 2002. ISBN 978-0072881387.

13 SKOLNIK, M. (Ed.). **Radar Handbook**. 3. ed.: McGraw-Hill, 2008. ISBN 978-0-07-148547-0.

14 BUTRICA, A. J. **To See the Unseen: A History of Planetary Radar Astronomy**. NASA, 1996.

15 WIESBECK, W. **Radar Systems Engineering**. 16. ed.: Institut für Hochfrequenztechnik und Elektronik, 2010.

16 MIKHELSON, I. V.; BAKHTIARI, S.; ELMER, T. W.; SAHAKIAN, A. V. Remote Sensing of Heart Rate and Patterns of Respiration on a Stationary Subject Using 94-GHz Millimeter-Wave Interferometry. In: 6. IEEE Transactions on Biomedical Engineering. IEEE, June 2011. v. 58.

17 DADAFSHAR, M. **Accelerometer and Gyroscopes Sensors: Operation, Sensing, and Applications**. Application Note 5830. Maxim Integrated Products, Inc. 2014. Available from: <`https://pdfserv.maximintegrated.com/en/an/AN5830.pdf`>. Visited on: 15 May 2019.

18 SPARKFUN ELECTRONICS. **Accelerometer Basics**. Available from: <`https://learn.sparkfun.com/tutorials/accelerometer-basics/all`>. Visited on: 15 May 2019.

19 ANALOG DEVICES. **ADXL330 Datasheet**. Rev. A. 2007. Available from: <`https://www.analog.com/media/en/technical-documentation/data-sheets/adxl330.pdf`>. Visited on: 15 May 2019.

20 STMICROELECTRONICS. **Parameters and Calibration of a Low-g 3-axis Accelerometer**. Application Note 4508. June 2014.

21 CLIFFORD, M.; GOMEZ, L. **Measuring Tilt with Low-g Accelerometers**. Application Note 3107. Freescale Semiconductor. May 2005. Available from: <`www.nxp.com/files-static/sensors/doc/app_note/AN3107.pdf`>. Visited on: 15 May 2019.

22 NOVAK, L.; NEUZIL, P.; LI, J.; WOO, M. Ultrasensitive MEMS-based inertial system. In: SENSORS. IEEE, 2009. p. 552–554. DOI: `10.1109/ICSENS.2009.5398301`.

23 ELECTRONIC COMMUNICATIONS COMMITTEE (ECC) WITHIN THE EURO-
    PEAN CONFERENCE OF POSTAL AND TELECOMMUNICATIONS ADMINIS-
    TRATIONS (CEPT). **The European Table of Frequency**: Allocations and Ap-
    plications in the Frequency Range 8.3 kHz to 3000 GHz (ECA Table). European
    Communications Office, Oct. 2018.

24 KOZAKOFF, D. J. **Analysis of Radome-Enclosed Antennas**. 2. ed.: Artech
    House, 2010. ISBN 978-1-59693-441-2.

25 LIN CONSORTIUM. **LIN Specification Package**: Rev. 2.2A. 31 Dec. 2010.

26 NI-9220 Getting Started Guide. Available from: <`http://www.ni.com/pdf/manual`
    `s/378023a.pdf`>. Visited on: 15 May 2019.

27 NATIONAL INSTRUMENTS. **NI-9220 Datasheet**. 2017. Available from: <`http:`
    `//www.ni.com/pdf/manuals/378023a_02.pdf`>.

28 NI-DAQMX Download Page. Available from: <`http://www.ni.com/en-us/suppor`
    `t/downloads/drivers/download.ni-daqmx.html`>. Visited on: 15 May 2019.

29 NI-DAQMX Reference Help. Available from: <`http://zone.ni.com/reference/`
    `en-XX/help/370471W-01/`>. Visited on: 15 May 2019.

30 NI-DAQMX C Functions. Available from: <`http://zone.ni.com/reference/en-`
    `XX/help/370471W-01/TOC3.htm`>. Visited on: 15 May 2019.

31 MATLAB Official Website. Available from: <`https://www.mathworks.com/produc`
    `ts/matlab.html`>. Visited on: 15 May 2019.

32 CHON, K. H.; DASH, S.; JU, K. Estimation of Respiratory Rate From Photoplethys-
    mogram Data Using Time–Frequency Spectral Estimation. In: IEEE Transactions on
    Biomedical Engineering. IEEE, 14 Apr. 2009. p. 2054–2063. DOI: `10.1109/TBME.`
    `2009.2019766`.

33 ADDISON, P. S.; WATSON, J. N.; MESTEK, M. L.; MECCA, R. S. Developing an
    algorithm for pulse oximetry derived respiratory rate (RRoxi): a healthy volunteer
    study. In: 1. JOURNAL of Clinical Monitoring and Computing. Springer, 10 Jan.
    2012. v. 26, p. 45–51. DOI: `10.1007/s10877-011-9332-y`.

34 KIMURA, Y.; OKAMURA, K.; WATANABE, T. et al. Time-frequency analysis of
    fetal heartbeat fluctuation using wavelet transform. **American Journal of Physi-
    ology: Heart and Circulatory Physiology**, v. 275, n. 6, h1993–h1999, 1998. DOI:
    `10.1152/ajpheart.1998.275.6.H1993`.

35 ISRAEL, S. A.; IRVINE, J.; CHENG, A. et al. ECG to identify individuals. **Pattern
    Recognition**, v. 38, p. 133–142, 2005.

36   GOLDBERGER, A.; GOLDBERGER, Z.; SHVILKIN, A. **Goldberger's Clinical Electrocardiography: A Simplified Approach**. 9. ed.: Elsevier, May 2017. p. 1–275. ISBN 978-0-323-40169-2.

37   TAGGART, P.; GIBBONS, D.; SOMERVILLE, W. Some Effects Of Motor-Car Driving On The Normal And Abnormal Heart. **The British Medical Journal**, v. 4, n. 5676, p. 130–134, 1969.

38   ZUŻEWICZ, K.; ROMAN-LIU, D.; KONARSKA, M. et al. Heart rate variability (HRV) and muscular system activity (EMG) in cases of crash threat during simulated driving of a passenger car. **International Journal of Occupational Medicine and Environmental Health**, v. 26, n. 5, p. 710–723, 2013. DOI: `10.2478/s13382-013-0148-5`.

Appendix

A DAS: Folders and Files Structure

```
|   main.mlapp
|
+---app
|       app_accel_frequency.mlapp
|       app_accel_spectrogram_X.mlapp
|       app_accel_spectrogram_Y.mlapp
|       app_accel_spectrogram_Z.mlapp
|       app_accel_time.mlapp
|       app_preferences.mlapp
|       app_radar_frequency.mlapp
|       app_radar_spectrogram_I.mlapp
|       app_radar_spectrogram_Q.mlapp
|       app_radar_time.mlapp
|       app_test_setup.mlapp
|       preferences.iee
|
+---img
|       IEE_150x81.jpg
|       iee_icon.ico
|
+---lib
|       check_daq_error.m
|       get_daq_device.m
|       is_file_populated.m
|       is_multiple_call.m
|       load_libs.m
|       load_spectrogram.m
|       NIDAQmx.h
|       NIDAQmx.m
|       NIDAQ_config_read_analog.m
|       NIDAQ_read_analog.m
|       preferences_get_default.m
|       preferences_load_from_file.m
|       preferences_save_to_file.m
|       reset_daq_device.m
```

```
|        reset_task.m
|        setup_get_default.m
|        setup_save_to_file.m
|        store_data_in_fifo.m
|        str2bool.m
|        update_axes_title.m
|        update_plot.m
|        VarHandle.m
|        voltage2gs.m
|
\---recordings
```